Nonlinear Viscoelastic Behavior of Ligaments and Tendons: Models and Experiments

Frances Maria Davis

Dissertation submitted to the Faculty of
Virginia Polytechnic Institute and State University
in partial fulfillment of the requirements for the degree of

Doctor of Philosophy
in
Engineering Mechanics

Raffaella De Vita, Chair
Romesh C. Batra
Michael L. Madigan
Ishwar K. Puri
Pavlos P. Vlachos

April 23, 2013
Blacksburg, Virginia

Keywords: Ligament, Tendon, Nonlinear Viscoelasticity, Stress relaxation, Small-angle x-ray diffraction (SAXD)

Nonlinear Viscoelastic Behavior of Ligaments and Tendons: Model and Experiments

Frances M. Davis

ABSTRACT

Ligaments and tendons are rope-like structures in our body that possess time- and history-dependent material properties. Despite the many advances made in experimental and theoretical biomechanics, the material properties of these biological structures are still not fully characterized. This dissertation represents a step forward in the development of combined theoretical and experimental tools that capture the time- and history-dependent material properties of ligaments and tendons.

The mechanical behavior of bundles of collagen fibers which form ligaments and tendons was investigated. Axial stress-stretch data and stress relaxation data at different axial stretches were collected by testing rat tail tendon fascicles. The experimental results demonstrated, for the first time, that the shape of the normalized axial stress relaxation curve depends on the axial stretch level thus suggesting that the fascicles are nonlinear viscoelastic. A constitutive model was then formulated within the nonlinear integral representation framework proposed by Pipkin and Rogers (1968). Unlike the well-known quasi-linear viscoelastic model, the proposed constitutive law was able to capture the observed nonlinearities in the stress relaxation response of rat tail tendon fascicles.

By extending the constitutive model for collagen fiber bundles, a new nonlinear three-dimensional model for the stress relaxation of skeletal ligaments was formulated. The model accounts for the contribution of the collagen fibers and the group substance in which they are embedded. Published uniaxial experimental data on the stress relaxation of human medial collateral ligaments were used to determine the model parameters. The model predictions for simple shear in the fiber direction, simple shear transverse to the fiber direction, and equibiaxial extension were then examined and, for the case of simple shear in the fiber direction, such predictions were found to be in good agreement with published experimental data.

The relationship between the mechanical response and structure of suspensory ligaments was examined by performing state-of-the-art small angle x-ray diffraction experiments in tandem with incremental stress relaxation tests. Specifically, small angle x-ray diffraction was used to measure changes in strain and orientation of collagen fibrils during the stress relaxation tests. Throughout the tests the collagen fibrils were found to gradually orient towards the loading direction. However, the collagen fibril strain did not change significantly suggesting that collagen fibers do not play a significant role in dissipating load during stress relaxation.

Dedication

To my mother, who loves me unconditionally with all her heart. Thank you for always keeping me in your thoughts and prayers.

To my father, whose faith in me always surprises me, amazes me, and humbles me. Thank you for always believing I am bigger than life's obstacles.

To my brother Martin, who helped me kick off my last year of graduate school with a cross-country trip. Thank you for helping me keep life in perspective and sending me some of your good luck this year.

To my brother Berkley, who sent this quote by Albert Camus while I was writing my final two chapters

> In the midst of chaos, I found there was, within me, an invincible calm.
> In the midst of winter, I found there was, within me, an invincible summer.
> And that makes me happy.
> For it says that no matter how hard the world pushes against me,
> within me, theres something stronger, something better, pushing right back.

To my Nanny, who always makes me smile. Thank you for all the laughs, the hugs, the kisses, and the stories.

To Ellen, who reminds me to work hard and *play* hard. Thank you for keeping my spirits up when the work was most difficult.

Acknowledgments

First and foremost, I would like to express sincere appreciation and gratitude to my advisor, Dr. Raffaella De Vita, for her guidance and mentorship during my graduate studies. I am also grateful to my committee members, Drs. Romesh Batra, Micheal Madigan, Ishwar Puri, and Pavlos Vlachos, for their guidance and thought provoking suggestions. I would be remiss if I did not recognize the contributions Drs. Jon Almer and Joseph Orgel, who mentored me during my summer appointment at Argonne National Laboratory.

I would also like to thank all of the members of the Mechanics of Soft Biological Systems Laboratory, particularly Matt Webster and Ting Tan, for all of the help and advice you all have provided. I am especially grateful to the members of Dr. Orgel's research group at Illinois Institute of Technology, particularly Rama Sashank and Dr. Olga Antipova, for all their help and guidance on performing x-ray diffraction studies. Last but not least, I would like to thank my fellow doctoral students, Jess Dibelka and Tim Hartman, for your feedback, support, and friendship over these last five years.

Funding Acknowledgments

This work was supported by Nation Science Foundation Graduate Research Fellowship and the Ford Foundation Pre-Doctoral Fellowship.

The work presented in Chapter 5 was completed at Argonne National Laboratory. Use of the Advanced Photon Source, an Office of Science User Facility operated for the U.S. Department of Energy (DOE) Office of Science by Argonne National Laboratory, was supported by the U.S. DOE under Contract No. DE-AC02-06CH11357. The project was supported by grants from the National Center for Research Resources (2P41RR008630-17) and the National Institute of General Medical Sciences (9 P41 GM103622-17) from the National Institutes of Health. The content is solely the responsibility of the authors and does not necessarily reflect the official views of the National Center for Research Resources, National Institute of General Medical Sciences or the National Institutes of Health.

Contents

List of Figures

1 Introduction

1.1 Motivation & Aims

Ligaments and tendons are dense fibrous connective tissues. Tendons connect muscle to bone while skeletal ligaments connect bone to bone and suspensory ligaments support internal organs. Skeletal ligaments and tendons work together to stabilize motion at a joint whereas suspensory ligaments keep internal organs, for instance the uterus and bladder, anchored in place.

Due to the role of tendons and skeletal ligaments in motion at a joint, they are susceptible to injury from overuse and sudden movements [1, 2]. In fact medical spending on tendon and skeletal ligaments injuries exceeds five billion dollars per year [1, 3]. The high incidence of tendon and skeletal ligament injuries is linked with increased participation in recreational sports activities [4, 5]. The Achilles tendon and medial collateral ligament, for example, are commonly injured during sporting activities such as skiing, soccer, football, and ice hockey [5, 6]. Following a complete tear of the ligament or tendon, joint instability occurs and the injury may require surgical intervention to restore joint stability.

The suspensory ligaments supporting internal organs are not immune to injury. In women suffering from pelvic organ prolapse, the cardinal and uteroscaral ligaments become lax allowing the position of the pelvic organs they support to shift downward and, in the most acute cases, protrude out of the vaginal canal [7]. More than 300,000 women in the United States undergo surgical reconstruction for pelvic organ prolapse every year with the resulting medical costs approaching one billion dollars [8].

For the most severe injuries, when the ligament or tendon is completely torn or becomes excessively lax, surgical reconstruction is required. During surgical repair of skeletal ligaments and tendons, sutures are placed to close the gap between the ruptured ends as seen in Figure 1.1(a). In surgical reconstruction for pelvic organ prolapse, the cardinal and uterosacral

ligaments are detached from the uterus and used to suspend the vagina from the uterosacral and cardinal ligaments (Figure 1.1(b)). In both cases, the ligament or tendon is strained in an ad-hoc way to tension the repaired ligament or tendon [7, 9, 10, 11, 12] but, over time, this tension decreases as the tissue undergoes stress relaxation. Improper selection of the initial tension can predispose the patient to long-term surgical complications such as site pain, osteoarthritis, or a recurrence of pelvic organ prolapse [7, 13].

(a)

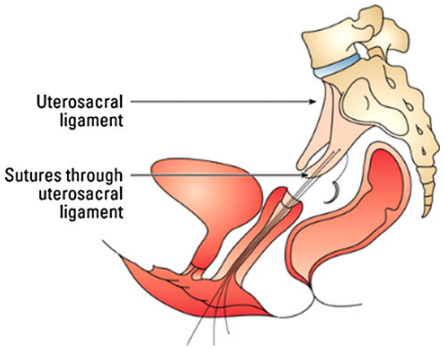

(b)

Figure 1.1: Surgical repair techniques using (a) the Krackow 4 strand suture for Achilles tendon repair [9] with permission from SAGE Publications, see Appendix C and (b) transvaginal suspension from the uterosacral-cardinal ligament complex for treatment of pelvic organ prolapse [7] with permission from Springer, see Appendix C.

Robust constitutive models, which characterize and predict the stress relaxation behavior of ligaments and tendons, are needed to improve surgical reconstruction. This dissertation aims to develop anisotropic finite strain constitutive relationships to describe the stress relaxation behavior of soft collagenous tissues. Specifically the objectives of this dissertation are:

- *Characterize the strain-dependent stress relaxation behavior of collagen fiber bundles by performing uniaxial stress relaxation experiments on rat tail tendon fascicles.*
- *Develop a constitutive relation for the stress relaxation behavior of collagen fiber bundles using the integral representation of Pipkin and Rogers [14, 15].*
- *Formulate a three dimensional constitutive relationship to describe the stress relaxation behavior of skeletal ligaments.*
- *Determine the role of collagen fibrils in the stress relaxation response of the cardinal ligament using small angle x-ray diffraction (SAXD).*

1.2 Summary of Chapters

In Chapter 2, the morphology and mechanical properties of ligaments and tendons are discussed, followed by a brief review of the viscoelastic models commonly employed to describe the relaxation behavior of ligaments and tendons.

Computational models offer an efficient method to determine the optimal initial tension for ligaments and tendons during surgical reconstruction. However, the literature lacks reliable constitutive relations which can be implemented in computational tools, such as finite element models, for the evaluation of new surgical techniques [16]. As a first step towards developing a three dimensional viscoelastic constitutive model, the strain dependent stress relaxation behavior of collagen fiber bundles is characterized using rat tail tendon fascicles in Chapter 3. Using the collected experimental data a constitutive relation is formulated for the nonlinear stress relaxation behavior of parallel collagen fiber bundles. In Chapter 4, the constitutive model for the stress relaxation response of collagen fiber bundles developed in Chapter 3 is extended to three-dimensions. The constitutive relation is developed by assuming that skeletal ligaments are composed of a compliant isotropic matrix reinforced by collagen fiber bundles.

Only recently has experimental data been published on the tensile properties of the cardinal and uteroscaral ligaments [17, 18, 19, 20]. Much is still unknown about the viscoelastic response of these ligaments. In Chapter 5, the stress relaxation response of swine cardinal ligaments is investigated using mechanical and diffraction studies. The small angle x-ray diffraction experiments completed at BioCAT in Argonne National Laboratory are used to examine the link between the structural changes that occur at the nano-scale and the macro-scale viscoelastic response of the cardinal ligament. Conclusions and future directions for this research are presented in Chapter 6.

2 Literature Review

2.1 Ligament and Tendon Morphology

Collagen is the primary building block of ligaments and tendons and comprises 70-80% of their dry weight [21]. Collagen fibers are hierarchical structures and can be subdivided into fibrils, sub-fibrils, microfibrils, and tropocollagen. Using an electron microscope at magnifications approaching 100,000×, a banded repeat can be seen in collagen fibrils which spans 67 nanometers and is known as the D-period.

In ligaments, collagen fibers are loosely organized in bundles along the long axis of the ligament (Figure 2.1 (a)). The hierarchical organization of tendons is similar except that collagen fibers aggregate into discrete bundles called fascicles that are surrounded by a sheath called the paratenon (Figure 2.1 (b)) [22]. The paratenon allows for the movement of fascicles against the surrounding tissue. In ligaments and tendons, fibroblasts, also called tenocytes when found in tendons, are located between the collagen fibers and act as mechanotransducers, synthesizing collagen for repair and maintenance in response to mechanical loading [23].

Collagen fibers, in both ligaments and tendons, are embedded in ground substance, a hydrated gel-like matrix that is composed of water, proteoglycans, and other proteins [24]. In addition to collagen fibers, elastin is also embedded in the ground substance. Elastin is a rubber-like protein, which helps the tissue to stretch and recoil. Elastin comprises 10-15% of ligament dry weight but only 1-3% of tendon dry weight [25]. Water is the principal component of the ground substance and accounts for 55-60% of ligament's and tendon's total weight [21]. Proteoglycans compose approximately 3% of ligament's and tendon's dry weight and consist of a core protein with one or more covalently bonded glygosaminoglycan (GAG) chains [25]. Proteoglycans help hydrate the tissue, bind cells in the extracellular matrix, and serve as connectors between neighboring collagen fibers [26].

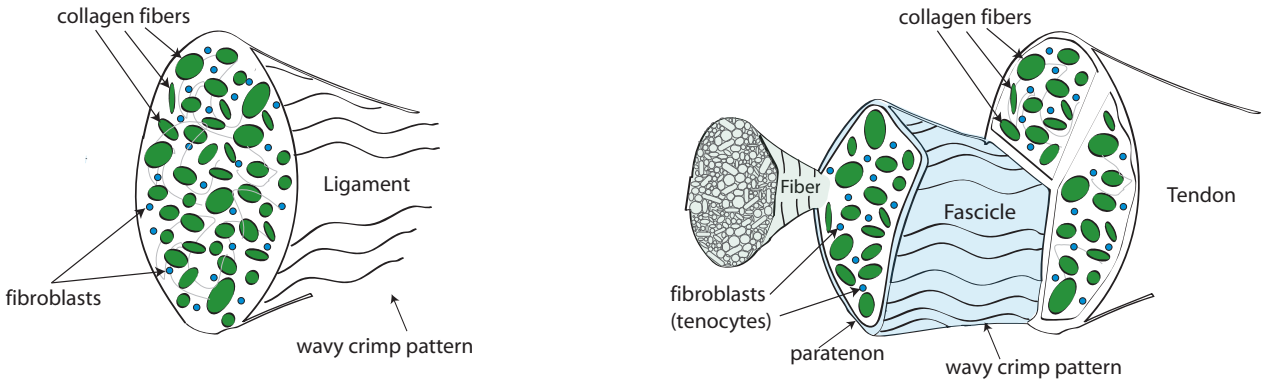

(a) (b)

Figure 2.1: Morphology of (a) ligaments and (b) tendons.

2.2 Mechanical Properties

2.2.a Quasi-Static properties

While there are variations in the properties of ligaments and tendons based on location in the body, when stretched along their long axis they exhibit similar behavior (Figure 2.2). The typical axial stress-strain behavior displays three distinct regions: toe region, linear region, and yield or failure region. In the toe region, the wavy collagen fibers that make up the tissue are gradually recruited to support load at different strains and become straight. The gradual straightening of the collagen fibers leads to an increase in the tangent modulus (slope of the axial stress-strain curve). The length of the toe region varies among different ligaments and tendons with the maximum axial strain at the end of the toe region ranging from 1% to 8% [27]. When the majority of collagen fibers become straight, the tangent modulus takes on a constant value since the axial stress-strain curve is approximately linear. The slope of this fairly linear portion of the stress-strain curve is generally the value reported as the elastic modulus for ligaments or tendons. As the collagen fibers begin to break, a reduction in modulus is observed. This change in modulus marks the beginning of the yield or failure region. In this region substantial damage to the ligament or tendon takes place.

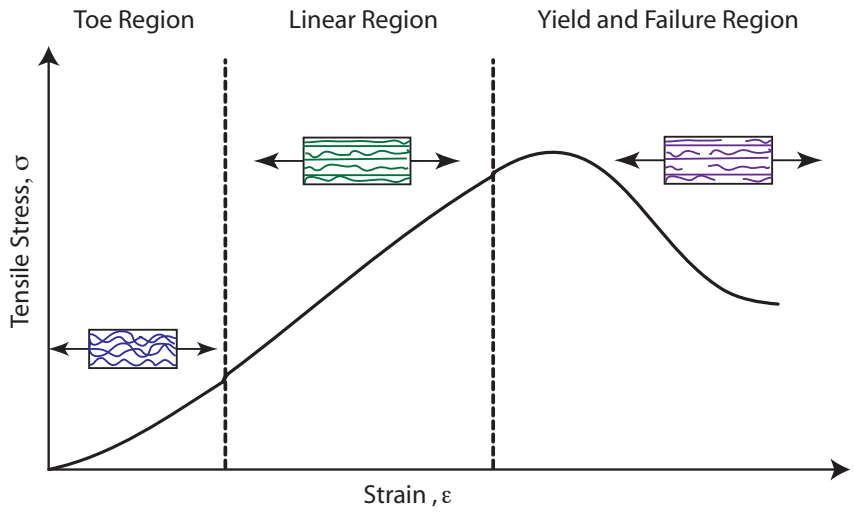

Figure 2.2: General axial stress-strain behavior of ligaments and tendons and structural changes of the collagen fibers.

2.2.b Viscoelastic properties

Ligaments and tendons are viscoelastic solids that exhibit time- and history-dependent properties. When they are held at a constant displacement, the stress decays overtime and this behavior is known as *stress relaxation* (Figure 2.3 (a)). When a constant load is applied the strain increases over time and the tissue *creeps* (Figure 2.3 (b)). When cyclically loaded in uniaxial tension at a constant strain or load rate, the unloading axial stress-strain curve does not follow the loading curve (Figure 2.3 (c)). As the number of cycles increase the loading and unloading axial stress-strain curves generally shift to the right until a steady repeatable behavior is achieved. This behavior is known as *hysteresis*. Ligaments and tendons also exhibit *strain rate dependency* (Figure 2.3 (d)). However, the effects of strain rate on the mechanical properties for samples tested in uniaxial tension are influential only over large changes in strain rate, such as, for example, 0.01/s to 1/s [24].

The viscoelastic behavior of soft tissues is physiologically relevant. Several investigators have reported that ligaments and tendons creep and relax at physiologic stresses and strains, respectively [28, 29, 30, 31]. For example, during static stretching a ligament or tendon is held at a fixed displacement over time and, as the stretch is held, the tissue relaxes. Since the primary aim of this dissertation is to investigate the stress relaxation behavior of ligaments and tendons, further review of the viscoelastic behavior of ligaments and tendons will focus only on the relaxation behavior. The next two subsections discuss experiments designed to quantify the general stress relaxation response of ligaments and tendons and experiments

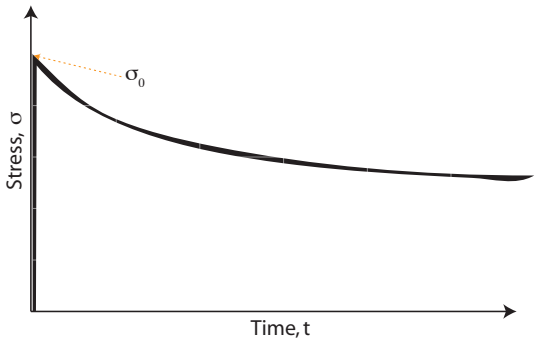

(a) Stress Relaxation

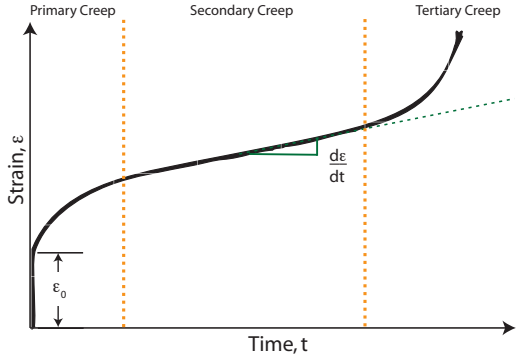

(b) Creep

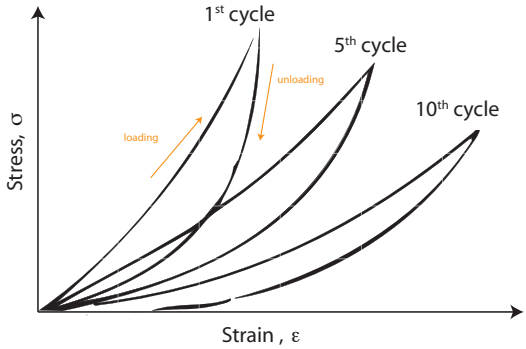

(c) Hysteresis

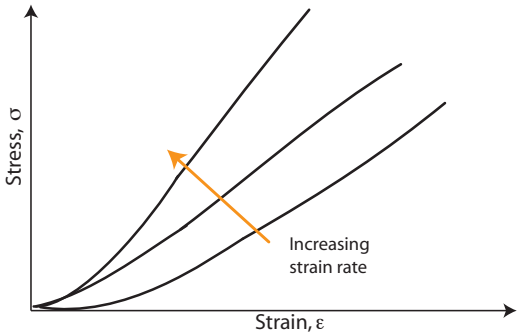

(d) Strain Rate Effects

Figure 2.3: Typical viscoelastic phenomena in ligaments and tendons

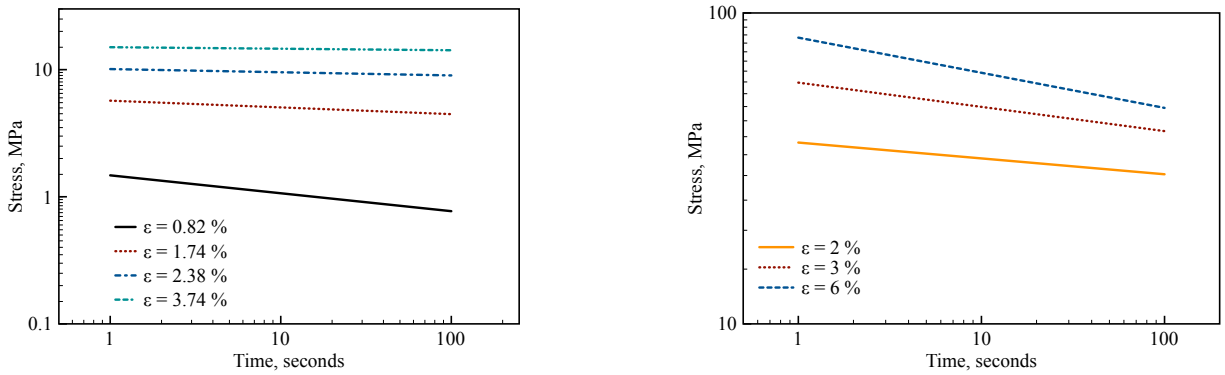

Figure 2.4: The stress relaxation behavior of (a) rat medial collateral ligaments [32] and (b) porcine digital flexor tendons [34] at different levels of axial strain, ε, generated from fit equations reported in each of the cited articles to describe the experimental data. Note that a log-log scale is used here. The changes in relaxation rate are graphically represented by changes in the slope.

designed to gain insight into how the structural hierarchy of ligaments and tendons influences the viscoelastic response of the tissue.

Stress Relaxation

To determine if the rate of stress relaxation depends on strain level, Provenzano et al. [32], Hingorani et al. [33], and Duenwald et al. [34] performed stress relaxation tests at multiple strain levels on rat and rabbit medial collateral ligaments (MCLs) and porcine digital flexor tendons, respectively. In the studies on MCLs as the strain level increased the rate of relaxation decreased (Figure 2.4 (a)). Conversely, in the study by Duenwald et al. [34] on digital flexor tendons as the strain level increased the rate of relaxation increased (Figure 2.4 (b)). This indicates that ligaments and tendons not only exhibit elastic non-linearities, as previously described in Section 2.2.a, but a nonlinear stress relaxation response as well.

In an effort to determine the contribution collagen fibers to the stress relaxation response Bonifasi-Lista et al. [35] conducted incremental stress relaxation tests on specimens excised from human MCLs in the in the longitudinal and transverse directions. The authors demonstrated that for specimens cut transverse to the fiber direction the rate of relaxation was largely unaffected by strain level. In the samples tested in the longitudinal direction, the rate of relaxation increased as the strain level increased. The results of the study suggests that the nonlinear stress relaxation response in the longitudinal direction is due to the collagen fibers.

van Dommelen et al. [31] examined how the strain-history during an incremental stress relaxation test influences the viscoelastic response of human MCLs. When stress relaxation tests were performed by applying consecutive strains in decreasing order (8%, 6.4%, 4.8%, and 3.2%) the maximum stresses were roughly 3 times greater than when the sequence was reversed (3.2%, 4.8%, 6.4%, and 8%). The authors however did not discuss if the rate of relaxation was affected by changing the sequence of incremental strains applied during testing. Consequently when examining the influence of strain level on the stress relaxation behavior of ligaments and tendons, performing only one stress relaxation test per specimen is preferred over incremental stress relaxation tests.

Structural Changes during Viscoelastic Phenomena

Several investigators have designed experiments to gain insight into the structural response of ligaments and tendons during creep and relaxation. The resulting experiments produced several theories on the origin of viscoelasticity in ligaments and tendons such as the inherent viscoelasticity of collagen fibers [36, 37, 38, 39], the inherent viscoelasticity of the extracellular matrix [38, 40, 41], and the interaction of collagen fibers with proteoglycans [42, 43]. No consensus has been reached.

Small angle x-ray diffraction experiments have been used to measure changes in the D-period (67 nm repeat) of collagen fibrils during mechanical testing. The observed changes in the D-period are representative of the strain experienced by a collagen fibril. Gupta et al. [38] have reported that the collagen fibrils in rat tail tendon fascicles relax when the fascicle is held at a fixed displacement suggesting that collagen may be intrinsically viscoelastic. This conclusion is supported by the results of two studies by Thornton et al. [36, 44] who used crimp analysis to show that fiber recruitment occurs in ligaments during creep. For the rabbit MCLs tested at 4.1 MPa the percentage of straight fibers increased on average from 9% to 22% during a 20-minute creep test. From the changes in fiber crimp the investigators deduced that the ligament acts to minimize creep by recruiting more fibers, thereby thereby distributing the creep load to more fibers and lessening the creep load on each collagen fiber.

Several authors have attributed the stress relaxation behavior of ligaments and tendons to matrix viscoelasticity and matrix fiber interactions. Screen [41] and Gupta et al. [38] examined the stress relaxation response of rat tail tendon fascicles by measuring the relaxation response of individual collagen fibers and the amount of fiber sliding that occurs during a macro-scale stress relaxation test using tenocytes as markers. Both authors concluded that fiber sliding is the dominant structural mechanism during stress relaxation at strains between 2-6%, speculating that during stress relaxation load is dissipated by fiber sliding and increasing shear in the matrix [38, 41]. The findings of Thornton and colleagues support these conclusions. When crimp analysis was used while performing stress relaxation exper-

iments, no significant difference was detected between the percentage of straight fibers pre- and post- relaxation [36, 44]. The absence of changes in fiber recruitment during relaxation implies that the matrix components or the interaction of the matrix and fibers are largely responsible for the dissipation of load.

Since the proteoglycans decorin and biglycan form bridges between neighboring collagen fibers, several authors have undertaken experiments to quantify the contribution of these proteoglycans to the mechanical behavior of ligaments and tendons. Uniaxial tensile tests to failure were performed on rat tail tendon fascicles [42] and human MCLs [45], which had the GAGs that form interfibrillar proteoglycans decorin and biglycan removed and control samples. Less than a 5% change was observed in the failure loads between the control group and the group with the GAGs removed. In addition, Lujan et al. [43] compared the stress relaxation behavior of human MCLs that had the same GAGs removed and controls. The authors were able to show with 95% confidence that the removal of GAGs had less than a 5% effect on the relaxation behavior. From these results, the three groups of investigators conclude that the interfibrillar proteoglycans decorin and biglycan have a limited influence on stress relaxation and uniaxial tensile behavior of ligaments and tendons.

2.3 Viscoelastic Constitutive Models

Constitutive models are mathematical models which describe the mechanical properties of a material. The section is further subdivided into the two common approaches for developing constitutive models: phenomenological and structural. In structural models, a mechanical response for each of the tissues' components is assumed and then a method is developed to combined the response of each component and determine the gross mechanical response of the tissue. In phenomenological models, empirical observations about the tissue's mechanical response guide the development of a constitutive relation that is consistent with the theories of classical mechanics. The reviewed models are by no means exhaustive but do lay the foundation for the models developed in the subsequent chapters.

2.3.a Phenomenological models

Three phenomenological models used to describe the stress relaxation behavior of ligaments and tendons are reviewed: the quasi-linear viscoelastic (QLV) model [24, 46, 47], nonlinear superposition model [33, 48, 49], and Schapery's theory [49, 50]. The models presented are all one-dimensional (generalizable to three-dimensions) and use infinitesimal strain theory.

Quasi-Linear Viscoelasticity

The quasi-linear viscoelastic model (QLV) popularized by Fung [24] has been widely adopted to describe the viscoelastic response soft tissues [46, 51, 52, 53]. For sample in a uniform state of uniaxial stress and strain, the QLV model for stress relaxation is the following:

$$\sigma(\epsilon, t) = \int_0^t G(t-\tau)\frac{d\sigma^e(\epsilon)}{d\epsilon}\frac{d\epsilon}{d\tau}d\tau \tag{2.1}$$

where $\sigma(\epsilon, t)$ is the axial stress (axial force divided by the undeformed cross-sectional area), ϵ is the infinitesimal axial strain, t is the time, $G(t-\tau)$ is the reduced relaxation function and $\sigma^e = \sigma^e(\epsilon)$ is a function that describes the instantaneous elastic response. In Eq. (2.1), $G(t)$ defines the time dependent relaxation behavior and is independent of the applied axial strain, ϵ, requiring the relaxation response at every strain level to be the same when normalized by the initial axial stress at $t = 0$. Note that the nonlinear axial stress-strain response of soft tissues is captured by appropriate selection of the function $\sigma^e(\epsilon)$. If the function $\sigma^e(\epsilon)$ is assumed to be linear, the Boltzman superposition integral from linear viscoelastic theory is recovered.

Although several investigators have used the QLV theory to describe the stress relaxation behavior of ligaments and tendons [46, 47, 51, 53, 54, 55], this theory cannot capture the coupled strain and time dependence that has been observed experimentally [32, 33, 56]. To this end, the applicability of other nonlinear viscoelastic models such as nonlinear superposition and Schapery's theory have been evaluated [49].

Nonlinear Superposition

Nonlinear superposition alters the superposition requirement from linear viscoelasticity, so that when a step change in the axial strain is applied from ϵ_1 to ϵ_2 the change in axial stress is the sum the recovery response from the removal of ϵ_1 and the relaxation response from applying the axial strain, ϵ_2 (See Figure 2.5). In addition, it allows the relaxation function, $R(\epsilon, t)$, to depend on strain level making it an appropriate choice to describe the stress relaxation behavior ligaments and tendons. The single integral form of the nonlinear superposition model for a sample under uniform state of uniaxial stress and strain is

$$\sigma(\epsilon, t) = \int_{-\infty}^t R\left(\epsilon(\tau), t-\tau\right)\frac{d\epsilon}{d\tau}d\tau\,. \tag{2.2}$$

A common choice for the relaxation function, $R(\epsilon(\tau), t-\tau)$, is the power law form where $R(\epsilon, t) = A(\epsilon)t^{B(\epsilon)}$. The function $A(\epsilon)$ defines the uniaxial stress-strain behavior while $B(\epsilon)$ describes rate of stress relaxation. To reproduce the nonlinear behavior of ligaments

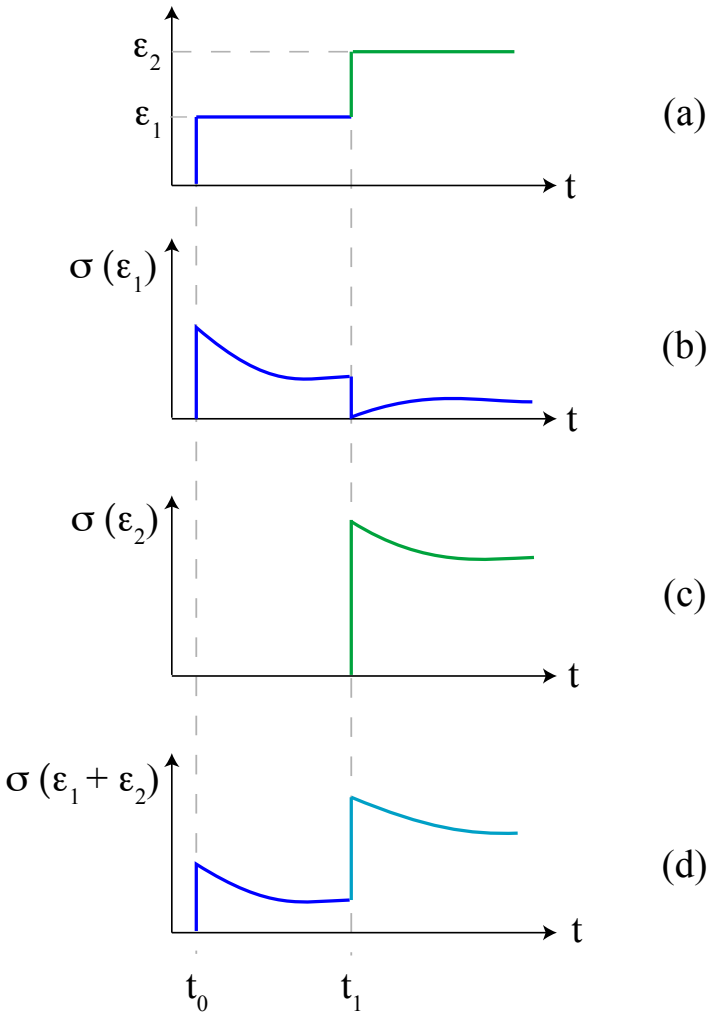

Figure 2.5: Time-dependent response to a two-step strain input. (a) Applied strains ε_1 at t_0 and ε_2 at t_1. (b) Resulting stress response as a function of time due to the application and removal of ε_1. The stress relaxation relaxation response for ε_1 acts from t_0 to t_1 and the recovery response from the removal of ε_1 acts from t_1 to t. (c) Resulting stress response as a function of time due to the application of a step strain ε_2 at t_1. (d) Stress relaxation response for the strain history presented in (a) according to modified superposition principle.

and tendons the functions $A(\epsilon)$ and $B(\epsilon)$ must be determined. If the relaxation function, $R(\epsilon(\tau), t-\tau)$, is taken to be a separable function of time and strain, $R(\epsilon, t) = G(t)\sigma^e(\epsilon)$, the QLV model is recovered.

The ability of the single integral form of the nonlinear superposition model to capture the stress relaxation and recovery behavior of porcine digital flexor tendons was evaluated by Duenwald and colleagues [34, 57]. Experimental studies found that recovery proceeded at a much slower rate than relaxation and the single integral form of the nonlinear superposition model was unable to capture these differing rates of relaxation and recovery. As a result, the model predictions significantly overestimated the stresses during recovery.

Schapery's Theory

Schapery's theory was derived using the principles of thermodynamics where axial strain is considered an internal variable. According to Schapery's theory, for a sample under a uniform uniaxial state of stress and strain, the stress response for an arbitrary strain history can be calculated from:

$$\sigma(\epsilon, t) = h_e(\epsilon)E_\infty + h_1(\epsilon)\int_0^t \Delta E(\rho(t) - \rho'(\tau))\frac{dh_2(\epsilon)}{d\tau}d\tau \tag{2.3}$$

where ρ and ρ' are reduced time parameters defined below,

$$\rho(t) = \int_0^t \frac{dt'}{a_e[\epsilon(t')]} \qquad \rho'(\tau) = \int_0^\tau \frac{dt'}{a_e[\epsilon(t')]}\,. \tag{2.4}$$

The parameter $E(t) = \frac{\sigma(t)}{\epsilon}$ is the stress relaxation modulus, E_∞ is the stress relaxation modulus as time approaches infinity and $\Delta E = E(t) - E_\infty$ is the transient component of the stress relaxation modulus. The functions $h_e(\epsilon)$, $h_1(\epsilon)$, $h_2(\epsilon)$ and $a_e(\epsilon)$ describe the strain dependent viscoelastic properties. When all of the functions, $h_e(\epsilon)$, $h_1(\epsilon)$, $h_2(\epsilon)$ and $a_e(\epsilon)$, are set to one, linear viscoelastic theory is recovered. Commonly, $h_1(\epsilon)$ and $a_e(\epsilon)$ are set to one and the transient modulus, ΔE, is modeled with a power law relationship where $\Delta E = C\rho^n$. For this case two parameters C and n and two functions, $h_e(\epsilon)$ and $h_2(\epsilon)$ must be determined to describe the nonlinear relaxation behavior exhibited by ligaments and tendons.

Duenwald et al. [57] subjected porcine digital flexor tendons and MCLs to three-step incremental stress relaxation tests. The sample was held at a strain, ε, for 100s, and then was allowed to recover at a strain of 1% for 100 seconds. After which a second 100 s stress relaxation test was performed at the initial strain, ε. To assess the predictive capabilities of the QLV model, the nonlinear superposition model, and Schapery's theory, the stress response during recovery and the second stress relaxation test were predicted using parameters determined by fitting data from the first stress relaxation test. Although QLV, nonlinear

superposition, and Schapery's theory were able to *fit* the experimental data from the first stress relaxation test well, only Schapery's theory accurately *predicted* the recovery response and second relaxation test.

2.3.b Structural models

Structural models are constitutive equations developed in terms of the tissue's microstructure. The formulation of structural models offers several advantages such as providing parameters in the model which can be compared with the mechanical properties of the individual tissue components. In the formulation of structural models an assumption must be made about the origin of viscoelasticity in the tissues. In the majority of models collagen fibers are considered the source of the tissue's viscoelastic behavior [36, 58, 59].

Lanir [58] developed a model for tendon viscoelastic behavior where elastin fibers are treated as linear elastic and the collagen fibers as linear viscoelastic. He then used a probability density function to account for the gradual recruitment of the collagen fibers. The model predicted different rates of relaxation at different strain levels but was not compared with experimental data.

Einat and Lanir [59] developed a similar model that included only the contribution of collagen fibers. Each collagen fiber was modeled as quasilinear viscoelastic. The gradual recruitment of the collagen fibers was accounted for using a probability density function. The model fit experimental relaxation data for sheep digital extensor tendons at varying strain levels well. The authors speculated that their model would be able to predict recovery phenomena better than QLV. However the recovery predictions were not compared with experimental data.

Thornton el al. [56] reported that creep and relaxation proceed at different rates. Further they discovered that the creep response could not be accurately predicted from stress relaxation data using QLV theory. However, ligament creep could be predicted from stress relaxation when fiber recruitment was incorporated [36]. In their model, the waviness of collagen fibers in the ligament is assumed to vary linearly across the width of the ligament. Collagen fibers are considered linear viscoelastic and creep after they become straight. At each time increment, the number of straight fibers is calculated, so that newly recruited fibers can be added to the model and start to creep. The addition of fiber recruitment significantly improved the model results for predicting the creep behavior from stress relaxation for rabbit MCLs.

The model by Sopakayang and De Vita [60] also examined the interrelation of stress relaxation and creep. In contrast to the other models discussed, the matrix (ground substance) is taken as the source of the tissue's viscoelastic response. In their model, the matrix is

modeled as linear viscoelastic. The collagen fibers are gradually recruited and when a collagen fiber becomes straight it behaves as a linear spring. The model captured the creep and relaxation response of the rabbit MCLs well. However when the model was used to predict creep behavior from relaxation data, the resulting predictions were only able to capture the creep behavior qualitatively. The creep strains were underestimated and the authors speculated that to improve the model it would be necessary to include additional components that account for the irreversible damage that occurs during creep.

3

A Nonlinear Constitutive Model for the Stress Relaxation Behavior of Collagen Fiber Bundles

This chapter was originally published as a journal article in the Annals of Biomedical Engineering [61]. It is available at http://dx.doi.org/10.1007/s10439-012-0596-2 .

3.1 Introduction

Ligaments and tendons are dense fibrous soft connective tissues: ligaments connect bone to bone and support internal organs while tendons connect muscle and bone. They are primarily composed of collagen and elastin fibers embedded in a ground substance of water, proteoglycans, and glycoproteins, all of which are produced and organized by the resident cells. Collagen is the primary load bearing component and the most abundant protein constituting 65 to 80% of the tissues' dry weight. It has a well-known hierarchical organization: collagen molecules are packed together to form collagen fibrils, collagen fibrils aggregate to form collagen fibers, and collagen fibers are arranged in distinct, parallel, wavy bundles known as *fascicles* [62].

As many collagenous tissues, ligaments and tendons exhibit long-term viscoelastic behavior: they relax when held at a constant displacement and creep when subjected to a constant load. The origin of their long-term viscoelasticity is still unknown but has been recently attributed to collagen [63]. In order to study the intrinsic viscoelastic properties of collagen, fascicles found in rat tail tendons are often tested. This is due their high content of collagen: 90 to 95% of the dry weight of rat tail tendon fascicles is comprised of collagen [64]. In an early study by Rigby et al. [65], for example, fascicles isolated from rat tail tendons were used to determine the effect of temperature on stress relaxation. More recently, rat tail tendons have been mechanically tested to understand the role of proteoglycans [54] and collagen

fiber sliding [38, 41] in stress relaxation. However, none of these investigations focused on characterizing the strain dependent stress relaxation response of these fascicles.

Investigating the strain dependent stress relaxation of ligaments and tendons is essential for designing replacement grafts with mechanical properties similar to native tissues and establishing surgical reconstruction methods and post-operative rehabilitation protocols. For example, during reconstructive surgeries, ligaments, tendons, and their replacement grafts are often strained in an *ad-hoc* manner by the surgeons to achieve a desired tension. However, this tension decreases over time due to the viscoelasticity of the tissues depending on the applied strain. An excessive decrease in tension can have detrimental effects: it causes laxity in the tissues that predisposes one to the recurrence of injuries and leads to other musculoskeletal disorders such as osteoarthritis [13]. Thus, the dependence of stress relaxation on the applied strain in ligaments, tendons, and their replacement grafts must be accurately characterized to establish guidelines in surgical procedures and enhance their outcome.

The most popular viscoelastic model employed for soft collagenous tissues is the quasi-linear viscoelastic (QLV) model proposed by Fung [24]. The QLV model is attractive due to the ease of implementation: quasi-static tensile tests and stress relaxation tests at a single strain level are sufficient to compute its parameters. For a specimen under uniform uniaxial loading, the QLV model for stress relaxation is the following:

$$\sigma(\epsilon, t) = \int_0^t G(t-\tau)\frac{d\sigma^e(\epsilon)}{d\epsilon}\frac{d\epsilon}{d\tau}d\tau \tag{3.1}$$

where $\sigma(\epsilon, t)$ is the axial stress, ϵ is the infinitesimal axial strain, t is the time, $G(t-\tau)$ is the normalized relaxation function and $\sigma^e = \sigma^e(\epsilon)$ is a function describing the instantaneous elastic response. In the QLV model, the relaxation behavior is modeled as a separable function of time, $G(t)$, and strain, $\sigma^e(\epsilon)$. Yet, recent experimental evidence demonstrated that stress relaxation in ligaments and tendons is strain dependent and, hence, cannot be modeled using a separable relaxation function of time and strain [32, 33, 56, 57].

Nonlinear superposition and Schapery's theory have been proposed as alternatives to QLV theory in order to describe the strain dependent stress relaxation exhibited by ligaments and tendons [33, 34, 49, 57]. The proposed viscoelastic models are, however, one-dimensional and valid only when the tissues are subjected to small strains. Finite strains experienced by ligaments and tendons have been considered in a three-dimensional viscoelastic model proposed by Johnson et al. [66]. This model has been derived within Pipkin and Rogers's nonlinear integral representation [14] but has then been tested by assuming that the tensorial relaxation function is a separable function of time and strain. This assumption leads to a finite strain form of the QLV model thus contradicting current experimental findings. Furthermore, in the model proposed by Johnson et al. [66] ligaments and tendons are erroneously assumed to be isotropic. While the above cited models capture the long-term viscoelasticity of lig-

aments and tendons, a robust three-dimensional constitutive models that accounts for the strain dependent stress relaxation behavior experienced by these tissues must be developed. As a first step, the contribution of collagen fibers to the stress relaxation behavior needs to be examined.

In this chapter, a nonlinear viscoelastic constitutive model that describes the stress relaxation behavior of collagen fiber bundles is presented. The model is derived within the nonlinear integral series representation developed by Pipkin and Rogers [14] and recently proposed for anisotropic materials by Rajagopal and Wineman [15]. In order to account for the collagen's nonlinearities and orientation in the tissue, the proposed tensorial relaxation function is a non-separable function of the strain invariants and time. Tensile axial stress-stretch data and stress relaxation data collected at multiple axial stretches from rat tail tendon fascicles are used to compute the model parameters. Moreover, a comparison of the proposed model with the predictions of the QLV model is also presented.

3.2 Theoretical Formulation

An incompressible nonlinear viscoelastic constitutive model is proposed to describe the stress relaxation response of collagen fiber bundles. The model is formulated within the nonlinear viscoelastic framework set forth by Pipkin and Rogers [14] by considering recent theoretical developments by Rajagopal and Wineman [15] for anisotropic materials. Most importantly, the model can capture the dependence of stress relaxation on strain, which has been experimentally observed in ligaments and tendons and attributed to the response of collagen fibers [32, 33, 34, 57].

3.2.a Constitutive model

In order to describe the nonlinear viscoelastic behavior of collagen fiber bundles, the integral series representation proposed by Pipkin and Rogers [14] is considered. As previously done by other investigators [15, 67, 66], only the first term of the integral series, which is a single integral with a nonlinear integrand, is used. For small strains this single integral representation is equivalent to the single integral form of the nonlinear superposition model (Section 2.3.a) [48, 49, 68].

The first Piola-Kirchhoff stress tensor, $\mathbf{P}(t)$, at any time t has the form [15]:

$$\mathbf{P}(t) = -p(t)\mathbf{F}^{-\mathrm{T}}(t) + \mathbf{F}(t)\left(\mathbf{R}[\mathbf{C}(t), 0] + \int_0^t \frac{\partial \mathbf{R}[\mathbf{C}(\tau), t-\tau]}{\partial(t-\tau)} d\tau\right) \tag{3.2}$$

where $\mathbf{F}(t)$ is the deformation gradient tensor, $\mathbf{C}(t) = \mathbf{F}(t)^{\mathrm{T}}\,\mathbf{F}(t)$ is the right Cauchy-Green deformation tensor, $\mathbf{R}[\mathbf{C}(\tau), t-\tau]$ is the tensorial relaxation function, and p is the Lagrange multiplier that accounts for incompressibility. In Eq. (3.2) no deformation is assumed to occur prior to time $t = 0$ and the term $\mathbf{F}(t)\mathbf{R}[\mathbf{C}(t), 0]$ represents the instantaneous elastic contribution to the total stress at time t.

The use of the right Cauchy-Green deformation tensor, $\mathbf{C}(t)$, as the strain measure in the tensorial relaxation function, $\mathbf{R}[\mathbf{C}(\tau), t-\tau]$, guarantees that the principle of material frame indifference is satisfied [69]. In order to meet fading memory requirements, the tensorial relaxation function must be a monotonically decreasing function of time: the partial derivative of $\mathbf{R}[\mathbf{C}(\tau), t-\tau]$ with respect to $t-\tau$ must be always negative. Assuming that the stress-free reference configuration was occupied at $t = 0$, in the absence of deformation, the tensorial relaxation function is identically zero. Finally, in the absence of explicit time dependence in the tensorial relaxation function, Eq. (3.2) yields the general nonlinear elastic constitutive equation with $\mathbf{R}[\mathbf{C}(\tau)] = 2\frac{\partial W}{\partial \mathbf{C}}$ where W is the so-called strain energy density function.

A collagen fiber bundle is assumed to be transversely isotropic and incompressible so that the tensorial relaxation function can be defined in terms of a scalar potential density function, $\tilde{W}$, as done by Rajagopal and Wineman [15]:

$$\mathbf{R}[\mathbf{C}(\tau), t-\tau] = 2\frac{\partial \tilde{W}(I_1(\tau), I_2(\tau), I_4(\tau), I_5(\tau), t-\tau)}{\partial \mathbf{C}} \tag{3.3}$$

where $I_1(\tau)$, $I_2(\tau)$, $I_4(\tau)$, and $I_5(\tau)$ are the strain invariants defined as follows [69]

$$I_1(\tau) = \mathrm{tr}(\mathbf{C}(\tau))\,, \quad I_2(\tau) = \frac{1}{2}(I_1^2(\tau) - \mathrm{tr}(\mathbf{C}^2(\tau)) \\ I_4(\tau) = \mathbf{M}\cdot\mathbf{C}(\tau)\mathbf{M}\,, \quad I_5(\tau) = \mathbf{M}\cdot\mathbf{C}^2(\tau)\mathbf{M} \tag{3.4}$$

and $\mathbf{M}$ is a unit vector that defines the axis of transverse isotropy in the reference configuration. The scalar potential density function does not depend on $I_3(\tau) = \det\mathbf{C}(\tau)$ since the strain invariant is identically equal to 1 due to the incompressibility assumption.

The tensorial relaxation function $\mathbf{R}[\mathbf{C}, t-\tau]$ presented in Eq. (3.3) can be alternatively written as

$$\mathbf{R}[\mathbf{C}, t-\tau] = k_1\mathbf{1} + k_2\mathbf{C} + k_3\mathbf{M}\otimes\mathbf{M} + k_4\left[\mathbf{M}\otimes(\mathbf{C}\mathbf{M}) + (\mathbf{C}\mathbf{M})\otimes\mathbf{M}\right] \tag{3.5}$$

where k_1, k_2, k_3, and k_4 are functions of the strain invariants $I_1(\tau)$, $I_2(\tau)$, $I_4(\tau)$, $I_5(\tau)$ and $t-\tau$ defined as

$$k_1 = 2\left(\frac{\partial\tilde{W}}{\partial I_1} + I_1\frac{\partial\tilde{W}}{\partial I_2}\right), \quad k_2 = -2\frac{\partial\tilde{W}}{\partial I_2}\,, \quad k_3 = 2\frac{\partial\tilde{W}}{\partial I_4}\,, \quad k_4 = 2\frac{\partial\tilde{W}}{\partial I_5}\,. \tag{3.6}$$

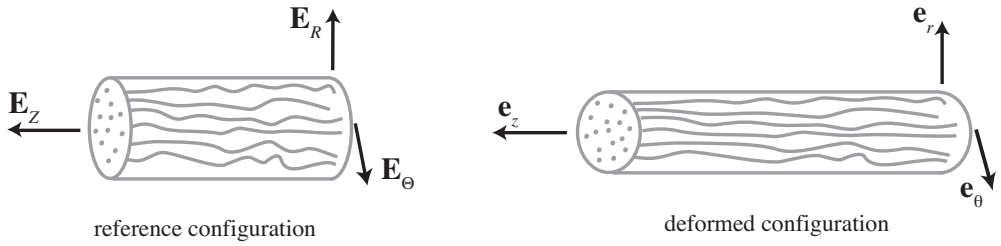

Figure 3.1: Schematic of the rat tail tendon fascicle's deformation. Note that the axis of transverse isotropy in the reference configuration, $\mathbf{M}$, is equal to $\mathbf{E}_Z$.

Note that, for ease of notation, the dependence on the strain invariants and time has been dropped in Eqs. (3.5)-(3.6).

In this study, the proposed framework is reduced to one dimension and the tensorial relaxation function $\mathbf{R}[\mathbf{C}, t-\tau]$ is assumed to depend only on the strain invariant I_4. Thus the functions k_1, k_2, and k_4 are identically zero thereby limiting the types of finite deformations that can be described [70, 71]. Specifically, the tensorial relaxation function is assumed to be

$$\begin{aligned}\mathbf{R}[I_4(\tau), t-\tau] &= k_3(I_4(\tau), t-\tau)\,\mathbf{M}\otimes\mathbf{M} \\ &= \left\{c_1\left[e^{c_2(I_4(\tau)-1)}-1\right]\right\}\left[(\,1-\alpha(I_4(\tau))\,)\,e^{-(t-\tau)\,\beta(I_4(\tau))}+\alpha(I_4(\tau))\right]\mathbf{M}\otimes\mathbf{M} \quad (3.7)\end{aligned}$$

where c_1 and c_2 are non-negative constants and $\alpha(I_4(\tau))$ and $\beta(I_4(\tau))$ are functions of the strain invariant $I_4(\tau)$. In Eq. (3.7), the function of $I_4(\tau)$ in the first curly brackets is used to describe the strain stiffening elastic behavior of collagen fibers [24, 72, 73]. Specifically, the parameters c_1 and c_2 describe the instantaneous elastic response. The function in the second square brackets is used to describe the normalized relaxation behavior [67]. The function $\alpha(I_4(\tau))$ describes the ratio of the equilibrium stress to the initial stress and is referred to the *elastic fraction* while the function $\beta(I_4(\tau))$ defines the *strain dependent relaxation rate*. A finite strain form of the QLV model for stress relaxation is recovered when α and β are constants (not functions of $I_4(\tau)$).

3.3 Determination of Material Parameters

3.3.a Uniaxial deformation

The proposed model is tested with experimental data collected by stretching rat tail tendon fascicles along their long axis. The fascicle is assumed to undergo an isochoric homogeneous

axisymmetric deformation schematically presented in Figure 3.1 and defined by

$$r = \lambda(t)^{-1/2} R\,, \quad \theta = \Theta\,, \quad z = \lambda(t)\, Z \tag{3.8}$$

where $(R,\, \Theta,\, Z)$ and $(r,\, \theta,\, z)$ represent the coordinates of a generic point in the reference and deformed configurations, respectively, and $\lambda = \lambda(t)$ is the axial stretch. The orthonormal bases $\{\mathbf{E}_R,\, \mathbf{E}_\Theta,\, \mathbf{E}_Z\}$ and $\{\mathbf{e}_r,\, \mathbf{e}_\theta,\, \mathbf{e}_z\}$ in the reference and current configurations, respectively, are defined such that $\mathbf{E}_Z$ and $\mathbf{e}_z$ are unit vectors parallel to the direction of loading. Moreover, the collagen fibers are assumed to be aligned along $\mathbf{E}_Z$ in the reference configuration so that $\mathbf{M} = \mathbf{E}_Z$ (Figure 3.1).

It follows that the deformation gradient tensor, $\mathbf{F}(t)$, and the right Cauchy-Green deformation tensor, $\mathbf{C}(t)$, are given by

$$\mathbf{F}(t) = \frac{1}{\sqrt{\lambda(t)}}\mathbf{e}_r \otimes \mathbf{E}_R + \frac{1}{\sqrt{\lambda(t)}}\mathbf{e}_\theta \otimes \mathbf{E}_\Theta + \lambda(t)\mathbf{e}_z \otimes \mathbf{E}_Z\,,$$
$$\mathbf{C}(t) = \frac{1}{\lambda(t)}\mathbf{E}_R \otimes \mathbf{E}_R + \frac{1}{\lambda(t)}\mathbf{E}_\Theta \otimes \mathbf{E}_\Theta + \lambda^2(t)\mathbf{E}_Z \otimes \mathbf{E}_Z\,. \tag{3.9}$$

The first Piola-Kirchhoff stress tensor that defines the instantaneous elastic stress can be computed by evaluating Eq. (3.2) at time $t = \tau$ with the tensorial relaxation function given by Eq. (3.7) and the tensor $\mathbf{F}$ and $\mathbf{C}$ given by Eq. (3.9). Assuming a traction-free boundary condition on the lateral surface of the tested fascicles leads to $p = 0$ in Eq. (3.2). Then the only non-zero component of the first Piola-Kirchhoff stress tensor has the form

$$\mathrm{P}_{zZ}(t) = \lambda(t) c_1 \left[e^{c_2 (\, \lambda^2(t) - 1\,)} - 1 \right]\,. \tag{3.10}$$

Stress relaxation can be modeled using Eqs. (3.2), (3.7) and (3.9) by assuming that $\lambda(t) = \lambda$ is constant. Then, the only non-zero component of the first Piola-Kirchhoff stress tensor that defines stress relaxation is

$$\mathrm{P}_{zZ}(t) = \lambda c_1 \left[e^{c_2\,(\lambda^2 - 1)} - 1 \right] \left[\big(\, 1 - \alpha(\lambda^2)\,\big)\, e^{-t\beta(\lambda^2)} + \alpha(\lambda^2) \right]\,. \tag{3.11}$$

In summary, for a bundle of parallel collagen fibers two parameters, c_1 and c_2, need to be determined to characterize the uniaxial instantaneous elastic behavior while the same parameters, c_1 and c_2, and two functions, $\alpha(\lambda^2)$ and $\beta(\lambda^2)$, need to be found to characterize the uniaxial stress relaxation behavior.

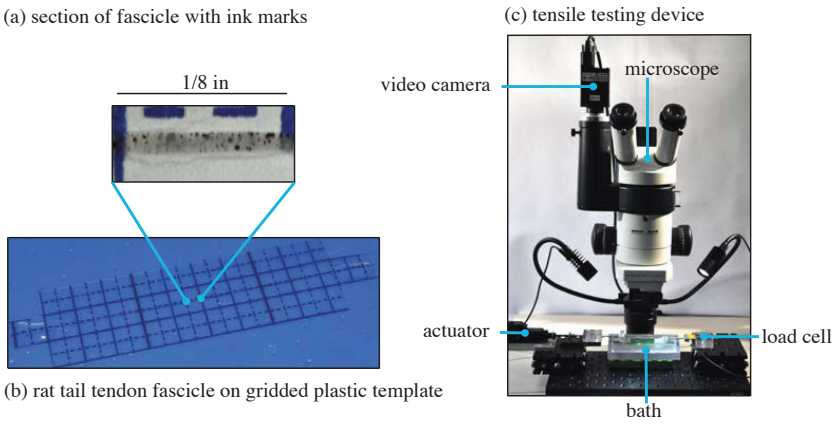

Figure 3.2: Preparation of rat tail tendon fascicle and custom designed micro-tensile testing device.

3.4 Experimental Methods

Twenty-six rat tail tendon fascicles were subjected to tensile tests followed by stress relaxation tests. Two male Sprague Dawley rats were used in this study: one rat (rat A) weighed 235 g and the other rat (rat B) weighed 236 g. The animals were acquired from a different study, which did not affect the musculoskeletal system or collagen development, in accordance with an approved Virginia Tech IACUC protocol. Immediately after sacrifice, the tails were isolated from the rats and their skin was removed using a wire stripper. Groups of fascicles were then teased out from the proximal end of the tails with fine tipped tweezers under a stereomicroscope (Stereoscope Stemi 2000C, Zeiss). The least amount of force necessary to free the fascicles was used to minimize their stretching. The fascicles were then separated, wrapped in paper towels soaked in phosphate buffered saline solution, and stored frozen ($-20°$C). Twelve to twenty-four hours before testing, the fascicles were placed in a refrigerator at $2°$C and before testing they were allowed to come to room temperature for one hour.

The fascicles were trimmed to a uniform length chosen to be 77 mm based on experimental results by Legerlotz et al. [27]. Images of each fascicle were collected using the stereomicroscope. The width of each fascicle was measured at six locations from the images using ImageJ (ImageJ v. 1.44, National Institutes of Health). The value of the width ranged from 0.153 to 0.496 mm. The cross-sectional area was calculated using the average of the six measured values of the width and assuming a circular cross-section. The computed values of the area varied from 0.019 to 0.194 mm^2. Black ink was then sprayed on the surface of the fascicles using an airbrush (Professional 150, Badger Airbrush Co.) in order to produce marks with suitable contrast for strain calculation (Figure 3.2(a)). The two ends of each fascicle were fixed to a piece of gridded plastic template using cyanoacrylate glue (Figure

3.2(b)) to ensure their straight alignment during mounting on a custom built micro-tensile testing device. The main components of the micro-tensile testing device used to perform the mechanical experiments are shown in Figure 3.2(c). A 8.9 N (2 lb) load cell (LSB 200, Futek) with a resolution of $\pm$ 0.002 N was used to measure the load and a micro-scale linear actuator (T-NA Series, Zaber Technologies) with a $\pm$ 8 μm accuracy was employed to stretch the specimens. Screw down grips and a bath for the testing device were custom made primarily of polycarbonate.

For each test, the two ends of the fascicle attached to the gridded plastic template, were secured to the grips. The plastic template, cured glue, and screw down clamps contributed to gripping the fascicle and prevented its slippage. The portion of the plastic template not secured to the grips was cut with a pair of scissors and removed. The fascicle was then immersed in the bath that was filled with phosphate buffered saline solution. It was preloaded to 0.01 N and then preconditioned at 6 mm/min to 0.4 mm for 5 cycles followed by a 5 minute recovery period. Preconditioning was performed to establish a consistent strain history for all samples [65]. The configuration assumed by the fascicle following recovery was taken as the reference configuration. The twenty-six fascicles were stretched at 6 mm/min to different displacement values corresponding to 0.75 mm ($n = 7$), 1.25 mm ($n = 7$), 1.75 mm ($n = 7$) or 2.25 mm ($n = 5$) and subsequently held for 10 minutes for stress relaxation testing.

The load and displacement data were simultaneously recorded at 20 Hz using LabVIEW software (LabVIEW 2009, National Instruments). The axial nominal stress, $\mathrm{P_{zZ}}$, was computed by dividing the current load by the initial cross-sectional area. A charge coupled device (CCD) camera (Stingray F-080B, Allied Vision) was used along with a stereomicroscope (Wild M3Z, Heerbrugg) to record images of the fascicle for the duration of the tests. A center region of the fascicle was selected for strain analysis and the displacement of the ink marks was measured using a digital image correlation method implemented in MATLAB (MATLAB v. 7.10, MathWorks)[74]. The right Cauchy-Green deformation tensor, $\mathbf{C}$, and, hence, the axial stretch λ were calculated from the measured displacements by assuming that the fascicle undergoes the deformation presented in Eq. (3.8). For comparison purposes, the Green-St. Venant strain tensor $\mathbf{E}$ related to $\mathbf{C}$ by $\mathbf{E} = \frac{1}{2}(\mathbf{C} - \mathbf{1})$ was also computed. Specifically, the component E_{ZZ} of the Green-St. Venant strain $\mathbf{E}$ related to the axial stretch λ by $\mathrm{E}_{ZZ} = \frac{1}{2}(\lambda^2 - 1)$ is reported.

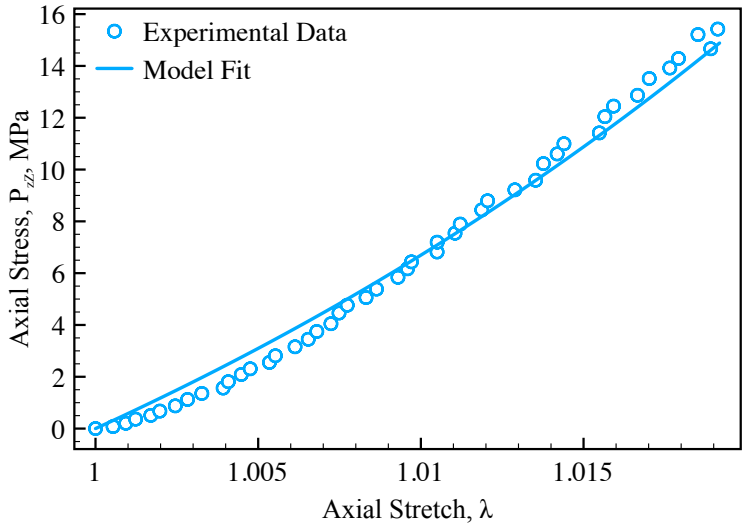

Figure 3.3: Typical tensile axial stress-stretch curve collected from one rat tail tendon fascicle and model fit to data with $c_1 = 20.27$ MPa and $c_2 = 14.15$ ($R^2 = 0.99$).

3.5 Results

3.5.a Elastic response

Axial stress-stretch data were obtained from twenty-six rat tail tendon fascicles by performing tensile tests as previously described. These data were collected by stretching the fascicles along their long axis up to the four displacement levels (0.75, 1.25, 1.75, or 2.25 mm) that were then held constant during the stress relaxation experiments. These displacements were found to correspond to axial stretch values lower than 1.0566 ($E_{ZZ} = 5.82\%$) and the experimental data obtained fell within the toe-region or linear region of the stress-strain curves [65, 27]. A representative axial stress-stretch curve for a fascicle, which was subsequently tested for stress relaxation at an axial stretch of 1.0199 ($E_{ZZ} = 2.00\%$), is shown in Figure 3.3. It can be clearly seen that the fascicle exhibits the typical nonlinear elastic strain-stiffening behavior of soft collagenous tissues.

The axial stress-stretch data were used to compute the model parameters c_1 and c_2 that define the instantaneous elastic response of the fascicle. Toward this end, Eq. (3.10) was fit to these data by employing a nonlinear least squares algorithm implemented in MATLAB and imposing that the model parameters were non-negative. The least squares function and its gradient were supplied to a built-in minimization function called *fmincon* and the trust-region reflective algorithm was utilized [75].

The proposed model for the instantaneous elastic response of the fascicle could fit the axial

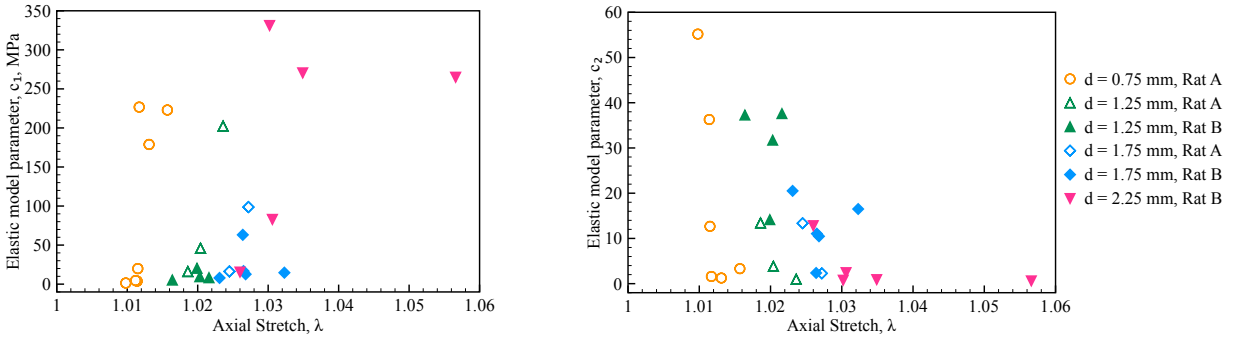

(a) (b)

Figure 3.4: The elastic parameters (a) c_1 and (b) c_2 as a function of the axial stretch, λ, determined by the displacement, d, kept constant during stress relaxation experiments.

stress-stretch data well with $0.86 < R^2 < 0.99$. In Figure 3.3, the model fit to the representative axial stress-stretch data is presented. For this data set, the parameters were found to be $c_1 = 20.27$ MPa and $c_2 = 14.15$ ($R^2 = 0.99$). The values of the parameters c_1 and c_2 obtained by fitting the axial stress-stretch data collected from each rat tail tendon fascicle are plotted versus the maximum axial stretches in Figure 3.4. They are represented with the same symbol and color when they are computed by fitting data from fascicles stretched up to an equal displacement. Note that the maximum axial stretch is the axial stretch held constant during the subsequent stress relaxation experiment. The values of the parameter c_1 ranged from 1.424 MPa to 331 MPa and the values of the parameter c_2 varied between 0.77 and 69.27.

3.5.b Stress relaxation response

Stress relaxation data were collected by subjecting rat tail tendon fascicles to constant displacements ranging from 0.75 mm to 2.25 mm. Due to inter-specimen variability, an equal displacement applied to different fascicles was found to induce different axial stretches. The displacements used during stress relaxation experiments produced axial stretches in the fascicles that varied from 1.0098 ($E_{ZZ} = 0.98\%$) to 1.0566 ($E_{ZZ} = 5.82\%$). The stress relaxation data normalized by the initial stress value are presented in Figure 3.5 for five representative fascicles. From Figure 3.5, one can see that the shape of the stress relaxation curve changes with axial stretch (or strain). These results suggest that the QLV theory cannot be employed to describe the stress relaxation behavior of rat tail tendon fascicles. According to the QLV model, the normalized stress relaxation function, $G(t)$ in Eq. (3.1), is independent of strain and thus should be identical regardless of the strain level considered.

The stress relaxation data collected at different axial stretches were used to determine the

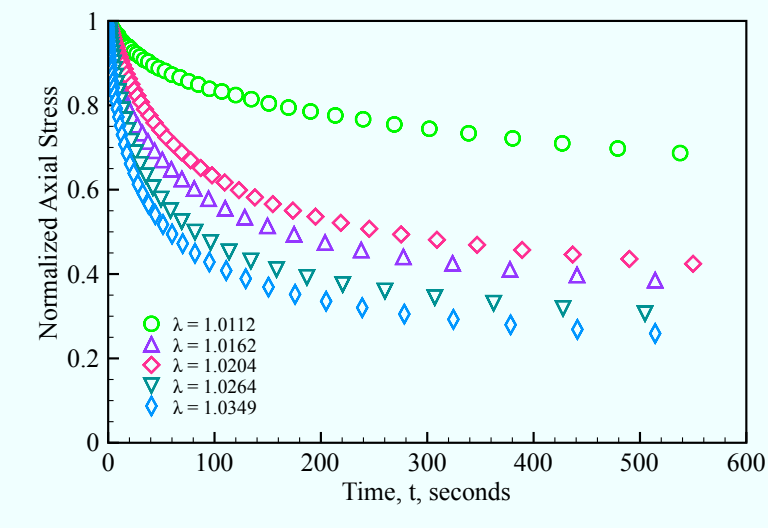

Figure 3.5: Normalized stress relaxation curves at axial stretches, λ, equal to 1.0112, 1.0162, 1.0204, 1.0264 and 1.0349 which correspond to axial strain, E_{ZZ}, equal to 1.13%, 1.65%, 2.06%, 2.67% and 3.55%, respectively. The axial stress, P_{zZ}, is normalized by the axial stress at $t = 0$, P_{zZ} (0).

values of $\alpha(I_4)$ and $\beta(I_4)$ in Eq. (3.11) with $I_4 = \lambda^2$. As described above, a nonlinear least squares algorithm was implemented in MATLAB with $\alpha(I_4)$ constrained to be between 0 and 1 and $\beta(I_4)$ constrained to be non-negative. Note that when curve fitting Eq. (3.11) to each set of stress relaxation data, the values of the parameters c_1 and c_2 were fixed to those previously computed by fitting the corresponding set of axial stress-stretch data.

The proposed model was able to capture the strain dependent stress relaxation behavior well ($0.80 < R^2 < 0.99$). In Figure 3.6 the value $\alpha(I_4)$ and $\beta(I_4)$ are plotted versus $I_4 = \lambda^2$. These values are represented with the same symbol and color when they are computed by fitting stress relaxation data obtained from fascicles stretched up to the same displacement. As I_4 increased, $\alpha(I_4)$ tended to decrease (Figure 3.6a) while $\beta(I_4)$ was found to increase (Figure 3.6b). However, as seen in Figure 3.6, there was significant variability in the values of $\alpha(I_4)$ and $\beta(I_4)$. A function of the form $\alpha(I_4) = c_3 e^{c_4(I_4-1)}$ was then fit to the $\alpha(I_4)$ versus I_4 data with $c_3 = 0.7318$ and $c_4 = -14.69$ ($R^2 = 0.68$) and a function of the form $\beta(I_4) = c_5(I_4 - 1)$ was fit to the $\beta(I_4)$ versus I_4 data with $c_5 = 0.2084$ ($R^2 = 0.30$). These curve fits were performed in an attempt to suggest the form of the functions that characterize the stress relaxation response of collagen fiber bundles.

Stress relaxation data sets at three additional axial stretches are shown on a log-log scale in Figure 3.7 along with model fits obtained with the proposed model and model predictions from the QLV. The QLV model used is given by Eq. (3.11) with $\alpha(I_4) = \alpha$ and $\beta(I_4) = \beta$ constant and independent of strain. Because the parameters α and β are independent of

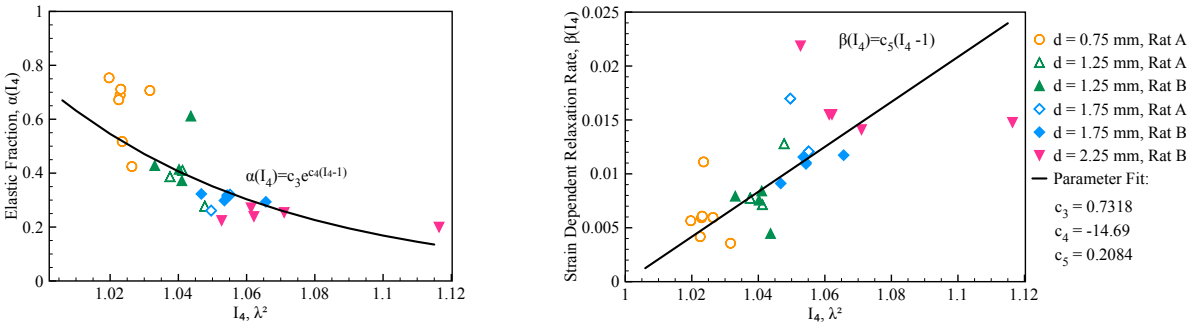

(a) (b)

Figure 3.6: Elastic fraction, $\alpha(I_4)$, (a) and strain dependent relaxation rate, $\beta(I_4)$, (b) as functions of the strain invariant $I_4 = \lambda^2$. The values of $\alpha(I_4)$ and $\beta(I_4)$ are computed by fitting Eq. (3.11) to stress relaxation data collected at different axial stretches that are determined by different displacements, d, as indicated in the legend. The curves obtained by plotting the values of $\alpha(I_4)$ and $\beta(I_4)$ versus I_4 are then fit to $\alpha(I_4) = c_3 e^{c_4(I_4-1)}$ where $c_3 = 0.7318$, $c_4 = -14.69$ ($R^2 = 0.68$) and $\beta(I_4) = c_5(I_4 - 1)$ where $c_5 = 0.2084$ ($R^2 = 0.30$), respectively (solid line).

strain, they were computed by fitting stress relaxation data collected at one axial stretch level, chosen to be 1.0098 ($E_{ZZ} = 0.98\%$). The values of these parameters were found to be $\alpha = 0.7537$ and $\beta = 5.649 \times 10^{-3} \frac{1}{s}$. For each stress relaxation curve, the parameters c_1 and c_2 in the QLV model were set equal to the values computed by fitting the corresponding axial stress-stretch data. As expected the QLV and proposed models coincide at the axial stretch used for the fitting. However, it can be observed that the QLV model can capture the stress relaxation response at the other two axial stretches only for the first 5-10 seconds of the tests.

3.6 Discussion

In this study, a novel constitutive law was formulated for the stress relaxation response of collagen fiber bundles. The model was derived within the nonlinear integral representation proposed by Pipkin and Rogers [14] and recently extended to anisotropic materials by Rajagopal and Wineman [15]. The tensorial relaxation function, which appears in this representation, was assumed to be a non-separable function of the strain invariants and time. In order to compute the model parameters, uniaxial tensile tests and uniaxial stress relaxation tests at four different displacement values on rat tail tendon fascicles were conducted. The experimental results confirmed previous findings on the nonlinear viscoelasticity of ligaments and tendons [33, 34, 49, 57]. They showed that the widely used QLV theory is inadequate

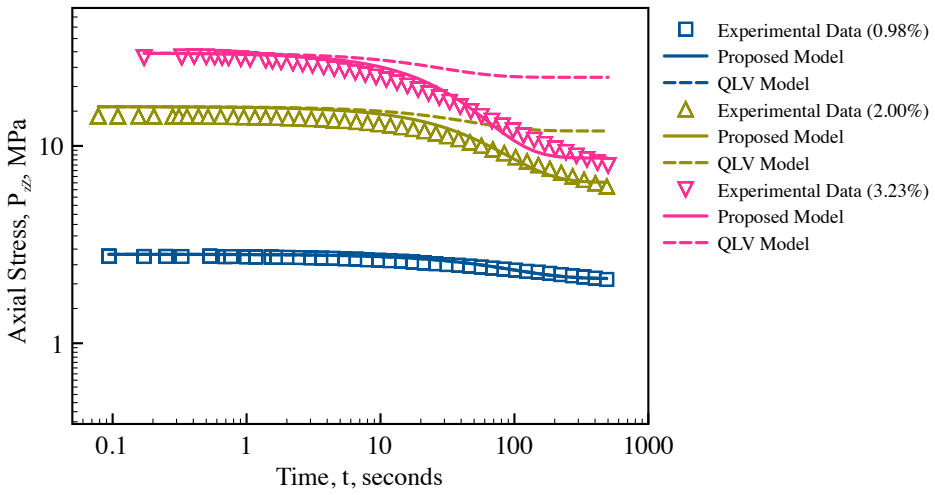

Figure 3.7: Experimental stress relaxation curves (symbols) for rat tail tendon fascicles at axial stretches λ =1.0098, 1.0199, and 1.0323 which correspond to axial strains E_{ZZ} =0.98%, 2.00% and 3.28%, respectively, proposed model fit to data (solid line), and comparison to QLV model (dashed line). The parameters in the QLV model are obtained by fitting data collected at E_{ZZ} =0.98% and predicts the same shape for the normalized stress relaxation curves regardless of the axial strain.

to describe the strain dependent stress relaxation behavior of soft collagenous tissues. The proposed model was then successfully fit to the experimental data by assuming that the fascicle undergoes an isochoric axisymmetric deformation. Unlike previous constitutive models, the proposed model accounts for finite strains and the strain dependent stress relaxation behavior that is typical of soft collagenous tissues.

The elastic behavior of rat tail tendon fascicles was found to be nonlinear as expected [27, 65] (Figure 3.3). However, the initial nonlinear region of the axial stress-strain curve, the so-called toe region, was observed within axial stretch values that correspond to strain values smaller than the 3 to 5% strain values reported by other authors [27, 65]. Shortening of the toe region may be due to differences in the experimental methods and protocols (e.g., preconditioning) and the longer length (77 mm) of the specimens used in this study. Indeed, in rat tail tendon fascicles the strain to failure decreases and the modulus increases as their length increases [27]. As a consequence, the extent of the toe region is also expected to decrease.

The axial stress-stretch data were used to find the parameters c_1 and c_2 that determine the instantaneous elastic response of fascicles. Because the extent of the toe and linear regions in these data varied the values of the parameters also varied (Figure 3.4). Some of the scatter in the data can be attributed due to the variability of the cross-sectional area of the tested fascicles [27, 76]. The length of the specimens used in this study was controlled and varied

less than 1% but their cross-section area ranged from 0.02 to 0.1 mm^2. One could note that the value of the parameter c_2 tended to decrease with the maximum axial stretch (Figure 3.4b) but no clear trend was found for the c_1 (Figure 3.4a).

The rat tail tendon fascicles displayed the strain dependent stress relaxation behavior attributed to collagen fibers in other soft collagenous tissues [32, 33, 34, 56, 57]. Overall as the axial stretch increased the amount of relaxed stress increased. However, due to the inherent variability of the specimens, this trend was not always observed. For example, in Figure 3.5 the specimen pulled to an axial stretch of 1.0180 ($E_{ZZ} = 1.82\%$) relaxed 65% of its initial stress while the specimen pulled to an axial stretch of 1.0204 ($E_{ZZ} = 2.06\%$) relaxed 59% of its initial stress. Similar results were reported by Screen et al. [41] when conducting incremental stress relaxation tests on rat tail tendon fascicles at strains less than 4%.

There are two major differences between the experimental protocol employed here and those employed in previous studies [32, 33, 38, 41]. First, direct stress relaxation tests, each conducted at a single axial stretch, were preferred over incremental stress relaxation tests. Direct stress relaxation tests likely provide more accurate information about the effect of strain on stress relaxation. The stress relaxation behavior studied by incremental stress relaxation tests may be affected by the history of incremental strains used during testing [31, 77]. Differences in the amount of stress relaxation measured from incremental and direct relaxation tests of rat tail tendon fascicles have been detected and quantified by Screen et al. [41]. Secondly, unlike previous experimental studies [32, 33, 38, 41], this study included preconditioning to the experimental protocol. Great care was taken in isolating the fascicles from the rat tail tendons and in handling and preparing the specimens for mechanical testing. However, the fascicles may have been stretched before mechanical testing. Thus, in an attempt to provide a more consistent strain history and reference state, the fascicles were preconditioned. Preconditioning has been reported to shorten or eliminate the toe region of the axial stress-strain curve [78] and alter the elastic modulus of spinal cord tissue [79] while its effect on the stress relaxation still needs to be investigated.

The QLV model is unable to capture the nonlinear viscoelastic behavior of collagen fiber bundles. In Figure 3.5, one can note that the normalized stress relaxation response depends on the axial stretch employed during testing. This behavior suggests that a separable relaxation function is not adequate to model stress relaxation in collagen fibers. Several investigators have shown that the stress relaxation behavior of other soft collagenous tissues cannot be modeled using a separable relaxation function [32, 33, 34, 56, 57]. In Figure 3.7, the QLV model is compared with the proposed model using the same methodology employed by Provenzano et al. [32]. However, we must note that in both cases, here and in the cited paper, the *predictions* of the QLV model are compared with *model fits*. Fitting the QLV model to stress relaxation data, each collected at different axial stretches, would provide a very good fit too. The purpose of the comparison in Figure 3.7 is to show that QLV model is unable to capture the stress relaxation behavior at multiple axial stretches using one set

of material parameters assumed to be independent of strain.

One limitation of this study was the inability to determine the functions $\alpha(I_4)$ and $\beta(I_4)$ that could fit well the data generated by the computed $\alpha(I_4)$ values versus I_4 and $\beta(I_4)$ values versus I_4 due to scatter in the experimental data (Figure 3.6). The elastic fraction, $\alpha(I_4)$, which represents the ratio of the equilibrium stress to the initial stress, was found to decrease with increasing axial stretch and was curve fit by an exponential function (Figure 3.6a). Other investigators have either not measured the elastic fraction [32, 33, 57] or have reported similar scatter in the data [38, 41]. The function $\beta(I_4)$, which represents the relaxation rate, was chosen to be a linear function of I_4 to best fit the computed $\beta(I_4)$ values versus I_4 (Figure 3.6b). This choice is consistent with the formulation by Roberts and Green [67] and the results of several experimental studies [32, 41, 57].

Future studies will be conducted to extend the proposed constitutive model to three-dimensions using multi-axial experimental data collected on collagenous tissues that undergo large strains such as the cardinal ligaments [20]. For these complex tissues, the definition of the tensorial relaxation function given in Eq. (3.7) will need to be modified so as to consider the contribution of other tissue components (e.g., elastin, ground substance, and proteoglycans). Finally, the tensorial relaxation function will be re-formulated to account for the structural changes that occur during stress relaxation at the fiber [56] and fibril [38] levels including damage. Indeed, the strain applied during stress relaxation can cause damage which needs to be addressed by future constitutive models. This can be accomplished using an approach similar to the ones outlined by one of the authors elsewhere [80, 81].

4

A Three-Dimensional Constitutive Model for the Stress Relaxation Response of Skeletal Ligaments

4.1 Introduction

Skeletal ligaments are soft connective tissues that connect bones to bones and stabilize the motion of joints. They are primarily composed of collagen fibers embedded in a ground substance of water, proteoglycans, and glycoproteins [62]. The collagen fibers constitute the primary load bearing components of these tissues.

Skeletal ligaments are viscoelastic materials exhibiting stress relaxation, creep, and hysteresis phenomena. Stress relaxation, which is the time-dependent decrease in stress under a constant stretch, is essential to the ligaments' proper function. Indeed, this viscoelastic phenomenon acts to attenuate the stress within the ligament, possibly protecting both the ligament and the surrounding structures from damage. Stress relaxation along the longitudinal axis of the ligaments has been thoroughly characterized [33, 34, 49, 57]. However, although the ligaments are primarily strained and stressed along this axis, the strain and stress distributions are three-dimensional and non-uniform due to their complex geometry and structure [82].

The importance of modeling the three-dimensional constitutive behavior of ligaments has been long recognized by the biomechanics community. In recent years, several investigators have put forward constitutive models to describe the three-dimensional elastic response of ligaments [40, 83, 84, 85] but only a few have attempted to capture the three-dimensional viscoelastic behavior [66, 73, 86]. These constitutive laws for stress relaxation have been formulated by assuming that the time-dependent and strain-dependent properties can be separated so that the normalized stress relaxation response is not dependent on strain. This assumption has been, however, questioned by experimental findings indicating that the normalized stress relaxation in the ligaments' longitudinal direction is strain-dependent

[32, 33, 35, 56].

Three-dimensional constitutive theories such as the nonlinear superposition [48], Schapery's theory [50], and the Pipkin-Rogers integral series [14] have been used to capture the strain-dependent normalized stress relaxation behavior of ligaments [33, 34, 49, 57, 61]. Most applications of these theories have been one-dimensional due to the lack of multi-axial experimental data. Ligaments have been mainly tested uni-axially along the collagen fibers' direction. To the authors' knowledge, the only experimental studies that characterize the elastic and viscoelastic properties of ligaments not only along the collagen fibers' direction but also along the direction transverse to the collagen fibers have been conducted by Weiss and his research group [35, 87]. The experimental results obtained by testing the ligaments in the direction transverse to the collagen fibers provided crucial information about the mechanical role of the group substance.

In this chapter, a three-dimensional constitutive law is presented to describe the stress relaxation behavior of skeletal ligaments. The constitutive model is formulated within the integral series representation proposed by Pipkin and Rogers [14] which has been recently employed by Rajagopal and Wineman [15] to characterize anisotropic nonlinear viscoelastic solids. The proposed model can capture the dependence of stress relaxation on strain, which has been observed experimentally in ligaments [32, 33, 57, 35] and is not captured by current three-dimensional models. In Section 4.2, the theoretical framework set forth by Pipkin and Rogers is introduced and a constitutive relation is proposed to describe the three-dimensional stress relaxation response of ligaments. In Section 4.3, published uniaxial experimental data on the elastic [87] and stress relaxation behavior [35] of human medial collateral ligaments (MCLs) tested along the fiber direction and transverse directions are used to determine the model parameters. After the model parameters are identified, the behavior of the model for simple shear in the fiber direction, simple shear transverse to the fiber direction, and equibiaxial extension are examined (Section 4.4).

4.2 Theoretical Framework

Skeletal ligaments are composed of an amorphous proteoglycan-rich matrix, the ground substance, which is reinforced by collagen fibers. Water is the primary component of the ground substance and accounts for more than 60% of ligament's weight [21]. Due to the high water content, ligaments are assumed to be incompressible. Moreover, ligaments are assumed to be transversely isotropic since the collagen fibers are preferentially aligned along their long axis.

4.2.a Constitutive model

The integral series representation proposed by Pipkin and Rogers [14] was selected to describe the three dimensional stress relaxation behavior of ligaments. Only the first term of the integral series is used. Therefore, the first Piola-Kirchhoff stress tensor, $\mathbf{P}(t)$, at any time t has the form [15]:

$$\mathbf{P}(t) = -p(t)\mathbf{F}^{-\mathrm{T}}(t) + \mathbf{F}(t)\left(\mathbf{R}[\mathbf{C}(t),0] + \int_{-\infty}^{t} \frac{\partial \mathbf{R}[\mathbf{C}(\tau), t-\tau]}{\partial(t-\tau)} d\tau\right) \tag{4.1}$$

where $\mathbf{F}(t)$ is the deformation gradient tensor, $\mathbf{C}(t) = \mathbf{F}^{\mathrm{T}}(t)\,\mathbf{F}(t)$ is the right Cauchy-Green deformation tensor, $\mathbf{R}[\mathbf{C}(\tau), t-\tau]$ is the tensorial relaxation function, and $p = p(t)$ is the Lagrange multiplier that accounts for incompressibility. Further, the term $\mathbf{F}(t)\mathbf{R}[\mathbf{C}(t),0]$ represents the instantaneous elastic contribution to the total stress at any time t.

In Eq. (4.1), the use of the right Cauchy-Green deformation tensor, $\mathbf{C}(t)$, as the strain measure in the tensorial relaxation function, $\mathbf{R}[\mathbf{C}(\tau), t-\tau]$, guarantees that the principle of material frame indifference is satisfied [69]. Assuming that the stress-free reference configuration was occupied at $t = 0$, in the absence of deformation the tensorial relaxation function is identically zero. The tensorial relaxation function must also be a monotonically decreasing function of time to meet fading memory requirements [69]. Note that Eq. (4.1) yields the general nonlinear elastic constitutive equation when time dependence is suppressed with $\mathbf{R}[\mathbf{C}(\tau)] = 2\frac{\partial W}{\partial \mathbf{C}}$ where W is the so-called strain energy density function.

Since skeletal ligaments are assumed to be transversely isotropic, the tensorial relaxation function $\mathbf{R}[\mathbf{C}(\tau), t-\tau]$ can be written as [69]

$$\mathbf{R}[\mathbf{C}(\tau), t-\tau] = k_1\mathbf{1} + k_2\mathbf{C}(\tau) + k_3\mathbf{M}\otimes\mathbf{M} + k_4\left[\mathbf{M}\otimes(\mathbf{C}(\tau)\mathbf{M}) + (\mathbf{C}(\tau)\mathbf{M})\otimes\mathbf{M}\right] \tag{4.2}$$

where $\mathbf{M}$ is the unit vector that defines the axis of transverse isotropy in the reference configuration and k_1, k_2, k_3, and k_4 are constitutive functions which depend on the strain invariants of $\mathbf{C}$, $I_1(\tau)$, $I_2(\tau)$, $I_4(\tau)$, $I_5(\tau)$, and $t-\tau$. The strain invariants of $\mathbf{C}$ are defined as:

$$I_1(\tau) = \mathrm{tr}(\mathbf{C}(\tau))\,, \quad I_2(\tau) = \frac{1}{2}(I_1^2(\tau) - \mathrm{tr}(\mathbf{C}^2(\tau))\,,$$
$$I_4(\tau) = \mathbf{M}\cdot\mathbf{C}(\tau)\mathbf{M}\,, \quad I_5(\tau) = \mathbf{M}\cdot\mathbf{C}^2(\tau)\mathbf{M}\,. \tag{4.3}$$

The strain invariant $I_3(\tau) = \det(\mathbf{C}(\tau)) \equiv 1$ since ligaments are assumed to be incompressible. Note that $I_1(\tau)$ and $I_2(\tau)$ are the principal invariants of $\mathbf{C}$ used to characterize the material response of incompressible isotropic solids. The additional invariants, $I_4(\tau)$ and $I_5(\tau)$, are associated with the anisotropy generated by the presence of a (collagen) fiber reinforcement.

It is well known that $I_4(\tau)$ is the square of the stretch in the fiber direction and, thus, has a clear physical interpretation. The physical interpretation of $I_5(\tau)$ cannot be given as easily but this invariant captures the effect of stretching and shearing in the fiber direction. Indeed, by denoting by C_{ij} the components of $\mathbf{C}$ in the Cartesian coordinate system with unit vector basis $\{\mathbf{E}_1, \mathbf{E}_2, \mathbf{E}_3\}$ and assuming that $\mathbf{M} = \mathbf{E}_3$, one has that $I_4(\tau) = C_{33}$ and $I_5(\tau) = C_{13}^2 + C_{23}^2 + C_{33}^2$.

The tensorial relaxation function is assumed to be given by

$$\mathbf{R}[\mathbf{C}, t-\tau] = 2\,\frac{\partial \tilde{W}(I_1(\tau), I_2(\tau), I_4(\tau), I_5(\tau), t-\tau)}{\partial \mathbf{C}}\,. \tag{4.4}$$

where $\tilde{W}$ is the scalar potential density function [15]. The constitutive functions k_1, k_2, k_3, and k_4 can be determined from the scalar potential density function using the following relationships:

$$k_1 = 2\left(\frac{\partial \tilde{W}}{\partial I_1} + I_1(\tau)\frac{\partial \tilde{W}}{\partial I_2}\right), \quad k_2 = -2\frac{\partial \tilde{W}}{\partial I_2}\,, \quad k_3 = 2\frac{\partial \tilde{W}}{\partial I_4}\,, \quad k_4 = 2\frac{\partial \tilde{W}}{\partial I_5} \tag{4.5}$$

where, for ease of notation, the dependence on the strain invariants of $\mathbf{C}$ and $t-\tau$ has been dropped.

4.2.b A tensorial relaxation function for ligaments

We assume that in skeletal ligaments the ground substance can be modeled as an isotropic matrix while the collagen fibers have a preferred orientation that is identified by the unit vector $\mathbf{M}$ in the reference configuration (Figure 4.1). Based on previous constitutive models for the mechanical response of ligaments [40, 73, 87], the tensorial relaxation function, $\mathbf{R}[\mathbf{C}(\tau), t-\tau]$, is split into the sum of a tensorial relaxation function representing the contribution of the ground substance, $\mathbf{R}_{gs}[I_1(\tau), t-\tau]$, and a tensorial relaxation function accounting for the contribution of the collagen fibers, $\mathbf{R}_{cf}[I_4(\tau), I_5(\tau), t-\tau]$.

$$\mathbf{R}[\mathbf{C}(\tau), t-\tau] = \mathbf{R}_{gs}[I_1(\tau), t-\tau] + \mathbf{R}_{cf}[I_4(\tau), I_5(\tau), t-\tau] \tag{4.6}$$

Writing the tensorial relaxation functions $\mathbf{R}_{gs}$ and $\mathbf{R}_{cf}$ in terms of the constitutive functions k_1, k_2, k_3, and k_4 has

$$\mathbf{R}_{gs}[I_1(\tau), t-\tau] = k_1\left(I_1(\tau), t-\tau\right)\mathbf{1} + k_2\left(I_1(\tau), t-\tau\right)\mathbf{C}(\tau) \tag{4.7}$$

and

$$\mathbf{R}_{cf}[I_4(\tau), I_5(\tau), t-\tau] = k_3\left(I_4(\tau), t-\tau\right)\mathbf{M}\otimes\mathbf{M} + k_4\left(I_5(\tau), t-\tau\right)\left[\mathbf{M}\otimes(\mathbf{C}(\tau)\mathbf{M}) + (\mathbf{C}(\tau)\mathbf{M})\otimes\mathbf{M}\right]. \quad (4.8)$$

The tensorial relaxation function, $\mathbf{R}[\mathbf{C}(\tau), t-\tau]$ in Eq. (4.6), is fully specified once the constitutive functions k_1, k_2, k_3, and k_4 are assigned. The selection of the constitutive functions is based on previous descriptions of the elastic and viscoelastic behavior of ligaments [24, 40, 73] the details of which will be presented later (See Sec. 4.5). Specifically, these functions are chosen to be:

$$k_1 = \left(c_1c_2e^{c_2(I_1(\tau)-3)} - \frac{c_1c_2}{2}I_1(\tau)\right)r_1(t) \quad (4.9)$$

$$k_2 = \frac{c_1c_2}{2}\,r_1(t) \quad (4.10)$$

$$k_3 = \begin{cases} c_3\left(e^{c_4(I_4(\tau)-1)}-1\right)r_2(I_4(\tau),t) & I_4(\tau) > 1 \\ 0 & I_4(\tau)\le 1 \end{cases} \quad (4.11)$$

$$k_4 = 0 \quad (4.12)$$

where the following functions $r_1(t)$ and $r_2(I_4(\tau), t)$ are defined as:

$$r_1(t) = (\,1-a\,)\,e^{-bt} + a \quad (4.13a)$$

$$r_2(I_4(\tau), t) = (\,1-\alpha(I_4)\,)\,e^{-t\,\beta(I_4)} + \alpha(I_4)\,. \quad (4.13b)$$

The model parameters c_1, c_2, c_3, c_4, a, and b are constants and $\alpha(I_4(\tau))$ and $\beta(I_4(\tau))$ are functions of the strain invariant $I_4(\tau)$. As a result of the decomposition of the tensorial relaxation function, Eqs. (4.9) and (4.10) capture the isotropic response of the ground substance while Eq. (4.11) accounts for the anisotropic contribution of the collagen fibers. We explicitly note that the function k_4 from Eq. (4.8) is taken to be identically zero as we have suppressed dependence on $I_5(\tau)$. This assumption is common in biomechanics and reduces the number of constitutive functions which must be determined [71]. In fact for many plane deformations where the fiber reinforcement lies in the plane, the invariants $I_4(\tau)$ and $I_5(\tau)$ are *not* independent [70]. For example, uniaxial tension tests along the fiber and transverse directions would not allow us to differentiate between the contributions of $I_4(\tau)$ and $I_5(\tau)$. For its simplicity of interpretation, $I_4(\tau)$ is preferred over $I_5(\tau)$ and as a result dependence of Eq. (4.8) on $I_5(\tau)$ has been omitted. Note that for ease of notation, the dependence of the strain invariants on τ is dropped for the remainder of this chapter.

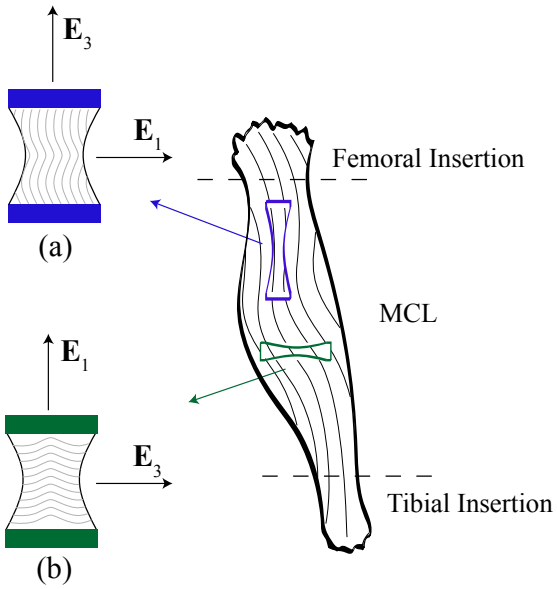

Figure 4.1: Schematic of the medial collateral ligament showing a samples cut in the (a) longitudinal (fiber) and (b) transverse direction. Note the axis of transverse isotropy in the reference configuration, $\mathbf{M}$, coincides with $\mathbf{E}_3$.

4.3 Identification of Model Parameters

Six parameters, c_1, c_2, c_3, c_4, a, b, and two functions $\alpha = \alpha(I_4)$ and $\beta = \beta(I_4)$, are needed to describe the elastic and relaxation response of ligaments. Experimental data on the quasi-static and stress relaxation response of ligaments along both the longitudinal and transverse directions (Figure 4.1) are used to determine the model parameters. For this reason, explicit expressions for the stresses in the longitudinal and transverse directions are derived for the elastic and stress relaxation behavior in Section 4.3.a. These expressions are fit to the experimental data using a nonlinear minimization algorithm as described in Section 4.3.b.

4.3.a Triaxial extension

The ligament is assumed to undergo an isochoric homogeneous axisymmetric deformation defined by

$$x_1 = \lambda_1(t)\, X_1\,, \quad x_2 = \lambda_2(t)\, X_2\,, \quad x_3 = \lambda_3(t)\, X_3 \tag{4.14}$$

where (X_1, X_2, X_3) and (x_1, x_2, x_3) represent the Cartesian coordinates of a generic point in the reference and deformed configurations, respectively, and $\lambda_1(t)$, $\lambda_2(t)$, and $\lambda_3(t)$ are the

axial stretches. The orthonormal bases $\{\mathbf{E}_1, \mathbf{E}_2, \mathbf{E}_3\}$ and $\{\mathbf{e}_1, \mathbf{e}_2, \mathbf{e}_3\}$ in the reference and deformed configurations, respectively, are aligned such that the collagen fibers are parallel to $\mathbf{E}_3$ in the reference configuration ($\mathbf{M} = \mathbf{E}_3$) as illustrated in Figure 4.1.

It follows that the deformation gradient tensor, $\mathbf{F}(t)$, and the right Cauchy-Green deformation tensor, $\mathbf{C}(t)$, are given by

$$\mathbf{F}(t) = \lambda_1(t)\,\mathbf{e}_1 \otimes \mathbf{E}_1 + \lambda_2(t)\,\mathbf{e}_2 \otimes \mathbf{E}_2 + \lambda_3(t)\,\mathbf{e}_3 \otimes \mathbf{E}_3\,,$$
$$\mathbf{C}(t) = \lambda_1^2(t)\,\mathbf{E}_1 \otimes \mathbf{E}_1 + \lambda_2^2(t)\,\mathbf{E}_2 \otimes \mathbf{E}_2 + \lambda_3^2(t)\,\mathbf{E}_3 \otimes \mathbf{E}_3\,. \quad (4.15)$$

Since the ligaments are assumed to be incompressible, we have

$$\lambda_1(t)\lambda_2(t)\lambda_3(t) = 1\,. \quad (4.16)$$

Elastic Behavior

The first Piola-Kirchhoff stress tensor that defines the instantaneous elastic stress for a triaxial extension can be computed by evaluating Eq. (4.1) at $t = \tau$ with the tensorial relaxation function given by Eqs. (4.2) and (4.9) - (4.12) and the tensors $\mathbf{F}$ and $\mathbf{C}$ given by Eq. (4.15). When the collagen fibers are stretched, $I_4 = \lambda_3^2(t) > 1$ and the first Piola-Kirchhoff stress tensor has the form:

$$\begin{aligned}\mathbf{P}(t) = &\left\{\frac{-p}{\lambda_1(t)} + \frac{\lambda_1(t)c_1c_2}{2}\left(2e^{c_2(I_1(t)-3)} - I_1(t) + \lambda_1^2(t)\right)\right\}\mathbf{e}_1 \otimes \mathbf{E}_1 \\ &+ \left\{\frac{-p}{\lambda_2(t)} + \frac{\lambda_2(t)c_1c_2}{2}\left(2e^{c_2(I_1(t)-3)} - I_1(t) + \lambda_2^2(t)\right)\right\}\mathbf{e}_2 \otimes \mathbf{E}_2 \\ &+ \left\{\frac{-p}{\lambda_3(t)} + \frac{\lambda_3(t)c_1c_2}{2}\left(2e^{c_2(I_1(t)-3)} - I_1(t) + \lambda_3^2(t)\right) + c_3\lambda_3(t)\left(e^{c_4(I_4(t)-1)} - 1\right)\right\}\mathbf{e}_3 \otimes \mathbf{E}_3\,.\end{aligned} \quad (4.17)$$

Longitudinal stretch Consider the case of a triaxial extension where the axial stretch $\lambda_3(t)$ is specified. The lateral surface of the ligament is assumed to be traction-free so that $\mathrm{P}_{11} = \mathrm{P}_{22} = 0$. Imposing these boundary conditions in Eq. (4.17) and using Eq. (4.16), one finds that $\lambda_1(t) = \lambda_2(t)$ and $\lambda_3(t) = \lambda_1^{-2}(t) = \lambda_2^{-2}(t)$. The only non-zero component of the stress tensor, P_{33}, can then be found in terms of the axial stretch $\lambda_3(t)$:

$$\begin{aligned}\mathrm{P}_{33}(t) = &\,c_3\lambda_3(t)\left(e^{c_4\left(\lambda_3^2(t)-1\right)} - 1\right) \\ &+ \frac{c_1c_2}{2\lambda_3(t)}\left(2e^{c_2\left(\lambda_3^2(t)+2\lambda_3^{-1}(t)-3\right)} - \lambda_3^{-1}(t)\right)\left(\lambda_3^2(t) - \lambda_3^{-1}(t)\right)\,.\end{aligned} \quad (4.18)$$

Transverse stretch Consider the case of a triaxial extension where the axial stretch $\lambda_1(t)$ is known. The traction-free boundary condition on the lateral surface requires that $\mathrm{P}_{22} = \mathrm{P}_{33} = 0$. Enforcing these boundary conditions in Eq. (4.17) and using Eq. (4.16) one finds that when the collagen fibers are compressed, $I_4 = \lambda_3^2(t) \leq 1$, $\lambda_3(t) = \lambda_2(t)$ and $\lambda_1(t) = \lambda_3^{-2}(t) = \lambda_2^{-2}(t)$. Then, the only non-zero component of the stress tensor is P_{11}

$$\mathrm{P}_{11}(t) = \frac{c_1 c_2}{2\lambda_1(t)} \left(\lambda_1^2(t) - \lambda_1^{-1}(t)\right) \left(2e^{c_2\left(\lambda_1^2(t)+2\lambda_1^{-1}(t)-3\right)} - \lambda_1^{-1}(t)\right) . \tag{4.19}$$

Stress Relaxation Behavior

The stress relaxation response for a ligament subjected to a triaxial extension can be described using Eqs. (4.1), (4.2), (4.9) - (4.12) and (4.15). The expression for the stress results in a system of nonlinear Volterra equations of the second kind that cannot be solved analytically for the general case of a triaxial extension [88]. However, for the case when one of the axial stretches is constant an analytical solution can be found. We consider two specific cases of a triaxial extension, the first where a constant longitudinal stretch, $\hat{\lambda}_3$, is specified and the second where a constant transverse stretch, $\hat{\lambda}_1$, is prescribed.

Longitudinal stretch Consider the specific case of a triaxial extension where a constant axial stretch along the fiber direction which is greater than one, $\lambda_3(t) = \hat{\lambda}_3$, is prescribed. The lateral surface of the ligament is assumed to be traction-free and, hence, $\mathrm{P}_{11}(t) = \mathrm{P}_{22}(t) = 0$ at all times t. In applying the boundary conditions one again finds that $\lambda_1(t) = \lambda_2(t)$ and $\hat{\lambda}_3 = \lambda_1^{-2}(t) = \lambda_2^{-2}(t)$. Then, the only non-zero component of the stress tensor, P_{33}, is

$$\begin{aligned}\mathrm{P}_{33}(t) = c_3\hat{\lambda}_3 \left(e^{c_4\left(\hat{\lambda}_3^2-1\right)} - 1\right) r_2\left(\hat{\lambda}_3^2, t\right) \\ + \frac{c_1 c_2}{2\hat{\lambda}_3} \left(2e^{c_2\left(\hat{\lambda}_3^2+2\hat{\lambda}_3^{-1}-3\right)} - \hat{\lambda}_3^{-1}\right) \left(\hat{\lambda}_3^2 - \hat{\lambda}_3^{-1}\right) r_1(t)\end{aligned} \tag{4.20}$$

where the functions r_1 and r_2 are defined in Eq. (4.13).

Transverse stretch Consider the case of a triaxial extension where the axial stretch, $\lambda_1(t)$, is specified to be constant, $\lambda_1(t) = \hat{\lambda}_1$. The traction-free boundary condition on the lateral surface requires that $\mathrm{P}_{22} = \mathrm{P}_{33} = 0$ at all times t. Enforcing the traction-free boundary conditions and making use of Eq. (4.16) one finds that, when $I_4 = \lambda_3^2(t) \leq 1$, $\lambda_3(t) = \lambda_2(t)$ and $\hat{\lambda}_1 = \lambda_3^{-2}(t) = \lambda_2^{-2}(t)$. The only non-zero component of the stress tensor, $\mathrm{P}_{11}(t)$, is found to be

$$\mathrm{P}_{11}(t) = \frac{c_1}{2\hat{\lambda}_1} \left(\hat{\lambda}_1^2 - \hat{\lambda}_1^{-1}\right) \left(2e^{c_2\left(\hat{\lambda}_1^2+2\hat{\lambda}_1^{-1}-3\right)} - \hat{\lambda}_1^{-1}\right) r_1(t) . \tag{4.21}$$

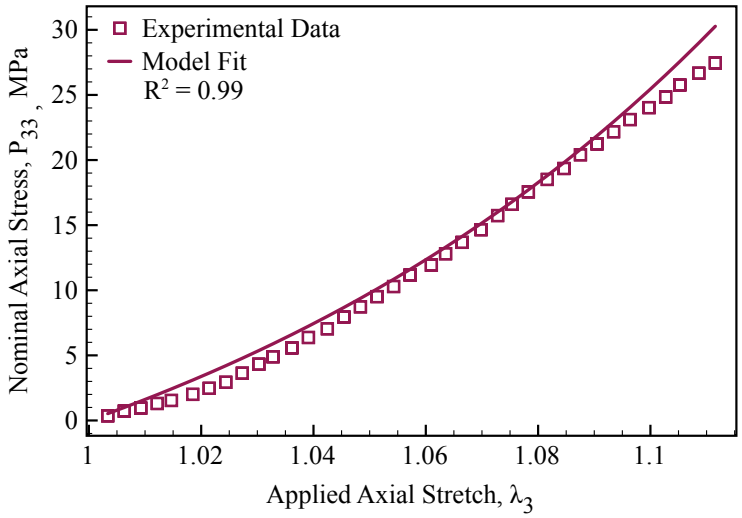

Figure 4.2: Stress-stretch experimental data obtained by Quapp and Weiss [87] for a human MCL stretched along the longitudinal (fiber) direction and model fit with $c_1 = 0.86$ MPa, $c_2 = 8.16$, $c_3 = 21.77$ MPa, and $c_4 = 3.30$.

4.3.b Parameter identification

Quasi-static stress-stretch data collected by performing uniaxial tensile tests on human MCLs along their longitudinal and transverse directions, as shown in Figure 4.1, were used to determine the elastic model parameters. PlotDigitizer (v. 2.5.1) was used to digitize the stress-stretch experimental data in Figure 4 of the manuscript published by Quapp and Weiss [87]. Values for the elastic material parameters, c_1, c_2, c_3, and c_4, were determined by minimizing the sum of the squared differences between the stresses computed using Eqs. (4.18) and (4.19) and those measured experimentally simultaneously. The built in minimization function, *fmincon*, in MATLAB (v. 7.12, MathWorks) was used while constraining the model parameters c_1, c_3, and c_4 to be non-negative and $c_2 > 0.36$. These restrictions were imposed on the values of the elastic model parameters to ensure that the material response is physically reasonable (See Appendix A). The values for the elastic material parameters c_1, c_2, c_3, and c_4 were found to be 0.86 MPa, 8.16, 21.77 MPa, and 3.30, respectively. The results of the curve fitting are presented in Figures 4.2 and 4.3. The model was able to fit well the stress-stretch data which were collected by testing the ligamentous specimens in their longitudinal and transverse directions ($R^2 > 0.99$). The nonlinear stiffening phenomenon in the stress-stretch curve of longitudinal specimens (Figure 4.2) and the approximately linear stress-stretch curve of transverse specimens (Figure 4.3) were captured.

The most comprehensive set of experimental data on the stress relaxation response of human MCLs was published by Bonifasi-Lista et al. [35]. Stress relaxation data were obtained by conducting uniaxial tests of ligamentous specimens in the longitudinal and transverse

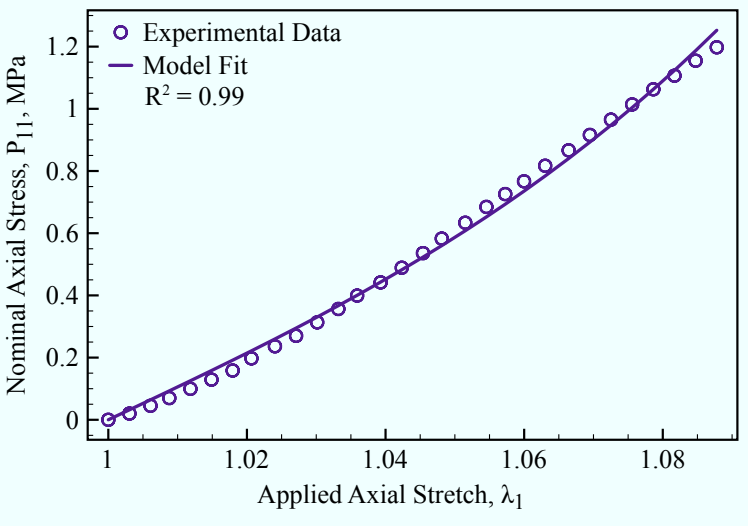

Figure 4.3: Stress-stretch experimental data obtained by Quapp and Weiss [87] for a human MCL stretched in the transverse direction and model fit with $c_1 = 0.86$ MPa and $c_2 = 8.16$.

directions at three different strain levels. While stress relaxation data collected at three strain levels are sufficient to determine if the tissue exhibits strain dependent stress relaxation behavior, this number of strain levels is insufficient to determine the functions $\alpha(I_4)$ and $\beta(I_4)$ that capture the strain-dependent stress relaxation response. Therefore, the functions $\alpha(I_4)$ and $\beta(I_4)$ were set to forms previously determined for collagen fiber bundles in Ch. 3 where $\alpha(I_4) = 0.73\, e^{-14.69(I_4-1)}$ and $\beta(I_4) = 0.2084\,(I_4 - 1)$ [61].

In order to determine the model parameters a and b, experimental data obtained by subjecting specimens to uniaxial stress relaxation tests along their transverse direction at a strain level of 8% were used. These data were digitized from Figure 4 in the manuscript published by Bonifasi-Lista et al. [35] using PlotDigitizer. The values of the parameters a and b were found by minimizing the sum of the squared differences between the theoretical stresses in Eq. (4.21) and the experimentally determined stresses. The parameters were constrained to satisfy the following conditions: $0 < a < 1$ and $b > 0$. See Appendix A for a discussion of how the constraints on the parameter values were determined.

Figure 4.4 shows the digitized experimental data and the results of the curve fitting. Overall the model is able to capture the stress relaxation response in the transverse direction but, at intermediate times, when $1 < t < 10$ s, the model over-predicts the normalized stress relaxation response.

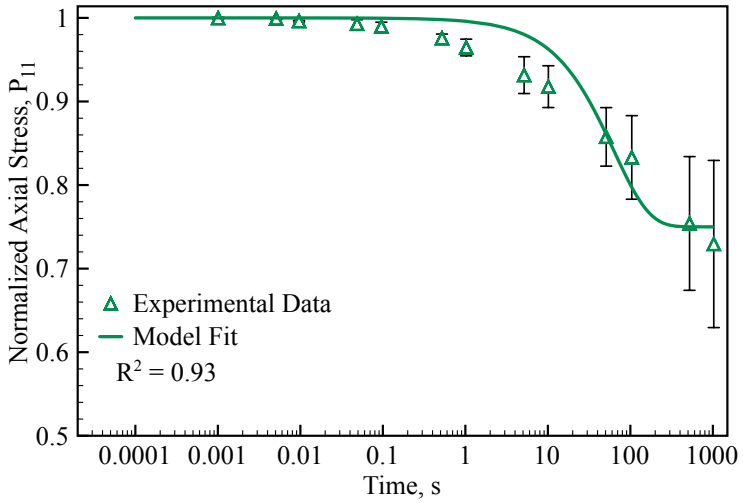

Figure 4.4: Normalized stress relaxation data for a uniaxial stress relaxation test in the transverse direction collected by Bonifasi-Lista et al. [35] on the human MCL and model fit where $a = 0.75$ and $b = 0.016$ 1/s.

4.4 Model Predictions

The performance of the model is further evaluated by considering its predictions for simple shear in the fiber direction, simple shear transverse to the fiber direction, and equibiaxial extension. In these predictions, the values of the material parameters and functions are fixed to those computed by fitting the uniaxial experimental data as described in the previous section. For convenience, the model parameters are $c_1 = 0.86$ MPa, $c_2 = 8.16$, $c_3 = 21.77$ MPa, $c_4 = 3.30$, $a = 0.75$, and $b = 0.016$ 1/s and the two functions which define the strain dependent stress relaxation behavior are $\alpha(I_4) = 0.73\, e^{-14.69(I_4-1)}$ and $\beta(I_4) = 0.2084\,(I_4 - 1)$. Note that for each of the predictions the *normalized* stress relaxation response is plotted to more easily visualize the influence of strain on the stress relaxation response. The stresses are always normalized by their initial value at $t = 0$.

4.4.a Simple shear in the fiber direction

Consider the isochoric plane deformation for simple shear in the fiber direction defined by

$$x_1 = X_1\,, \quad x_2 = X_2\,, \quad x_3 = \gamma(t)\,X_1 + X_3 \tag{4.22}$$

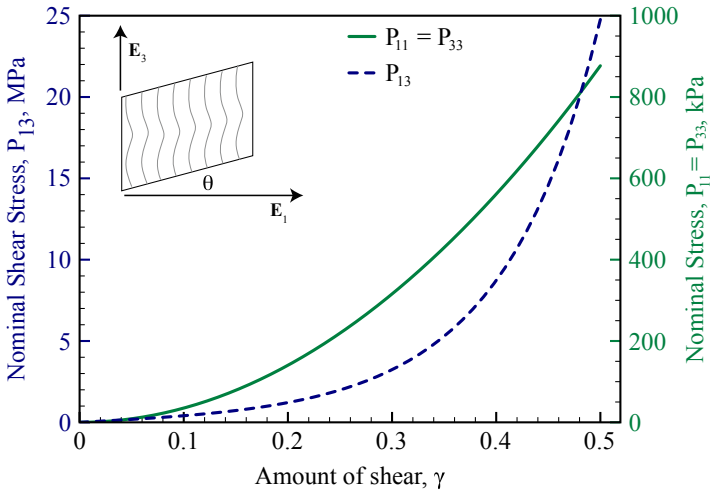

Figure 4.5: Predicted shear stress, P_{13} (left y-axis), and normal stresses, P_{11} and P_{33} (right y-axis), as a function of the amount of shear, γ, for a MCL sheared in the fiber direction. The insert shows a schematic of the shear deformation where the amount of shear, $\gamma = \tan\theta$.

where $\gamma(t)$ is the amount of shear. The deformation gradient tensor, $\mathbf{F}(t)$, and the right Cauchy-Green deformation tensor, $\mathbf{C}(t)$, then are

$$\begin{aligned}\mathbf{F}(t) &= \mathbf{e}_1 \otimes \mathbf{E}_1 + \mathbf{e}_2 \otimes \mathbf{E}_2 + \gamma(t)\,\mathbf{e}_3 \otimes \mathbf{E}_1 + \mathbf{e}_3 \otimes \mathbf{E}_3\,,\\ \mathbf{C}(t) &= \left(1+\gamma^2(t)\right)\,\mathbf{E}_1 \otimes \mathbf{E}_1 + \gamma(t)\,\left(\mathbf{E}_1 \otimes \mathbf{E}_3 + \mathbf{E}_3 \otimes \mathbf{E}_1\right) + \mathbf{E}_2 \otimes \mathbf{E}_2 + \mathbf{E}_3 \otimes \mathbf{E}_3\,. \quad (4.23)\end{aligned}$$

Calculating I_4 from Eq. (4.23), $I_4 = C_{33} = 1$, shows the collagen fibers are not stretched when the ligament is sheared in the fiber direction. Since $I_4 = 1$, the constitutive function, k_3, that describes the contribution of the collagen fiber reinforcement to the stress, given by Eq. (4.11), is always zero. As a result, simple shear in the fiber direction is governed by the isotropic response of the ground substance.

The instantaneous elastic response of a ligament subjected to simple shear in the fiber direction can be computed by evaluating Eq. (4.1) at $t = \tau$ where the tensorial relaxation function is defined by Eqs. (4.2) and (4.9)-(4.12). After assuming a plane stress boundary condition so that $P_{22} = 0$, p can be computed and its value substituted into Eq. (4.1). Then, the first Piola-Kirchhoff stress tensor takes the form

$$\begin{aligned}\mathbf{P}\,(t) = \frac{c_1 c_2 \gamma^2(t)}{2}\mathbf{e}_1 \otimes \mathbf{E}_1 + \frac{c_1 c_2 \gamma(t)}{2}\left(2e^{c_2\gamma^2(t)} - \gamma^2(t) - 1\right)\mathbf{e}_1 \otimes \mathbf{E}_3\\ + \frac{c_1 c_2 \gamma(t)}{2}\left(2e^{c_2\gamma^2(t)} - 1\right)\mathbf{e}_3 \otimes \mathbf{E}_1 + \frac{c_1 c_2 \gamma^2(t)}{2}\mathbf{e}_3 \otimes \mathbf{E}_3\,. \quad (4.24)\end{aligned}$$

In Figure 4.5, the shear stress, P_{13}, computed from Eq. (4.24) is plotted versus the amount

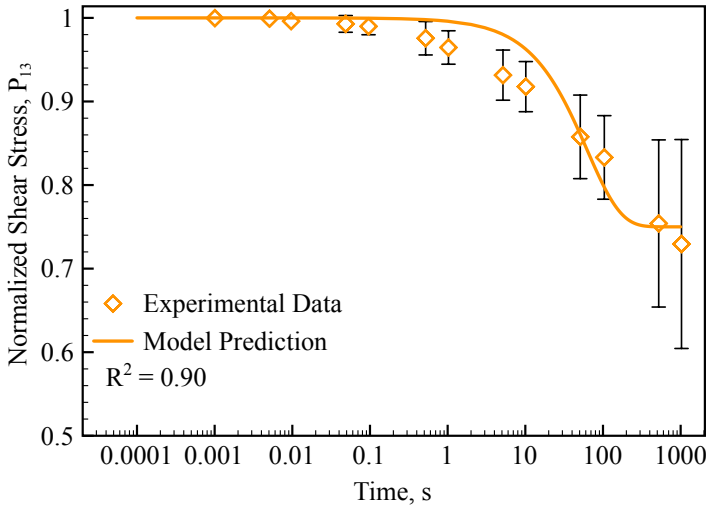

Figure 4.6: Prediction of the normalized shear stress, $P_{13}(t)$, when the MCL is sheared in the fiber direction and allowed to relax and normalized stress relaxation data obtained by Bonifasi-Lista et al. [35] for an applied shear of 0.35.

of shear on the left y-axis. The resulting curve is nonlinear exhibiting the strain-stiffening phenomenon that has been observed experimentally [40]. The stiffening effect becomes more pronounced for $\gamma > 0.20$. We note that the first Piola-Kirchhoff stress tensor, $\mathbf{P}$, is not symmetric, $P_{31} \neq P_{13}$ but, a similar relationship between P_{31} and γ is obtained. The two normal stresses required to generate a homogeneous shear are plotted in Figure 4.5 on the right y-axis. Notice that the normal stresses are an order of magnitude smaller than the shear stresses.

During stress relaxation, $\gamma(t)$ is constant, i.e. $\gamma(t) = \hat{\gamma}$. Then, the first Piola-Kirchhoff stress tensor that describes the stress relaxation behavior is calculated by evaluating Eqs. (4.2), (4.9)-(4.12), and (4.23) in Eq. (4.1) where $\gamma(t) = \hat{\gamma}$. Enforcing the plane stress boundary condition, which requires $P_{22} = 0$, the value for the Lagrange multiplier that accounts for incompressibility, p is determined and substituted into Eq. (4.1). The resulting stress tensor is:

$$\mathbf{P}(t) = \frac{c_1 c_2 \hat{\gamma}^2}{2} r_1(t)\, \mathbf{e}_1 \otimes \mathbf{E}_1 + \frac{c_1 c_2 \hat{\gamma}}{2}\left(2e^{c_2\hat{\gamma}^2} - \hat{\gamma}^2 - 1\right) r_1(t)\, \mathbf{e}_1 \otimes \mathbf{E}_3 + \frac{c_1 c_2 \hat{\gamma}}{2}\left(2e^{c_2\hat{\gamma}^2} - 1\right) r_1(t)\, \mathbf{e}_3 \otimes \mathbf{E}_1 + \frac{c_1 c_2 \hat{\gamma}^2}{2} r_1(t)\, \mathbf{e}_3 \otimes \mathbf{E}_3 \,. \quad (4.25)$$

recalling that the function $r_1(t)$ is given in Eq. (4.13).

As mentioned earlier, the ligament's response to simple shear in the fiber direction is governed by the isotropic response of the ground substance. Therefore, no strain dependent

stress relaxation behavior is observed for this type of deformation, as the strain dependent relaxation behavior is attributed only to the collagen fibers. In Figure 4.6, the predicted shear stress, $\mathrm{P}_{13}(t)$, is normalized by its value at $t = 0$ and plotted versus time. This prediction is directly compared with experimental data published by Bonifasi-Lista et al. [35] that were obtained by digitizing Figure 4 in their manuscript for $\hat{\gamma} = 0.35$. Good agreement ($\mathrm{R}^2 = 0.90$) was found between the experimental data and the model prediction. However, similar to the stress relaxation response for a stretch applied in the direction transverse to the fibers (Figure 4.4), at mid-range times, $t = 1 - 10$ s, the model over predicts the value of the normalized stress.

4.4.b Simple shear transverse to the fiber direction

The ligament is assumed to undergo an isochoric deformation in the $\mathbf{E}_1$-$\mathbf{E}_3$ plane for shear transverse to the fiber direction given by

$$x_1 = X_1 + \gamma(t)\, X_3\,, \quad x_2 = X_2\,, \quad x_3 = X_3 \tag{4.26}$$

where $\gamma(t)$ is the amount of shear. The deformation gradient tensor, $\mathbf{F}(t)$, and the right Cauchy-Green deformation tensor, $\mathbf{C}(t)$, are

$$\begin{aligned}\mathbf{F}(t) &= \mathbf{e}_1 \otimes \mathbf{E}_1 + \gamma(t)\, \mathbf{e}_1 \otimes \mathbf{E}_3 + \mathbf{e}_2 \otimes \mathbf{E}_2 + \mathbf{e}_3 \otimes \mathbf{E}_3\,,\\ \mathbf{C}(t) &= \mathbf{E}_1 \otimes \mathbf{E}_1 + \gamma(t)\, (\mathbf{E}_1 \otimes \mathbf{E}_3 + \mathbf{E}_3 \otimes \mathbf{E}_1) + \mathbf{E}_2 \otimes \mathbf{E}_2 + \left(1 + \gamma^2(t)\right) \mathbf{E}_3 \otimes \mathbf{E}_3\,.\end{aligned} \tag{4.27}$$

For this shear deformation, the collagen fibers are stretched as the ligament is sheared, $I_4 = \mathrm{C}_{33} = 1 + \gamma^2(t)$. As a result both the ground substance and the collagen fibers contribute to the ligament's response for simple shear transverse to the fiber direction.

The first Piola-Kirchhoff stress tensor for the the instantaneous elastic response is specified by evaluating Eq. (4.1) at $t = \tau$, with the tensorial relaxation function given by Eqs. (4.2) and (4.9)-(4.12) and substituting Eq. (4.27) for the tensors $\mathbf{F}$ and $\mathbf{C}$. The Lagrange multiplier p can be computed from the plane stress boundary condition $\mathrm{P}_{22} = 0$. Then, the first Piola-Kirchoff stress tensor for the instantaneous elastic response is

$$\begin{aligned}\mathbf{P}\left(\gamma(t)\right) = {} & \frac{c_1 c_2}{2}\gamma^2(t)\, \mathbf{e}_1 \otimes \mathbf{E}_1 + \frac{c_1 c_2 \gamma(t)}{2}\left(2e^{c_2\gamma^2(t)} - \gamma^2(t) - 1\right) \mathbf{e}_3 \otimes \mathbf{E}_1\\ & + \left[c_3\gamma(t)\left(e^{c_4\gamma^2(t)} - 1\right) + \frac{c_1 c_2 \gamma(t)}{2}\left(2e^{c_2\gamma^2(t)} - 1\right)\right] \mathbf{e}_1 \otimes \mathbf{E}_3\\ & + \left(c_3\left(e^{c_4\gamma^2(t)} - 1\right) + \frac{c_1 c_2}{2}\gamma^2(t)\right) \mathbf{e}_3 \otimes \mathbf{E}_3\,.\end{aligned} \tag{4.28}$$

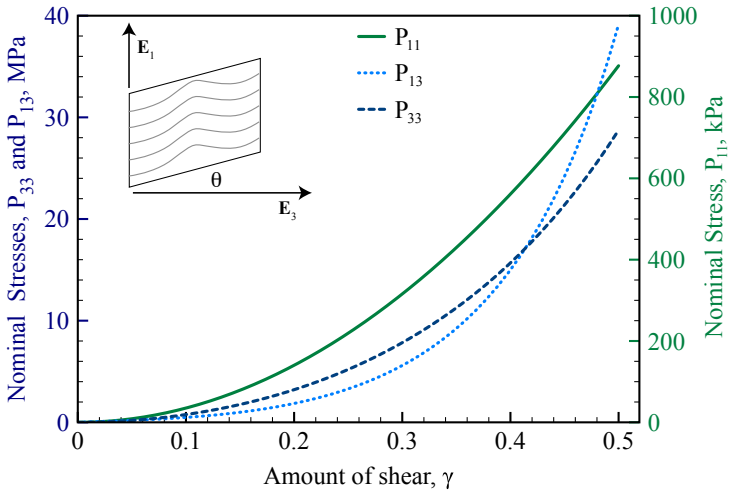

Figure 4.7: Predicted shear stress, P_{13}, and normal stress, P_{33}, (left y-axis) and the normal stress, P_{11}, (right y-axis) as a function of the amount of shear, γ, for a MCL sheared in the direction transverse to the fibers. The insert shows a schematic of the shear deformation where the amount of shear, $\gamma = \tan\theta$.

In Figure 4.7 the instantaneous elastic response given by Eq. (4.28) for the shear stress, P_{13}, versus the amount of shear is presented. The normal stresses, P_{11} and P_{33}, required to sustain the shear transverse to the fiber direction are also plotted in Figure 4.7. A comparison of Figures 4.5 and 4.7 shows that the shear stress, P_{13}, and the normal stress, P_{33}, are larger for the same amount of shear when the ligament undergoes simple shear transverse to the fiber direction. The increase in the shear stress, P_{13}, and normal stress, P_{33}, is due to the contribution of the collagen fibers. Notice that the normal stresses required to sustain shear transverse to the fiber direction are unequal with $P_{33} >> P_{11}$.

Stress relaxation for simple shear transverse to the fiber direction is described by taking Eqs. (4.1), (4.2) and (4.9)-(4.12) with the boundary condition $P_{22} = 0$ and assuming that $\gamma(t) = \tilde{\gamma}$ is constant. The first-Piola Kirchhoff stress tensor is

$$\begin{aligned}\mathbf{P}(t) = \frac{c_1c_2}{2}\tilde{\gamma}^2\, r_1(t)\, \mathbf{e}_1 \otimes \mathbf{E}_1 + \frac{c_1c_2\tilde{\gamma}}{2}\left(2e^{c_2\tilde{\gamma}^2} - \tilde{\gamma}^2 - 1\right) r_1(t)\, \mathbf{e}_3 \otimes \mathbf{E}_1 \\ + \left\{\frac{c_1c_2\tilde{\gamma}}{2}\left(2e^{c_2\tilde{\gamma}^2} - 1\right) r_1(t) + c_3\tilde{\gamma}\left(e^{c_4\tilde{\gamma}^2} - 1\right) r_2(1+\tilde{\gamma}^2, t)\right\} \mathbf{e}_1 \otimes \mathbf{E}_3 \\ + \left\{c_3\left(e^{c_4\tilde{\gamma}^2} - 1\right) r_2(1+\tilde{\gamma}^2, t) + \frac{c_1c_2}{2}\tilde{\gamma}^2\, r_1(t)\right\} \mathbf{e}_3 \otimes \mathbf{E}_3 \end{aligned} \quad (4.29)$$

Since the collagen fibers are stretched as the ligament is sheared, the normalized stress relaxation behavior for the shear stress, $P_{13}(t)$, and the normal stress, $P_{33}(t)$, exhibit strain dependency. In Figure 4.8 the normalized stress relaxation response for the shear stress,

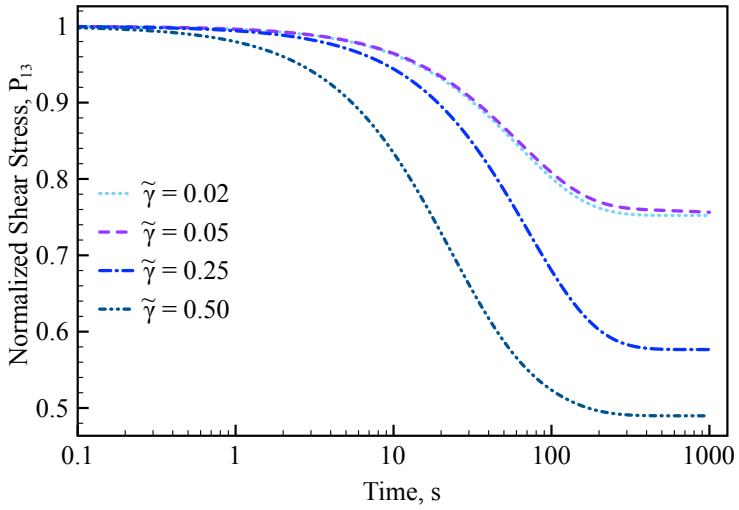

Figure 4.8: Prediction of the normalized shear stress, $P_{13}(t)$, for a MCL undergoing relaxation in shear transverse to the fiber direction at four levels of applied shear, $\tilde{\gamma} = 0.02$, 0.05, 0.25, 0.50.

$P_{13}(t)$, is plotted for four values of shear: $\tilde{\gamma} = 0.02$, 0.05, 0.25, 0.50. As the amount of shear increases, the value of the stress at equilibrium and the time to reach the equilibrium stress decrease.

4.4.c Equibiaxial extension

For an isochoric equibiaxial extension along the fiber direction $\mathbf{E}_3$ and along the axis aligned with $\mathbf{E}_1$ the deformation is assumed to be

$$x_1 = \lambda(t)\, X_1\,, \quad x_2 = \frac{1}{\lambda^2(t)}\, X_2\,, \quad x_3 = \lambda(t)\, X_3 \tag{4.30}$$

where $\lambda(t)$ is the amount of stretch. The deformation gradient tensor, $\mathbf{F}(t)$, and the right Cauchy-Green deformation tensor, $\mathbf{C}(t)$, respectively are given by

$$\mathbf{F}(t) = \lambda(t)\, \mathbf{e}_1 \otimes \mathbf{E}_1 + \frac{1}{\lambda^2(t)}\, \mathbf{e}_2 \otimes \mathbf{E}_2 + \lambda(t)\, \mathbf{e}_3 \otimes \mathbf{E}_3\,,$$
$$\mathbf{C}(t) = \lambda^2(t)\, \mathbf{E}_1 \otimes \mathbf{E}_1 + \frac{1}{\lambda^4(t)}\, \mathbf{E}_2 \otimes \mathbf{E}_2 + \lambda^2(t)\, \mathbf{E}_3 \otimes \mathbf{E}_3\,. \tag{4.31}$$

The ligament surface with outer normal $\pm\mathbf{E}_2$ is assumed to be traction-free and, hence, $P_{22} = 0$. Substituting Eqs. (4.2), (4.9)-(4.12), and (4.31) into Eq. (4.1) at time $t = \tau$ the first Piola-

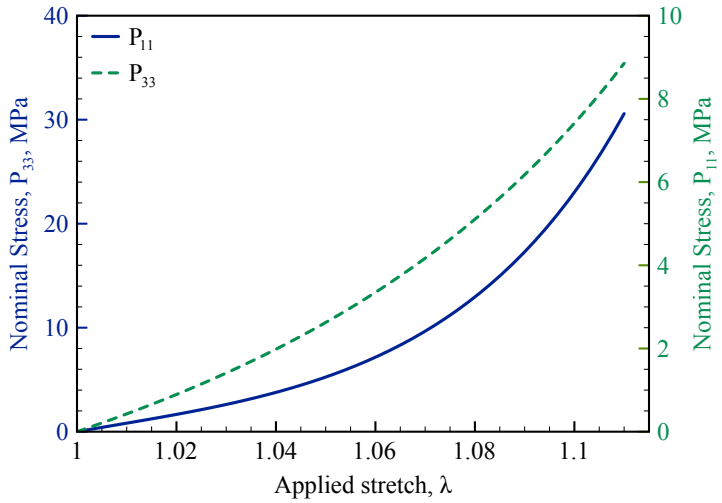

Figure 4.9: Predicted stress-stretch response for the normal stress P_{11} on the right y-axis and the normal stress P_{33} on the left y-axis for MCL subjected to an equibiaxial extension.

Kirchoff stress tensor for the instantaneous elastic response is computed. The Lagrange multiplier found by enforcing the boundary conditions is $p = \frac{c_1 c_2}{\lambda^4(t)} \left(e^{c_2\left(2\lambda^2(t)+\lambda^{-4}(t)-3\right)} - \lambda^2(t) \right)$. Then, the first Piola-Kirchhoff stress tensor becomes

$$\begin{aligned}\mathbf{P}\left(\lambda(t)\right) = &\frac{c_1 c_2\left(\lambda^6(t)-1\right)}{2\lambda^5(t)} \left(2e^{c_2(2\lambda^2(t)+\lambda^{-4}(t)-3)} - \lambda^2(t) \right) \mathbf{e}_1 \otimes \mathbf{E}_1 \\ &+ \left[\frac{c_1 c_2\left(\lambda^6(t)-1\right)}{2\lambda^5(t)} \left(2e^{c_2(2\lambda^2(t)+\lambda^{-4}(t)-3)} - \lambda^2(t) \right) + c_3\lambda(t) \left(e^{c_4(\lambda^2(t)-1)} - 1 \right) \right] \mathbf{e}_3 \otimes \mathbf{E}_3 \,. \quad (4.32)\end{aligned}$$

Figure 4.9 shows the model predictions for a ligament subjected to an equibiaxial extension along $\mathbf{E}_3$ and $\mathbf{E}_1$. As expected for an equibiaxial extension, the stresses generated at the same stretch are much higher in the fiber direction.

The stress tensor that describes the stress relaxation response is found by using Eqs. (4.1), (4.2), (4.9) - (4.12), and (4.31) assuming that the equibiaxial stretch, $\lambda(t) = \widehat{\lambda}$, is constant. Again the value for p is determined by enforcing the traction-free boundary condition on the surfaces with the outer normal $\pm\mathbf{E}_2$. The first Piola-Kirchhoff is then

$$\begin{aligned}\mathbf{P}(t) = &\frac{c_1 c_2\left(\widehat{\lambda}^6-1\right)}{2\widehat{\lambda}^5} \left(2e^{c_2\left(2\widehat{\lambda}^2+\widehat{\lambda}^{-4}-3\right)} - \widehat{\lambda}^2 \right) r_1(t)\, \mathbf{e}_1 \otimes \mathbf{E}_1 \\ &+ \left(\frac{c_1 c_2\left(\widehat{\lambda}^6-1\right)}{2\widehat{\lambda}^5} \left(2e^{c_2\left(2\widehat{\lambda}^2+\widehat{\lambda}^{-4}-3\right)} - \widehat{\lambda}^2 \right) r_1(t) + c_3\widehat{\lambda} \left(e^{c_4\left(\widehat{\lambda}^2-1\right)} - 1 \right) r_2\left(\widehat{\lambda}^2, t\right) \right) \mathbf{e}_3 \otimes \mathbf{E}_3 \quad (4.33)\end{aligned}$$

In Figure 4.10, the normalized stress relaxation response at four levels of stretch, $\widehat{\lambda} = 1.01$,

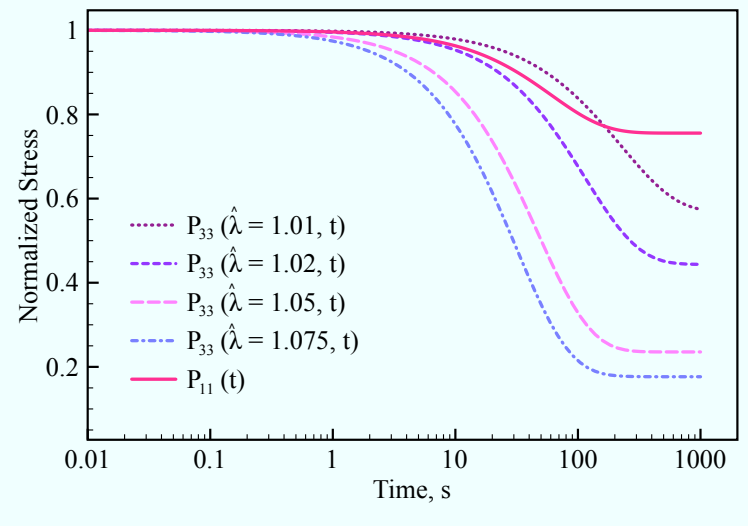

Figure 4.10: Predicted normalized stress relaxation response along the $\mathbf{E}_1$ direction, $P_{11}(t)$ (solid line), and the $\mathbf{E}_3$ direction, $P_{33}(t)$ (dashed lines), for a MCL allowed to relax at a constant equibiaxial stretch, $\widehat{\lambda}$. In the fiber direction, the stretch level influences the normalized stress relaxation behavior so four representative stretch levels are plotted, $\widehat{\lambda} = 1.01$, 1.02, 1.05, and 1.075.

1.02, 1.05, and 1.075, is shown for $P_{33}(t)$. The normalized stress at equilibrium and the time it takes for the normalized stress relaxation response to reach equilibrium both decrease with increasing values of the applied stretch. The normalized stress relaxation response in the transverse direction, $P_{11}(t)$, which is independent of the stretch, is also plotted in Figure 4.10.

4.5 Discussion

In this study, a three-dimensional finite strain nonlinear viscoelastic constitutive relation was proposed to describe the stress relaxation response of ligaments. The constitutive relation extends the model put forward in Chapter 3 on the uniaxial stress relaxation response of collagen fiber bundles to three dimensions by accounting for the contribution of the ground substance. The model parameters were identified from the uniaxial elastic and stress relaxation behavior of the MCL in the longitudinal and transverse directions. Overall the proposed tensorial relaxation function was able to fit the elastic and relaxation response in uniaxial tension well while including non-linear stiffening, finite strains, and strain dependent relaxation behavior in the fiber direction. The model parameters identified were then used to predict the ligament response in simple shear in the fiber direction, simple shear transverse to the fiber direction, and equibiaxial extension. For stress relaxation during shear in the

fiber direction, it was possible to compare the results of the model prediction with published experimental data [35]. The model prediction was in good agreement ($R^2 = 0.90$) with the experimental data suggesting the model may be capable of accurately predicting the response of the MCL under loading conditions not used to determine the model parameters. However, further validation with experiments are necessary to quantify the predictive capabilities of the model.

The choice of the tensorial relaxation function and the constitutive functions, k_1, k_2, k_3, and k_4, which describe the three dimensional viscoelastic response of the ligament, was a critical component of this work. The tensorial relaxation function was determined by considering the separate contributions of the collagen fibers and ground substance as presented in Eq. (4.6). Specifically, the collagen fibers were assumed to be responsible for the nonlinear stress-stretch behavior in the fiber direction and the strain-dependent normalized stress relaxation response. The ground substance was assumed to govern the nonlinear stiffening behavior observed for simple shear in the fiber direction.

The elastic behavior of ligaments is defined by $\mathbf{R}[\mathbf{C}, 0]$, that is

$$\mathbf{R}\left[\mathbf{C}, 0\right] = k_1(I_1, 0)\,\mathbf{1} + k_2(I_1, 0)\,\mathbf{C} + k_3(I_4, 0)\,\mathbf{M} \otimes \mathbf{M} + k_4\left(I_5, 0\right)\left[\mathbf{M} \otimes (\mathbf{C}(\tau)\mathbf{M}) + (\mathbf{C}(\tau)\mathbf{M}) \otimes \mathbf{M}\right] . \quad (4.34)$$

Simple forms for the constitutive functions, $k_1(I_1, 0)$ and $k_2(I_1, 0)$, that describe the elastic response of the ground substance were considered. These include those leading to the neo-Hookean and Mooney-Rivlin models which were unable to reproduce the nonlinear strain stiffening observed experimentally for shear in the fiber direction [40]. Therefore the strain energy proposed by Weiss et al. [40] was adopted to model the contribution of the ground substance to the elastic stresses, that is $\tilde{W} = c_1 e^{c_2(I_1-3)} - \frac{1}{2}c_1 c_2\,(I_2 - 3)$ where the constitutive functions $k_1(I_1, 0)$ and $k_2(I_1, 0)$ can be found by substituting $\tilde{W}$ into Eq. (4.5). The strain-stiffening stress-stretch behavior in the fiber direction was captured using an exponential function in I_4. The collagen fibers only contribute to the stress when the collagen fibers are stretched, $I_4 > 1$. When the collagen fibers are compressed, $I_4 < 1$, the collagen fibers are assumed to buckle immediately and not contribute to the stress. We note that the constitutive function $k_4(I_5, 0)$ was set to zero. For an in-depth comparison of the differences in behavior for a transversely isotropic strain energy that depends on I_5 as opposed to I_4 the reader is referred to the manuscript by Merodio and Ogden [70].

Experiments on the stress relaxation behavior of ligaments in the transverse direction have shown that for strains between 8-12% the normalized relaxation behavior is independent of strain. As a result the normalized relaxation response of the ground substance can be described with just two parameters, a and b (Eq. (4.13a)). In order to select the normalized stress relaxation response of the collagen fibers, we assumed that the collagen fibers exhibit the strain-dependent normalized stress relaxation response as suggested by our previous work

in Chapter 3 (Eq. (4.13b). The functions $\alpha(I_4)$ and $\beta(I_4)$ were selected to describe strain dependent changes in the ratio of the initial stress to the equilibrium stress and the relaxation rate, respectively. The published experimental data on the uniaxial stress relaxation response of ligaments in the fiber direction support the assumption that the normalized relaxation response is a function of strain [33, 32, 35, 34, 57]. However, some authors have reported that for large strains the normalized stress relaxation response in the fiber direction becomes independent of strain [89, 33]. In ligaments where this is the case, the current model could be amended so that the functions $\alpha(I_4)$ and $\beta(I_4)$ incorporate a switching criteria and take on a second set of constant values for large values of strain.

Two important assumptions were made in the determination of the model parameters. First we assumed that quasi-static stress-stretch data could be used to describe the instantaneous elastic behavior. Realistically, the stress-stretch response of ligaments is dependent on the strain rate. Therefore the model could be refined by considering the strain rate dependency. This could be accomplished employing the structural approach presented by De Vita and Slaughter [90] or the phenomenological approach presented by Limbert and Middleton [73]. The second assumption made was that the functions $\alpha(I_4)$ and $\beta(I_4)$ previously determined for collagen fiber bundles could be used to describe the stress relaxation response of the collagen fibers in the MCL (See Sec. 3.5.b). We expect that, although the strain-dependent relaxation behavior could be adequately described using the same forms of $\alpha(I_4)$ and $\beta(I_4)$, the values of the constants that define these functions may be different.

When subjecting a nonlinear elastic specimen to shear, tractions must be applied on all of its inclined faces in order to maintain a homogeneous shear deformation [69, 91] and, therefore, the normal stresses are non-zero (Figures 4.5 and 4.7). The experimental apparatus used to perform the shear test cannot provide all of the normal tractions required to maintain a homogeneous strain field. Altering the specimen aspect ratio and clamping pressure can minimize inhomogeneities in the strain field [83, 92] but only for small shear strains can a relatively homogeneous shear be produced without supplying the required normal stresses. One possible method to account for these inhomogeneities is to use optical techniques such as digital image correlation (DIC) to capture the spatial variation in the strain field [93].

5

Characterization of the Stress Relaxation Response of Swine Cardinal Ligaments using SAXD

5.1 Introduction

Pelvic floor disorders such as pelvic organ prolapse and urinary incontinence affect one in three adult women and represent a major public health concern [94, 95]. In the United States alone, more than 400,000 women undergo surgery for pelvic organ prolapse or urinary incontinence with an annual cost of more than one billion dollars [8, 96]. While the etiology of pelvic floor disorders is almost certainly multifactorial, aging and the hormonal changes that accompany menopause likely play a role as most women only become symptomatic over the age of 50 [97]. Epidemiological studies indicate that the structural and mechanical alterations that occur during pregnancy and delivery may damage the vagina, uterus, and the cardinal and uterosacral ligaments which support them (Figure 5.1) [98]. In fact, a recent imaging study has shown that in more than 85% of pelvic organ prolapse cases the cardinal and uterosacral ligaments are lax [99, 100], supporting the hypothesis that biomechanical changes in these suspensory ligaments is a critical factor in the progression of pelvic floor disorders. Biomechanical studies on the structural and mechanical changes these ligaments undergo due to pregnancy and aging are necessary to gain a better understanding of the mechanisms that lead to pelvic floor disorders and improve clinical intervention.

A small number of studies have attempted to measured the gross mechanical properties of the cardinal and uterosacral ligaments. The quasi-static failure properties of the uterosacral ligament in uniaxial tension have been measured using tissues collected from elderly female cadavers with no sign of pelvic floor disorder [17, 19] and Cynomolgus monkeys [20]. Similar to skeletal ligaments, the uterosacral ligament displayed a nonlinear elastic stress-strain response, including toe, linear, and failure regions (See Figure 2.2). The only study to date on the mechanical properties of the cardinal ligament quantified the quasi-static failure prop-

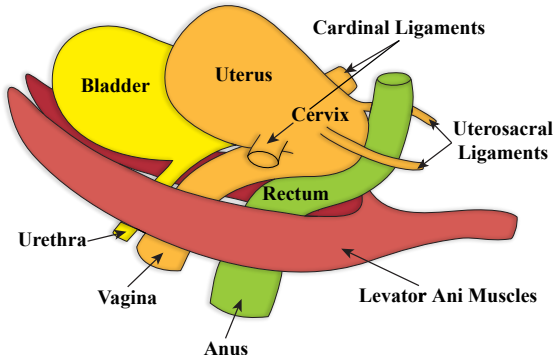

Figure 5.1: Schematic of the pelvic floor viewed from the side, with the cardinal ligaments identified.

erties of the swine cardinal ligament in uniaxial tension (See Appendix B). However, none of these mechanical experiments have attempted to investigate the viscoelastic response of the cardinal ligaments. Furthermore, the relationship between the structure and mechanical response of these suspensory ligaments has yet to be explored.

The purpose of this study is to investigate the stress relaxation response of the swine cardinal ligament. First, the gross stress relaxation response of the swine cardinal ligament is studied by performing uniaxial stress relaxation tests on swine cardinal ligaments at multiple levels of axial stretch. The experimental protocol was designed to determine whether the rate of relaxation is dependent on the applied stretch in the swine cardinal ligament. Second, in an attempt to learn more about the structural mechanisms that facilitate stress relaxation in the cardinal ligament, incremental stress relaxation tests were coupled with time-resolved small angle x-ray diffraction studies. Specifically, changes in the collagen fibril strain and orientation during a macro-scale incremental stress relaxation tests are measured.

5.2 Materials and Methods

5.2.a Sample dissection

Cardinal ligaments were obtained from five pregnant sows (234.6 $\pm$ 17.4 kg, body mass) which gave birth immediately before they were sacrificed. The animals were acquired from an unrelated study in accordance with an approved Virginia Tech IACUC protocol. Immediately after death, the cardinal ligaments were removed from the sow. First, the skin, adipose tissue, and muscle in the lower abdomen were cut to reveal the pubic symphysis. Next, a hack saw

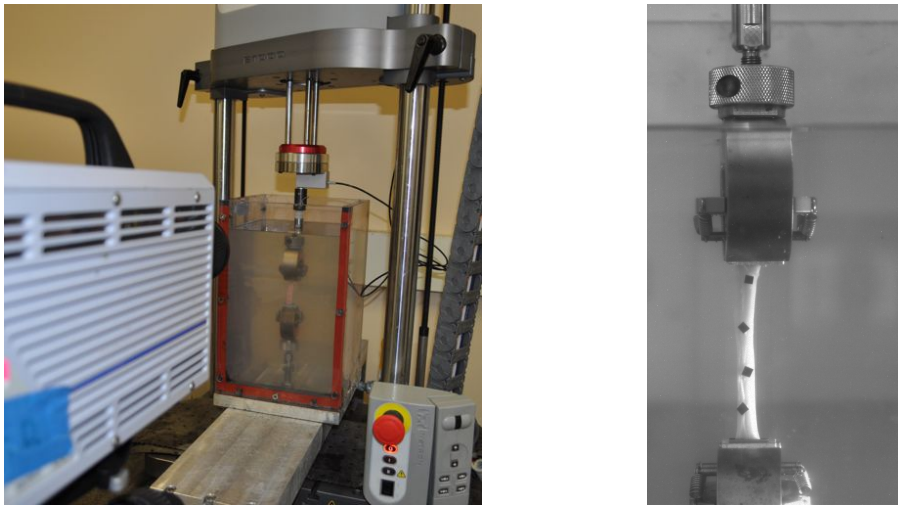

(a) (b)

Figure 5.2: Images of the test setup: (a) the tensile testing machine, camera, and hydration bath and (b) a representative image captured during the stress relaxation test.

was used to split the pubic symphysis and a rib spreader was inserted to open the pelvis so that the vagina, rectum, and bladder were clearly visible. Using a scalpel, the vagina, rectum, and bladder were extracted from the abdominal cavity as a unit. Then, the bladder and rectum were carefully dissected away from the vagina and discarded. The vagina was laid flat on a dissection table and any excess adipose tissue was removed from the cardinal ligaments. Finally, the cardinal ligaments were separated from the vagina and cut into rectangular strips approximately 7 mm wide by 115 mm long. These strips were oriented so that the physiologic loading direction coincided with the long axis of the sample. The samples were individually wrapped in plastic and stored frozen (-20 °C).

5.2.b Stress relaxation tests

One hour before testing the samples were removed from the freezer and allowed to come to room temperature. Images of each sample were collected using a stereo-microscope (Stemi 2000C, Zeiss) and the width of each specimen was measured at five locations using ImageJ (v. 1.44, National Institutes of Health). Digital calipers instrumented with a force gauge were employed to measure the thickness of each specimen at five locations under a 50 gf compressive load (Mitutoyo 573-291-20). Assuming a rectangular cross-section, the area for each specimen was calculated using the average width and thickness. To optically measure the axial stretch, four black plastic markers were adhered to the surface of the ligament using a drop of cyanoacrylate glue (Figure 5.2b).

Following application of the black plastic markers, the ends of each specimen were wrapped with sandpaper and mounted in a tensile testing machine (ElectroPuls E1000, Instron; 50 N load cell with a resolution of ± 0.05 N) equipped with a hydration bath (Figure 5.2a). A total of 25 stress relaxation tests were performed. Each sample was pre-loaded to 0.1 N and allowed to recover for two minutes. Then, the samples were stretched at 0.75 mm/sec up to different displacements corresponding to 8 mm ($n = 8$), 10 mm ($n = 3$), 13 mm ($n = 9$), or 15 mm ($n = 4$) and held for 5 minutes for stress relaxation testing. During each test, load, displacement, and camera images (Photron Ultima APX-RS; resolution 512 x 1024) were simultaneously captured at 10 Hz using BlueHill (v. 2.14, Instron). The motion of the black markers was tracked using image analysis software (ProAnalyst v. 1.5.3, Xcitex) and the average axial stretch, λ_z, over the gauge length was computed using a custom script in MATLAB (v. 7.12, MathWorks). The nominal axial stress, $\sigma(t)$, was calculated by dividing the load by the measured cross-sectional area.

After determining the nominal axial stress and average axial stretch, the data were plotted on a log-log scale and fit to a power law relationship:

$$\sigma(t) = \sigma_0 \, t^{-n} \tag{5.1}$$

where σ_0 is the initial nominal axial stress ($\sigma(t = 0)$), and n is the slope of the stress-time curve on a log-log scale. In line with previous studies on the stress relaxation response of ligaments [32, 33], n is termed the rate of stress relaxation. To fit the experimental data to Eq. (5.1), the nominal axial stress was first normalized by taking $\sigma(t)/\sigma_0$. Then, the log of the normalized stress and the log of the time were curve fit using a linear regression model to determine the rate of stress relaxation, n.

5.2.c Small angle x-ray diffraction (SAXD) measurements

Simultaneous incremental stress relaxation and diffraction experiments were performed on cardinal ligament specimens at the Advanced Photon Source on ID-18 (BioCAT) at Argonne National Laboratory (Lemont, IL). The diffraction experiments were performed with a focused beam size of 150 μm by 50 μm at a wavelength of 1.033 Å. Two dimensional x-ray diffraction frames were collected using a MAR CCD detector (MARCCD165, Rayonix LLC) with 2048 x 2048 pixel resolution. To calibrate the sample to detector distance (2.585 m) as well as the beam center location ($x = 1176$ pix, $y = 985$ pix) a silver behenate standard was used [101]. A schematic of the beamline setup is shown in Figure 5.3a.

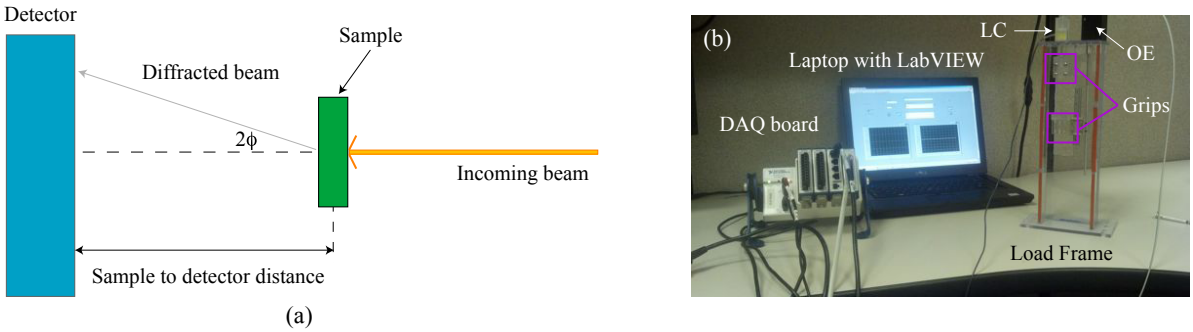

Figure 5.3: (a) Schematic of the beamline setup showing the scattering angle, ϕ, and (b) the custom load frame used to perform the incremental stress relaxation tests where LC, is the load cell and OE, is the optical encoder.

Tensile Testing Load Frame and Experimental Protocol

The specimens subjected to simultaneous diffraction and incremental stress relaxation tests were thawed at room temperature for one hour before the testing began. The width and thickness of each sample were determined at five locations using calipers and the area was computed from the average width and thickness assuming a rectangular cross-section. The ends of each sample were wrapped in sandpaper and placed in a custom load frame designed to fit within the space constraints on the beamline (Figure 5.3b). Sample hydration was maintained in the load frame by sandwiching the sample between two sheets of Kapton film wetted with PBS.

The custom load frame used to perform the incremental stress relaxation tests incorporates a 8.9 N load cell (LSB 200, Futek) with a resolution of ± 0.01 N and a linear optical encoder (Linear Probe Encoder, US Digital) with a total travel of 50.8 mm and a resolution of ± 50 μm to measure sample load and displacement, respectively. A micro-scale linear actuator (T-NA Series, Zaber Technologies) with ± 8 μm accuracy was employed to stretch the specimens. A custom code in LABVIEW (v. 8.2, National Instruments) was written to record the load and displacement data at 20 Hz during the relaxation tests.

Five samples were subjected to the incremental stress relaxation tests, each sample was preloaded to 0.02 N and allowed to recover for 75 s. Next, an incremental displacement of 5 mm was applied at a rate of 2 mm/s and the sample was allowed to relax for 100 s. Two additional incremental displacements of 5 mm, each with a corresponding relaxation time of 100 s, were performed to obtain a total of three incremental stress relaxation levels per sample. Small angle x-ray diffraction frames were collected immediately prior to the first step of the incremental stress relaxation test and every 10 s thereafter with an exposure time of 0.5 s for the duration of the incremental stress relaxation test. The average axial stretch, λ_z, over the gauge length of the sample was computed by dividing the current length by

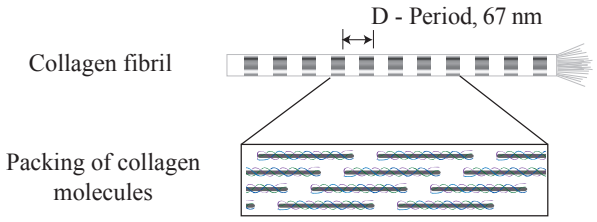

Figure 5.4: Structure of a collagen fibril.

the initial length. The nominal axial stress, $\sigma(t)$, was found by dividing the load by the measured cross-sectional area.

Analysis of Small Angle X-Ray Diffraction (SAXD) Patterns

Fibrillar collagen is a highly ordered hierarchical structure; Type I collagen molecules self-assemble into a quarter staggered packing arrangement resulting in a banded repeat that occurs every 67 nm known as the D-period [24] (Figure 5.4). The resulting SAXD pattern of Type I collagen shows meridional reflections that correspond to harmonic frequencies of this intrinsic spacing (67 nm, 67/2 nm, 67/3 nm ... $67/m$ nm) where m is an integer (Figure 5.8). The meridional reflections are identified by their order, m, for example, the reflection at 67/3 nm is referred to as the third order meridional reflection. The average strain state of the collagen fibrils imaged by the beam can be determined from the SAXD pattern by measuring changes in the location of these meridional reflections, which are indicative of changes in the D-period spacing. Information on the preferred orientation of collagen can also be identified from the SAXD frames by analyzing the intensity distribution of a single reflection. By correlating the data obtained from the incremental stress relaxation tests(λ_z and $\sigma(t)$) with the data on collagen fibril strain and orientation obtained from the diffraction images, the structural changes occurring at the fibril level can be related to the macroscopically measured stresses (or stretches).

The time series of diffraction frames collected during the incremental stress relaxation tests were analyzed for changes in the D-period spacing of the third and fifth order reflections of collagen using FIT2D software (v. 12.80, Andy Hammersly/ESRF) and a custom code developed by Sector 1 at the Advanced Photon Source in MATLAB. A one-dimensional profile of the scattering intensity versus the scattering angle, ϕ, was generated for each diffraction frame using the CAKE and INTEGRATE functions in FIT2D with an angular range of 360°, a radial range of 0 to 500 pixels and setting the number of azimuthal bins to 1. In the one dimensional profiles of scattering intensity versus scattering angle (Figure

5.9), the diffraction peaks observed in the profile arise from the hierarchical structure of collagen. Each observed peak (Figure 5.9) corresponds to the meridional reflections seen in the diffraction frames (Figure 5.8).

Using the custom MATLAB code, the diffraction peaks corresponding to the third and fifth order reflections for collagen in the one dimensional intensity profile were fitted to a Gaussian function, where the baseline of the curve is assumed to be linear. The equation for a Gaussian function with a linear baseline has the form:

$$y(\phi) = A \exp\left[-\left(\frac{\phi - \phi_0}{w}\right)^2\right] + B_1 + B_2\phi \tag{5.2}$$

where $y(\phi)$ is the fitted value of the scattering intensity, ϕ is the scattering angle, ϕ_0 is the peak position, A is the scattering intensity at the peak position, w is the width of the peak, and B_1 and B_2 are two parameters that account for the linear baseline. The peak position, ϕ_0, is related to the D-period spacing of collagen, d, through Bragg's law which states that $m\lambda = 2d\sin\phi$, where m is the integer that identifies the order of the peak and λ is the wavelength of the beam ($\lambda = 1.033$ Å). The changes in the D-period measured from the peak position, ϕ_0, can then be used to calculate the mean strain of the collagen fibrils defined as:

$$\varepsilon_f^{(m)}(t) = \frac{d^{(m)}(t) - d^{(m)}(t=0)}{d^{(m)}(t=0)} \tag{5.3}$$

where $d^{(m)}(t = 0)$ is measured from the last diffraction frame collected before the first incremental stress relaxation test begins. To determine how the strain state of the collagen fibrils changes during an incremental stress relaxation test, the mean fibril strain, $\varepsilon_f^{(m)}$, was plotted along with the tissue level nominal axial stress, $\sigma(t)$, versus time for each of the incremental stress relaxation tests.

To discern if the orientation of the collagen fibrils changes during the incremental stress relaxation tests, a one dimensional profile of integrated scattering intensity versus angular position, θ, was generated for each diffraction frame using the CAKE and INTEGRATE functions in FIT2D with an angular range of 360°, a radial range that corresponds to an annulus about the third meridional reflection and setting the number of radial bins to 1. The one-dimensional profile obtained was then normalized by the maximum value of the scattering intensity and plotted as a function of the angular position, θ. To visually inspect if the preferred orientation changes from either an applied stretch (change in relaxation strain level) or during the stress relaxation test, the fibril orientation distribution was plotted at seven times: before the start of the tests, after each incremental displacement of 5 mm was applied, and at the end of each incremental stress relaxation test.

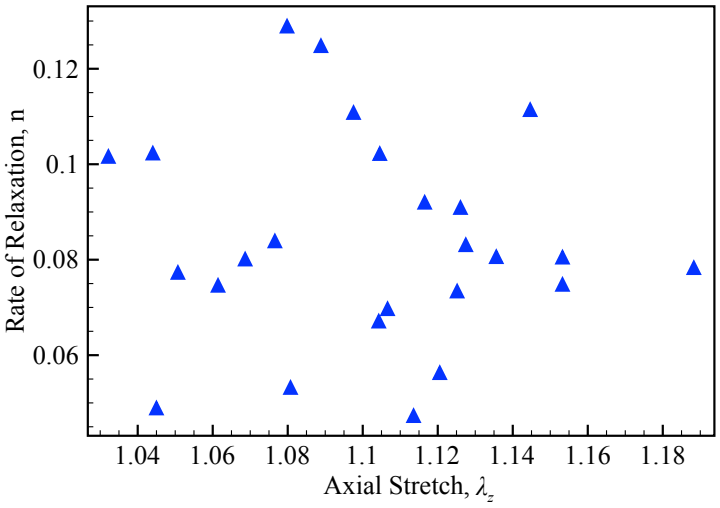

Figure 5.5: The rate of stress relaxation, n, as a function of the relaxation stretch level, λ_z. There is no clear trend in the rate of relaxation with respect to the applied axial stretch.

5.3 Results

5.3.a Stress relaxation response

To study the influence of the stretch level on the stress relaxation response of cardinal ligaments, the test samples were subjected to displacements between 8 and 15 mm. These values of the displacement were selected based on preliminary uniaxial tension tests to failure (See Appendix B) which found that the cardinal ligament began to fail at axial stretches between 1.13 - 1.18. For the twenty-five stress relaxation tests performed, the measured values of axial stretch, λ_z, varied from 1.03 to 1.19. In Figure 5.5, the relaxation rate was plotted versus the axial stretch. However, no clear trend in the data was observed and it was not possible to identify if the cardinal ligament exhibits stretch (or strain) -dependent stress relaxation behavior.

A trend was observed in how the relaxation behavior changes as function of the initial nominal stress. A plot of the rate of relaxation, n, as a function of the initial nominal stress, σ_0, is shown in Figure 5.6a. Notice that the rate of relaxation increased from 0.047 for an initial nominal stress of 65 kPa to 0.129 for an initial nominal stress of 87 kPa but, for larger stresses the rate of relaxation approaches a constant value of 0.078. Five representative points are also highlighted in Figure 5.6a and the normalized stress relaxation response for each of the highlighted samples is plotted in Figure 5.6b.

Statistical analysis was used to test the null hypothesis that there is no association between the initial nominal stress and the rate of relaxation. By performing a segmented analysis of

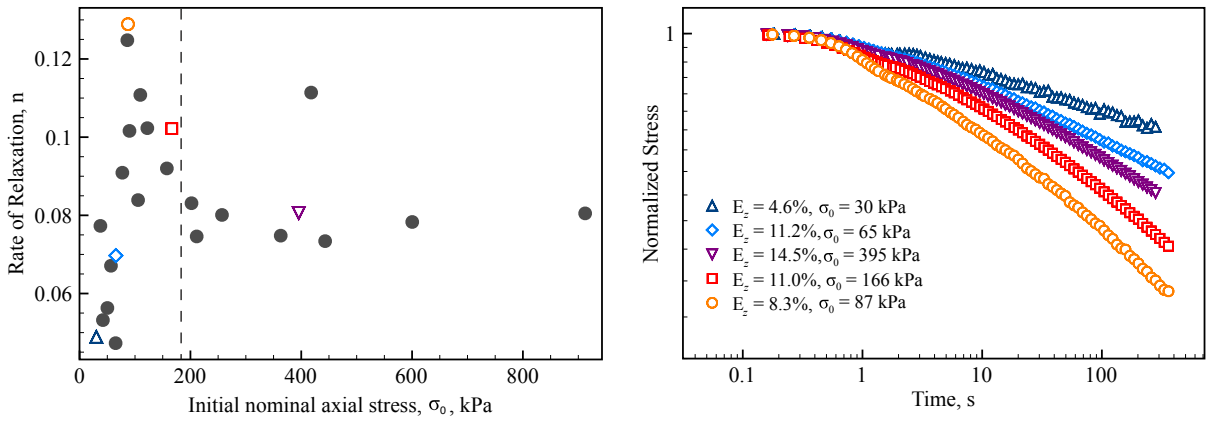

(a) (b)

Figure 5.6: The (a) rate of stress relaxation, n, as a function of the initial nominal stress with five representative samples highlighted where the rate of relaxation is determined from Eq. (5.1) and (b) the normalized stress relaxation response for the five highlighted samples. In the first segment, the rate of stress relaxation is associated with the initial nominal stress ($p = 0.012$). However as the initial nominal stress increases the rate of relaxation becomes steady ($n \approx 0.078$) and the rate of relaxation and the initial nominal stress are no longer correlated ($p = 0.96$).

covariance (ANCOVA), it was possible to account for the two distinct regions observed in Figure 5.6a. No a priori assumption was placed on the location of transition point between these regions, instead the segmented ANCOVA was run multiple times varying the transition point from 87 kPa to 211 kPa. The null hypothesis was rejected if the p-value was less than 0.05. The p-values for the segmented ANCOVA when the transition occurred at 166 kPa were 0.012 for the first segment and 0.96 for the second segment (Figure 5.6a). Selecting 166 kPa as the transition point produced the largest first segment where the null hypothesis was rejected and for all transition points less than 166 kPa the null hypothesis was always rejected.

5.3.b Simultaneous SAXD and stress relaxation tests

Tissue Level Stress Relaxation Response

For the samples that were subjected to simultaneous diffraction and stress relaxation tests the applied displacements ranged between 5 – 15 mm. The corresponding values of axial stretch, λ_z, varied from 1.06 to 1.17. For three samples the first applied stretch resulted in an exceptionally low load, in those cases the data from the first stretch was discarded.

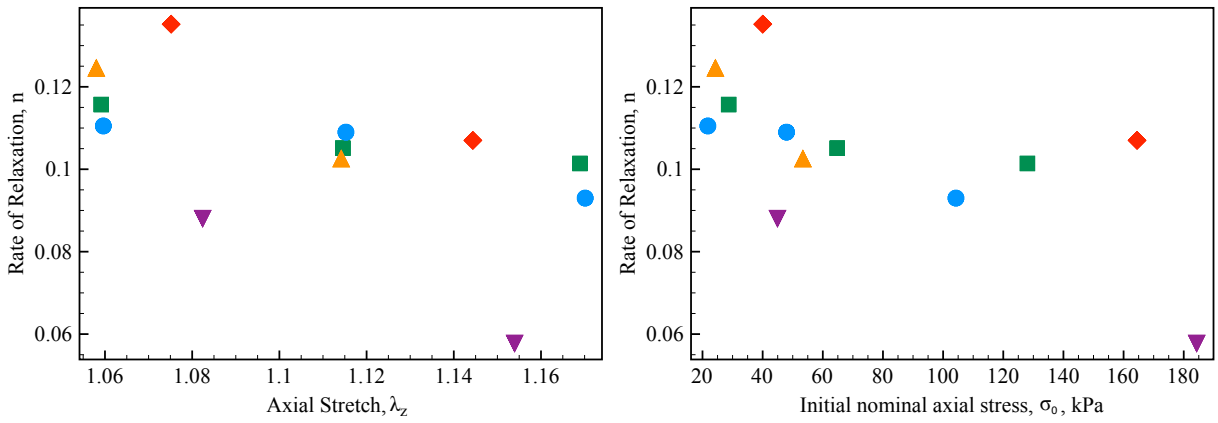

(a) (b)

Figure 5.7: (a) Rate of stress relaxation, n, as a function of the applied axial stretch, λ_z and (b) rate of stress relaxation, n, as a function of the initial nominal stress for the samples subjected to simultaneous small angle x-ray diffraction and increment stress relaxation test.

Similar to the previously described stress relaxation tests, the relaxation rate is plotted versus the applied axial stretch and initial nominal stress (Figure 5.7). Data points from the same sample are labeled with the same shape and color. In Figure 5.7a as the applied stretch increased, the rate of relaxation tended to decrease. Within each sample, as the initial nominal stress increased the rate of relaxation decreased, however the overall trend is less clear (Figure 5.7b). Due to the limited number of samples statistical analysis was not performed.

SAXD

An example of the diffraction images collected are shown in Figure 5.8. Differences can clearly be observed between the frame collected before the incremental stress relaxation test began (Figure 5.8a) and the frame collected at the end of the third incremental stress relaxation test (Figure 5.8b). Changes in the intensity and shape of diffraction pattern are seen in all of the observed rings. The blocks in Figure 5.8 point out the first, third, and fifth order meridional reflections of collagen. Note that the beam stop overshadows the first-order reflection and the second and fourth order reflections are weak. This is expected for collagen and led us to rely on the measurements from the third and fifth order reflections to describe changes in collagen fibril strain and orientation [102, 103].

In Figure 5.9, a one dimensional profile of scattering intensity as a function of scattering angle, ϕ, is shown for the two diffraction images in Figure 5.8. Again for clarity, the positions of the third and fifth order reflections of collagen are marked. It is clear that the baseline

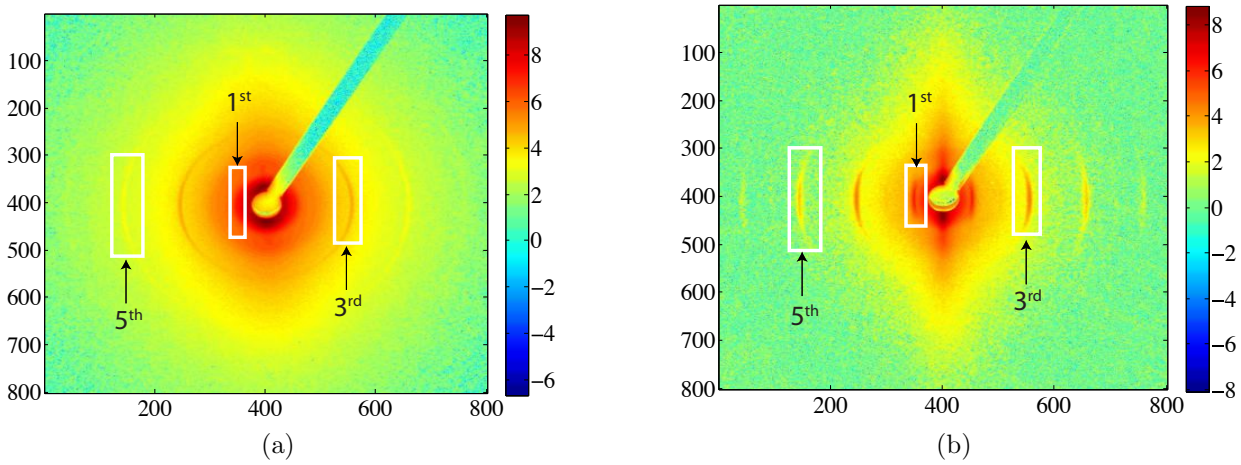

Figure 5.8: X-ray diffraction patterns of swine cardinal ligaments (a) captured prior to the start of the relaxation test (unloaded) and (b) captured the end of the third step of the incremental stress relaxation test. The color scale maps the log of the scattering intensity at each point. The first, third, and fifth order meridional reflections are marked in each image.

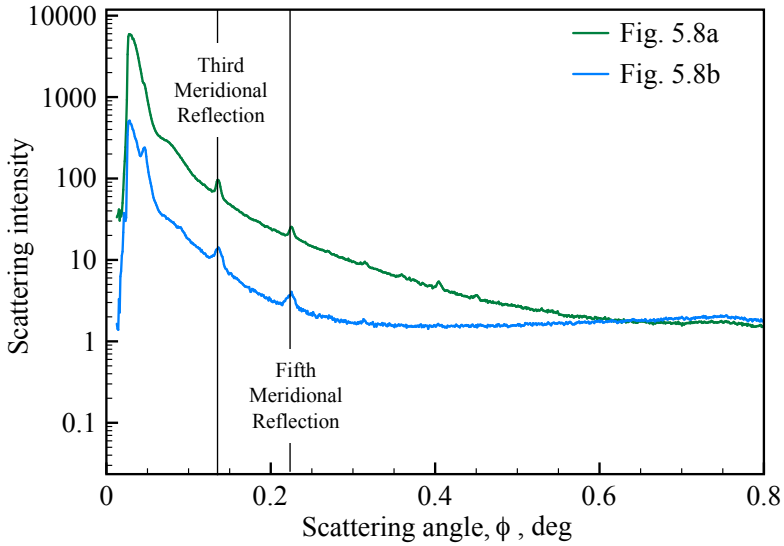

Figure 5.9: Scattering intensity as a function of the scattering angle, ϕ, in degrees, where the profiles are obtained from Figures 5.8a and 5.8b. The third and fifth meridional reflections for collagen are labeled. Note that the plot scale is semi-log y.

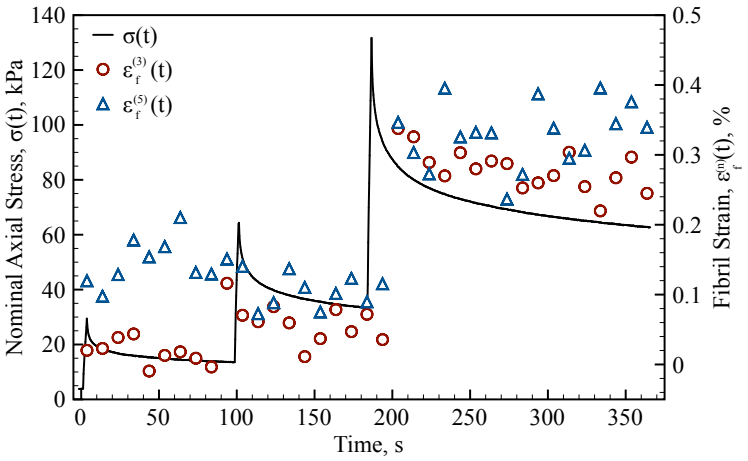

Figure 5.10: Plot of the incremental stress relaxation response (line, left y -axis) and the corresponding changes in the fibril strain, $\varepsilon_f^{(m)}(t)$, (points, right y-axis) measured from the third (○) and fifth (△) meridional reflections of collagen versus time for a representative sample. The axial strain, $E_z = \frac{\lambda_z^2 - 1}{2}$, applied at the tissue level for the three relaxation levels are 6.1%, 12.1%, and 18.3%, respectively.

of the one dimensional profile is not flat, justifying the use of linear function to describe the baseline in Eq. 5.2. The actual measured spacing for the third and fifth order reflections are 65.2 and 65.6 nm for Figure 5.8a and 65.4 and 65.8 nm for Figure 5.8b. These values were confirmed using a rat tail tendon standard, where the measured spacing was 66.7 and 67.0 nm for the third and fifth order reflections, respectively.

Nano-scale Response of the Collagen Fibrils

Changes in the collagen fibril strain computed from Eq. 5.3 were measured throughout the incremental stress relaxation tests. In Figure 5.10, the tissue level axial stress (left y -axis) and the fibril level strain (right y-axis) are both plotted versus the time. The strain induced at the fibril level by applying a stretch at the tissue level was much smaller than the tissue level strain. For example, at a tissue level strain of 18.3% for the third incremental stress relaxation test the strain at the fibril level was only 0.34%. Sharp changes in $\varepsilon_f^{(3)}(t)$ were observed when the second and third axial stretch were applied. However for the first stretch the fibril strain remains very close to zero. For the fibril strains measured from the fifth meridional reflection, when the first and third axial stretches were applied there was a sharp increase in $\varepsilon_f^{(5)}(t)$. The values of the fibril strain for both $\varepsilon_f^{(3)}(t)$ and $\varepsilon_f^{(5)}(t)$ remained relatively steady when the tissue level axial strain (stretch) was held constant.

The angular distribution of the collagen fibrils for a representative sample was determined

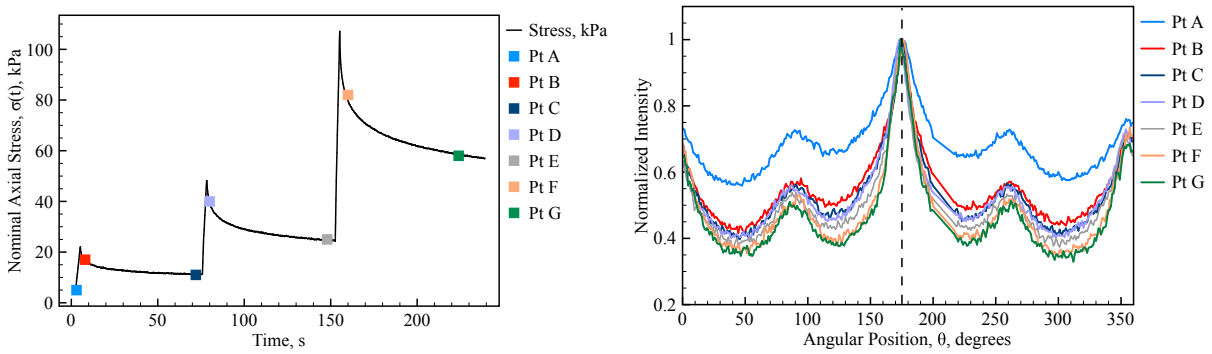

(a) (b)

Figure 5.11: (a) Plot of the tissue level incremental stress relaxation response for a representative sample with the times that were analyzed to find the orientation of the collagen fibrils marked. (b) Corresponding plots of normalized scattering intensity as a function of angular position, θ, for the points labeled in (a). Note that the dashed vertical black line shows the direction of loading for the stress relaxation test. To obtain the plots of normalized intensity as a function of angular position, the diffraction frames were integrated over small constant range of r, $147.88 < r < 164.80$ pix, which is the region for the third order reflection of collagen.

at the seven times pictured in Figure 5.11a: before the start of the test (Pt A), after each incremental displacement of 5 mm was applied (Pt B, Pt D, Pt F), and at the end of each incremental stress relaxation test (Pt C, Pt E, Pt G). The normalized scattering intensity as a function of angular position is shown in Figure 5.11b for the selected times. For reference, a horizontal line of uniform intensity indicates an isotropic array of collagen fibrils. When the collagen fibrils are preferentially aligned, the plot of scattering intensity versus angular position has a peak centered at the angle(s) of preferred orientation.

There is clearly a variation in the normalized scattering intensity as function of angular position at all times showing that the collagen fibrils in the tissue are equally spaced at 90°. As an increasing number of collagen fibrils become aligned with the loading direction, the widths of the peaks at 180° and 360° decrease while the overall height of the peaks increases. The most significant changes in fibril orientation occur after the first stretch is applied, between Pt. A and Pt. B. The changes that occur during stress relaxation and due to each subsequently applied stretch are small. However, it is clear that the collagen fibrils continue to reorient towards the loading direction throughout the incremental stress relaxation test.

5.4 Discussion

The gross stress relaxation response of the cardinal ligament was examined over a broad range of axial stretches (1.03 - 1.18). Due to large specimen to specimen variability determining whether the cardinal ligament exhibits stretch-dependent stress relaxation behavior was not possible. To clarify the type of viscoelastic behavior (linear, quasi-linear, nonlinear) exhibited by the cardinal ligament incremental stress relaxation tests must be preferred over direct stress relaxation tests. Although the stress relaxation behavior studied by incremental stress relaxation tests may be affected by the history of incremental strains (or stretches) used during testing [31, 77], it allows scatter in the data due to inter-specimen variability to be minimized. This variability is believed to be the reason why no relationship is observed between the stretch level and rate of relaxation in Figure 5.5. To minimize the strain history effects during incremental stress relaxation testing, a recovery period of ten times the length of the stress relaxation test is suggested between each stretch [32, 33].

Cardinal ligaments are hierarchical structures and respond to loading through structural reorganization and deformation at all levels of their hierarchy. A robust understanding of the mechanical response of the cardinal ligament can only be obtained by characterizing the response at these different hierarchical length scales. In this study, we have measured the stress relaxation response at the tissue and fibril levels by simultaneously collecting x-ray diffraction and mechanical data. This is the first SAXD study completed on the cardinal ligament and one of only a handful of studies that performed SAXD and mechanical experiments concurrently [38, 39, 104]. Using the time series of diffraction images collected during an incremental stress relaxation test, the collagen fibril strain due a macroscopically applied stretch was measured (Figure 5.10). The relatively low magnitude of the collagen fibril strains suggests that the majority of the deformation must occur in the ground substance. Moreover, the strain of the collagen fibrils does not significantly change during stress relaxation indicating that the load is most likely dissipated in the ground substance. These observations agree with measurements made by Screen [41] and Gupta et al. [38] at the collagen fiber level using rat tail tendon fascicles. Both authors concluded that during stress relaxation load is dissipated by fiber sliding and increasing shear in the matrix.

The use of SAXD also allowed the orientation of the collagen fibril reinforcement within the cardinal ligament to be measured for the first time. While the reorientation of collagen fibrils due to an stretch applied at the tissue level is well documented [104], the changes in collagen fibril orientation during stress relaxation have not been well studied. Throughout the stress relaxation test an increasing number collagen fibrils become aligned with the stretching direction (Figure 5.11). The mechanism driving this internal rearrangement of the collagen fibril network is unknown.

One limitation of this study was the strain measurement techniques used. First, the use of a

cyanoacrylate glue to adhere plastic markers to the specimen may have introduced errors in the strain measurement. The effect of the glue is expected to minimal since cyanoacrylate glue does not diffuse into the tissue and remains on the surface [105]. In addition, the effect of the glue is localized and as such should have a minimal impact on the average strain measurement over the gage length of the specimen. Second, it is not currently possible to directly compare the strains measured from the gross stress relaxation tests to those measured during the diffraction experiments since the strain measurement techniques differed. An image based technique was not utilized to measure the axial stretch during the diffraction experiments as the use of vacuum tubes, which reduce noise due to air scattering in the diffraction frames, made it impractical to install a camera.

For this study the porcine animal model was used to quantify the viscoelastic properties of the cardinal ligament. Non-human primates have the pelvic anatomy that is most similar to humans. Despite this advantage, the low availability and high expense in maintaining a primate colony has led us to seek a more cost effective animal model to study the development of pelvic floor disorders. The swine model was selected because sows develop spontaneous pelvic organ prolapse [106, 107] and the swine vagina and supportive connective tissues are very similar in structure to the human pelvic anatomy [106]. As a consequence of the fact that humans walk upright, the levator ani muscles in the pelvic floor (Figure 5.1) perform different functions in humans and swine [108, 109]. The levator ani muscles in humans play a role in pelvic support whereas for animals with a tail, such as swine, the levator ani muscles primarily control the motion of the tail [109]. This change in the role of the musculature combined with the fact that humans are bipedal means that the loads (or strains) experienced by cardinal ligament in swine is most likely different than those experienced by human cardinal ligaments [108].

This experimental study represents an important step towards developing a comprehensive understanding of the mechanical properties of the cardinal ligament. In the future, additional experimental studies must be performed on nulliparous and non-pregnant multiparous sows in order to identify the changes in mechanical properties of the cardinal ligament that are associated with pregnancy and parity. Currently only the passive response of the cardinal and uterosacral ligaments has been evaluated. To fully understand how these ligaments respond to loads *in vivo* it will be necessary to investigate how the contractile level of the smooth muscle cells within these ligaments contribute to the mechanical response.

6 Future Work

In this dissertation, the stress relaxation behavior of skeletal and suspensory ligaments has been discussed with the aim of using this information to improve surgical repairs. For skeletal ligaments, whose mechanical properties have been well characterized in the literature, constitutive models for strain-dependent stress relaxation response of collagen fiber bundles (Ch. 3) and the three-dimensional stress relaxation response of skeletal ligaments (Ch. 4) were proposed. For suspensory ligaments, the relationship between structure and mechanical response of the cardinal ligament was examined by carrying out simultaneous stress relaxation and x-ray diffraction experiments at Argonne National Laboratory (Ch. 5). The results of these studies into the stress relaxation behavior of ligaments suggested several research projects that can be carried out in the future.

Study the shear response of ligaments. In Chapter 4, a three dimensional model for the stress relaxation behavior of the skeletal ligaments was proposed. As a first step towards validation, the model prediction for stress relaxation when a ligament is sheared in the fiber direction was compared with published experimental data on the shear response of the medial collateral ligament (Sec. 4.4.a). However, the experimental apparatus used to perform the shear tests was not designed to apply all of the normal stresses necessary to maintain a homogeneous shear deformation [35]. Further study of ligament shear behavior is needed to determine if this experimental setup is valid approximation of simple shear in the fiber direction. The two dimensional strain field on the surface of the ligament must be measured to determine if a semi-homogeneous region of constant shear strain exists. If a homogeneous shear strain is not produced, an alternative method must be developed to perform the shear tests. Other experimental protocols have been suggested to perform shear test on rubbers [91] which might be adapted to soft tissues.

Additional experimental studies on the elastic and stress relaxation response of ligaments subjected to simple shear in the fiber direction would also provide much needed information on the mechanical response of the ground substance. Several investigators have suggested that load may be transferred within ligaments and tendons by shearing the ground substance

[38, 40, 41] highlighting the importance of understanding the mechanical response of the ground substance in shear.

Refine SAXD experiments. The small angle x-ray diffraction studies discussed in Chapter 5 could be refined in several ways. First, the incremental stress relaxation tests could include a long recovery period between each test. Complete recovery of rat and rabbit MCLs has been reported when the samples were allowed to recover for ten times the length of the relaxation test between stretches [32, 33]. During this time, the sample could be removed and allowed to recover in a fluid bath. Second, the data collection rate for the x-diffraction frames should be increased. The setup described in Section 5.2.c was limited and could only collect diffraction frames every 10 seconds (0.1 Hz). Additional structural data on the the early stages of the stress relaxation response, where the force changes most rapidly, could be captured by installing the specialized fast capture setup at BioCAT (ID-18). The fast capture setup allows diffraction frames to be captured with a time resolution of approximately 1 Hz. Third, thorough hydration studies need to be conducted. Although the ligament is sandwiched between two Kapton sheets wetted with PBS forming a mini-fluid bath during testing, it is possible that the mini-bath is insufficient to maintain the sample hydration for the entire test. To determine if any of the measured changes in fibril strain are due to dehydration, x-ray diffraction frames of unloaded samples should be collected over a period of three times the relaxation time. Finally, incremental stress relaxation studies must be repeated on the beamline with the shutter closed (no beam). Comparing the data collected with shutter open and the shutter closed will provide convincing mechanical evidence that the use of x-ray diffraction does not alter the mechanical properties.

Explore the effect of pregnancy, parity, and aging. The mechanical studies described in Chapter 5 were conducted on cardinal ligaments collected from full term multiparous sows that gave birth immediately before they were euthanized. At this point it is unclear how or if pregnancy and delivery affect the mechanical properties of the cardinal ligament. In humans, it has been reported that age [97] and parity [98] are critical risk factors for the development pelvic floor disorders. But, again their influence on the mechanical properties of the cardinal ligament is unknown. The elastic and viscoelastic properties of the cardinal ligaments in young nulliparous sows and older multiparous sows at multiple times Such a longitudinal study of the mechanical properties may help elucidate the role suspensory ligaments play in the development and progression of pelvic floor disorders. Furthermore, this information is essential for developing early stage interventions and improving surgical protocols to repair pelvic organ prolapse.

Bibliography

[1] Griffin, L., Agel, J., Albohm, M., Arendt, E., Dick, R., Garrett, W., Garrick, J., Hewett, T., Huston, L., and Ireland, M., 2000. "Noncontact anterior cruciate ligament injuries: risk factors and prevention strategies". *Journal of the American Academy of Orthopaedic Surgeons,* ***8***(3), pp. 141–150.

[2] Hauser, R., Dolan, E., Phillips, H., Newlin, A., Moore, R., and Woldin, B., 2013. "Ligament injury and healing: A review of current clinical diagnostics and therapeutics". *Open Rehabilitation Journal,* ***6***, pp. 1–20.

[3] Benhardt, H., and Cosgriff-Hernandez, E., 2009. "The role of mechanical loading in ligament tissue engineering". *Tissue Engineering Part B: Reviews,* ***15***(4), pp. 467–475.

[4] Khan, R. J. K., Fick, D., Brammar, T. J., Crawford, J., and Parker, M. J., 2004. "Interventions for treating acute Achilles tendon ruptures". In *The Cochrane Library*, Vol. 3. Chichester, UK: John Wiley & Sons, Ltd.

[5] Jozsa, L., and Kannus, P., 1997. "Histopathological findings in spontaneous tendon ruptures". *Scandinavian Journal of Medicine and Science in Sports,* ***7***(2), pp. 113–118.

[6] Schein, A., Matcuk, G., Patel, D., Gottsegen, C. J., Hartshorn, T., Forrester, D., and White, E., 2012. "Structure and function, injury, pathology, and treatment of the medial collateral ligament of the knee". *Emergency Radiology,* ***19***, pp. 489–498.

[7] Cvach, K., and Dwyer, P., 2012. "Surgical management of pelvic organ prolapse: abdominal and vaginal approaches". *World Journal of Urology,* ***30***, pp. 1–7.

[8] Subak, L., Waetjen, L., van den Eeden, S., Thom, D., Vittinghoff, E., and Brown,

J., 2001. "Cost of pelvic organ prolapse surgery in the United States". *Obstetrics & Gynecology,* ***98***(4), pp. 646–651.

[9] Magnussen, R. A., Glisson, R. R., and Moorman, C. T., 2011. "Augmentation of Achilles tendon repair with extracellular matrix xenograft". *The American Journal of Sports Medicine,* ***39***(7), pp. 1522–1527.

[10] Krackow, K. A., Thomas, S. C., and Jones, L. C., 1986. "A new stitch for ligament-tendon fixation". *The Journal of Bone and Joint Surgery (American),* ***68***, pp. 764 – 766.

[11] Speck, M., and Klaue, K., 1998. "Early full weightbearing and functional treatment after surgical repair of acute Achilles tendon rupture". *The American Journal of Sports Medicine,* ***26***(6), pp. 789–793.

[12] Willits, K., Amendola, A., Bryant, D., Mohtadi, N., Giffin, J., Fowler, P., Kean, C., and Kirkley, A., 2010. "Operative versus nonoperative treatment of acute Achilles tendon ruptures: A multicenter randomized trial using accelerated functional rehabilitation.". *The Journal of Bone and Joint Surgery (American),* ***92***(17), pp. 2767–2775.

[13] Bellemans, J., D'Hooghe, P., Vandenneucker, H., Damme, G. V., and Victor, J., 2006. "Soft tissue balance in total knee arthroplasty: Does stress relaxation occur perioperatively?". *Clinical Orthopaedics and Related Research,* ***452***, pp. 49–52.

[14] Pipkin, A. C., and Rogers, T. G., 1968. "A non-linear integral representation for viscoelastic behaviour". *Journal of the Mechanics and Physics of Solids,* ***16***(1), pp. 59–72.

[15] Rajagopal, K. R., and Wineman, A. S., 2009. "Response of anisotropic nonlinearly viscoelastic solids". *Mathematics and Mechanics of Solids,* ***14***(5), pp. 490–501.

[16] Weiss, J. A., Gardiner, J. C., Ellis, B. J., Lujan, T. J., and Phatak, N. S., 2005. "Three-dimensional finite element modeling of ligaments: Technical aspects". *Medical Engineering & Physics,* ***27***(10), pp. 845–861.

[17] Martins, P., Silva-Filho, A., Fonseca, A., Santos, A., Santos, L., Mascarenhas, T., Jorge, R., and Ferreira, A., 2012. "Strength of round and uterosacral ligaments: A biomechanical study". *Archives of Gynecology and Obstetrics.* 10.1007/s00404-012-2564-3.

[18] Reay Jones, N., Healy, J., King, L., Saini, S., Shousha, S., and Allen-Mersh, T., 2003. "Pelvic connective tissue resilience decreases with vaginal delivery, menopause and uterine prolapse". *British Journal of Surgery,* ***90***(4), pp. 466–472.

[19] Rivaux, G., Rubod, C., Dedet, B., Brieu, M., Gabriel, B., De Landscheere, L., Devos, P., Delmas, V., and Cosson, M., 2011. "Biomechanical characterisation of uterine

ligaments. Implications for the pelvic floor". *Pelvi-Perineologie,* ***6***(2), pp. 67–74.

[20] Vardy, M., Gardner, T., Cosman, F., Scotti, R., Mikhail, M., Preiss-Bloom, A., Williams, J., Cline, J., and Lindsay, R., 2005. "The effects of hormone replacement on the biomechanical properties of the uterosacral and round ligaments in the monkey model". *American Journal of Obstetrics and Gynecology,* ***192***(5), pp. 1741–1751.

[21] Kannus, P., 2000. "Structure of the tendon connective tissue". *Scandinavian Journal of Medicine and Science in Sports,* ***10***(6), pp. 312–320.

[22] Rowe, R., 1985. "The structure of rat tail tendon". *Connective Tissue Research,* ***14***(1), pp. 9–20.

[23] Scott, A., Cook, J. L., Hart, D. A., Walker, D. C., Duronio, V., and Khan, K. M., 2007. "Tenocyte responses to mechanical loading in vivo: A role for local insulin-like growth factor 1 signaling in early tendinosis in rats". *Arthritis & Rheumatism,* ***56***(3), pp. 871–881.

[24] Fung, Y. C., 1993. *Biomechanics, Mechanical Properites of Living Tissues*, 2nd ed. Springer-Verlag, New York.

[25] Martin, R. B., Burr, D. B., and Sharkey, N. A., 1998. *Skeletal Tissue Mechanics.* Springer-Verlag.

[26] Ilic, M., Carter, P., Tyndall, A., Dudhia, J., and Handley, C., 2005. "Proteoglycans and catabolic products of proteoglycans present in ligament". *Biochemical Journal,* ***385***, pp. 381–388.

[27] Legerlotz, K., Riley, G., and Screen, H., 2010. "Specimen dimensions influence the measurement of material properties in tendon fascicles". *Journal of Biomechanics,* ***43***(12), pp. 2274–2280.

[28] Hawkins, D., Lum, C., Gaydos, D., and Dunning, R., 2009. "Dynamic creep and pre-conditioning of the Achilles tendon in-vivo". *Journal of Biomechanics,* ***42***(16), pp. 2813–2817.

[29] Smutz, W., France, E., and Bloswick, D., 1995. "Measurement of creep strain of flexor tendons during low-force high frequency activities such as computer keyboard use". *Clinical Biomechanics,* ***10***(2), pp. 67–72.

[30] Pearson, S. J., Burgess, K., and Onambele, G. N. L., 2007. "Creep and the in vivo assessment of human patellar tendon mechanical properties". *Clinical Biomechanics,* ***22***(6), pp. 712–717.

[31] van Dommelen, J. A. W., Jolandan, M. M., Ivarsson, B. J., Millington, S. A., Raut, M., Kerrigan, J. R., Crandall, J. R., and Diduch, D. R., 2006. "Nonlinear viscoelastic

behavior of human knee ligaments subjected to complex loading histories". *Annals of Biomedical Engineering,* ***34***(6), pp. 1008–1018.

[32] Provenzano, P., Lakes, R., Keenan, T., and Vanderby, R., 2001. "Nonlinear ligament viscoelasticity". *Annals of Biomedical Engineering,* ***29***(10), pp. 908–914.

[33] Hingorani, R. V., Provenzano, P. P., Lakes, R. S., Escarcega, A., and Vanderby, R., 2004. "Nonlinear viscoelasticity in rabbit medial collateral ligament". *Annals of Biomedical Engineering,* ***32***(2), pp. 306–312.

[34] Duenwald, S. E., Vanderby, R., and Lakes, R. S., 2009. "Viscoelastic relaxation and recovery of tendon". *Annals of Biomedical Engineering,* ***37***(6), pp. 1131–1140.

[35] Bonifasi-Lista, C., Lakez, S., Small, M., and Weiss, J., 2005. "Viscoelastic properties of the human medial collateral ligament under longitudinal, transverse and shear loading". *Journal of Orthopaedic Research,* ***23***(1), pp. 67–76.

[36] Thornton, G. M., Frank, C. B., and Shrive, N. G., 2001. "Ligament creep behavior can be predicted from stress relaxation by incorporating fiber recruitment". *Journal of Rheology,* ***45***(2), pp. 493–507.

[37] Svensson, R. B., Hassenkam, T., Hansen, P., and Magnusson, S. P., 2010. "Viscoelastic behavior of discrete human collagen fibrils". *Journal of the Mechanical Behavior of Biomedical Materials,* ***3***(1), pp. 112–115.

[38] Gupta, H. S., Seto, J., Krauss, S., Boesecke, P., and Screen, H. R. C., 2010. "In situ multi-level analysis of viscoelastic deformation mechanisms in tendon collagen". *Journal of Structural Biology,* ***169***(2), pp. 183–191.

[39] Puxkandl, R., Zizak, I., Paris, O., Keckes, J., Tesch, W., Bernstorff, S., Purslow, P., and Fratzl, P., 2002. "Viscoelastic properties of collagen: Synchrotron radiation investigations and structural model". *Philosophical Transactions of the Royal Society of London Series B-Biological Sciences,* ***357***(1418), pp. 191–197.

[40] Weiss, J., Gardiner, J., and Bonifasi-Lista, C., 2002. "Ligament material behavior is nonlinear, viscoelastic and rate-independent under shear loading". *Journal of Biomechanics,* ***35***(7), pp. 943–950.

[41] Screen, H. R. C., 2008. "Investigating load relaxation mechanics in tendon". *Journal of the Mechanical Behavior of Biomedical Materials,* ***1***(1), pp. 51–58.

[42] Screen, H. R. C., Shelton, J. C., Chhaya, V. H., Kayser, M. V., Bader, D. L., and Lee, D. A., 2005. "The influence of noncollagenous matrix components on the micromechanical environment of tendon fascicles". *Annals of Biomedical Engineering,* ***33***(8), pp. 1090–1099.

[43] Lujan, T. J., Underwood, C. J., Jacobs, N. T., and Weiss, J. A., 2009. "Contribution of glycosaminoglycans to viscoelastic tensile behavior of human ligament". *Journal of Applied Physiology,* ***106***(2), pp. 423–431.

[44] Thornton, G. M., Shrive, N. G., and Frank, C. B., 2002. "Ligament creep recruits fibres at low stresses and can lead to modulus-reducing fibre damage at higher creep stresses: A study in rabbit medial collateral ligament model". *Journal of Orthopaedic Research,* ***20***(5), pp. 967–974.

[45] Lujan, T. J., Underwood, C. J., Henninger, H. B., Thompson, B. M., and Weiss, J. A., 2007. "Effect of dermatan sulfate glycosaminoglycans on the quasi-static material properties of the human medial collateral ligament". *Journal of Orthopaedic Research,* ***25***(7), pp. 894–903.

[46] Abramowitch, S. D., and Woo, S. L. Y., 2004. "An improved method to analyze the stress relaxation of ligaments following a finite ramp time based on the quasi-linear viscoelastic theory". *Journal of Biomechanical Engineering-Transactions of the ASME,* ***126***(1), pp. 92–97.

[47] DeFrate, L. E., and Li, G., 2007. "The prediction of stress-relaxation of ligaments and tendons using the quasi-linear viscoelastic model". *Biomechanics and Modeling in Mechanobiology,* ***6***(4), pp. 245–251.

[48] Findley, W. N., and Lai, J. S. Y., 1967. "A modified superposition principle applied to the creep of nonlinear viscoelastic material under abrupt changes in state of combined stress". *Transactions of the Society of Rhelolgy,* ***11***(3), pp. 361–380.

[49] Provenzano, P. P., Lakes, R. S., Corr, D. T., and Vanderby, R., 2002. "Application of nonlinear viscoelastic models to describe ligament behavior". *Biomechanics and Modeling in Mechanobiology,* ***1***(1), pp. 45–57.

[50] Schapery, R., 1969. "On the characterization of nonlinear viscoelastic materials". *Polymer Engineering and Science,* ***9***(4), pp. 295–310.

[51] Toms, S. R., Dakin, G. J., Lemons, J. E., and Eberhardt, A. W., 2002. "Quasi-linear viscoelastic behavior of the human periodontal ligament". *Journal of Biomechanics,* ***35***(10), pp. 1411–1415.

[52] Yang, W., Fung, T. C., Chian, K. S., and Chong, C. K., 2006. "Viscoelasticity of esophageal tissue and application of a QLV model". *Journal of Biomechanical Engineering-Transactions of the ASME,* ***128***(6), pp. 909–916.

[53] Funk, J. R., Hall, G. W., Crandall, J. R., and Pilkey, W. D., 2000. "Linear and quasi-linear viscoelastic characterization of ankle ligaments". *Journal of Biomechanical Engineering-Transactions of the ASME,* ***122***(1), pp. 15–22.

[54] Elliott, D. M., Robinson, P. S., Gimbel, J. A., Sarver, J. J., Abboud, J. A., Iozzo, R. V., and Soslowsky, L. J., 2003. "Effect of altered matrix proteins on quasilinear viscoelastic properties in transgenic mouse tail tendons". *Annals of Biomedical Engineering,* ***31***(5), pp. 599–605.

[55] Sarver, J. J., Robinson, P. S., and Elliott, D. M., 2003. "Methods for quasi-linear viscoelastic modeling of soft tissue: Application to incremental stress-relaxation experiments". *Journal of Biomechanical Engineering,* ***125***(5), pp. 754–758.

[56] Thornton, G. M., Oliynyk, A., Frank, C. B., and Shrive, N. G., 1997. "Ligament creep cannot be predicted from stress relaxation at low stress: A biomechanical study of the rabbit medial collateral ligament". *Journal of Orthopaedic Research,* ***15***(5), pp. 652–656.

[57] Duenwald, S. E., Vanderby, R., and Lakes, R. S., 2010. "Stress relaxation and recovery in tendon and ligament: Experiment and modeling". *Biorheology,* ***47***(1), pp. 1–14.

[58] Lanir, Y., 1980. "A microstructure model for the rheology of mammalian tendon". *Journal of Biomechanical Engineering-Transactions of the ASME,* ***102***(4), pp. 332–339.

[59] Einat, R., and Lanir, Y., 2009. "Recruitment viscoelasticity of the tendon". *Journal of Biomechanical Engineering,* ***131***(11).

[60] Sopakayang, R., and De Vita, R., 2011. "A mathematical model for creep, relaxation and strain stiffening in parallel-fibered collagenous tissues". *Medical Engineering & Physics,* ***33***(9), pp. 1056–1063.

[61] Davis, F., and De Vita, R., 2012. "A nonlinear constitutive model for stress relaxation in ligaments and tendons". *Annals of Biomedical Engineering,* ***40***(12), pp. 2541–2550.

[62] Amiel, D., Frank, C., Harwood, F., Fronek, J., and Akeson, W., 1983. "Tendons and ligaments: A morphological and biochemical comparison". *Journal of Orthopaedic Research,* ***1***(3), pp. 257–265.

[63] Shen, Z. L., Kahn, H., Ballarin, R., and Eppell, S. J., 2011. "Viscoelastic properties of isolated collagen fibrils". *Biophysical Journal,* ***100***(12), pp. 3008–3015.

[64] Dumitru, E., and Garrett, R., 1957. "Solubilization of rat tail tendon collagen". *Archives of Biochemistry and Biophysics,* ***66***(1), pp. 245–247.

[65] Rigby, B., Hirai, N., Spikes, J., and Eyring, H., 1959. "The mechanical properties of rat tail tendon". *The Journal of General Physiology,* ***43***(2), p. 265.

[66] Johnson, G. A., Livesay, G. A., Woo, S. L. Y., and Rajagopal, K. R., 1996. "A single integral finite strain viscoelastic model of ligaments and tendons". *Journal of*

Biomechanical Engineering-Transactions of the ASME, ***118***(2), pp. 221–226.

[67] Roberts, D., and Green, W., 1980. "Large axisymmetric deformation of a non-linear viscoelastic circular membrane". *Acta Mechanica,* ***36***(1), pp. 31–42.

[68] Oza, A., Vanderby, R., and Lakes, R., 2003. "Interrelation of creep and relaxation for nonlinearly viscoelastic materials: application to ligament and metal". *Rheologica Acta,* ***42***(6), pp. 557–568.

[69] Truesdell, C., Noll, W., and Antman, S., 2004. *The Non-linear Field Theories of Mechanics*, Vol. 3. Springer-Verlag.

[70] Merodio, J., and Ogden, R., 2005. "Mechanical response of fiber-reinforced incompressible non-linearly elastic solids". *International Journal of Non-Linear Mechanics,* ***40***, pp. 213 – 227.

[71] Holzapfel, G., and Ogden, R., 2009. "On planar biaxial tests for anisotropic nonlinearly elastic solids: A continuum mechanical framework". *Mathematics and Mechanics of Solids,* ***14***(5), pp. 474–489.

[72] Holzapfel, G. A., Gasser, T. C., and Ogden, R. W., 2000. "A new constitutive framework for arterial wall mechanics and a comparative study of material models". *Journal of Elasticity,* ***61***, pp. 1–48.

[73] Limbert, G., and Middleton, J., 2004. "A transversely isotropic viscohyperelastic material - application to the modeling of biological soft connective tissues". *International Journal of Solids and Structures,* ***41***(15), pp. 4237–4260.

[74] Eberl, C., Thompson, R., and Gianola, D., 2006. Digital image correlation and tracking with matlab: Matlab file exchange.

[75] Byrd, R. H., Schnabel, R. B., and Shultz, G. A., 1988. "Approximate solution of the trust region problem by minimization over two-dimensional subspaces". *Mathematical Programming,* ***40***, pp. 247–263.

[76] Atkinson, T., Ewers, B., and Haut, R., 1999. "The tensile and stress relaxation responses of human patellar tendon varies with specimen cross-sectional area". *Journal of Biomechanics,* ***32***(9), pp. 907–914.

[77] Panjabi, M., Moy, P., Oxland, T., and Cholewicki, J., 1999. "Subfailure injury affects the relaxation behavior of rabbit acl". *Clinical Biomechanics,* ***14***(1), pp. 24–31.

[78] Derwin, K. A., and Soslowsky, L. J., 1999. "A quantitative investigation of structure-function relationships in a tendon fascicle model". *Journal of Biomechanical Engineering-Transactions of the ASME,* ***121***(6), pp. 598–604.

[79] Cheng, S., Clarke, E. C., and Bilston, L. E., 2009. "The effects of preconditioning strain

on measured tissue properties". *Journal of Biomechanics,* ***42***(9), pp. 1360–1362.

[80] De Vita, R., and Slaughter, W. S., 2007. "A constitutive equation for the failure behavior of medial collateral ligaments". *Biomechanics and Modeling in Mechanobiology,* ***6***, pp. 189–197.

[81] Guo, Z. Y., and De Vita, R., 2009. "Probabilistic constitutive law for damage in ligaments". *Medical Engineering & Physics,* ***31***(9), pp. 1104–1109.

[82] Gardiner, J., and Weiss, J., 2003. "Subject-specific finite element analysis of the human medial collateral ligament during valgus knee loading". *Journal of Orthopaedic Research,* ***21***(6), pp. 1098–1106.

[83] Gardiner, J. C., and Weiss, J. A., 2001. "Simple shear testing of parallel-fibered planar soft tissues". *Journal of Biomechanical Engineering-Transactions of the ASME,* ***123***(2), pp. 170–175.

[84] Lanir, Y., 1983. "Constitutive-equations for fibrous connective tissues". *Journal of Biomechanics,* ***16***(1), pp. 1–12.

[85] Hurschler, C., Loitz-Ramage, B., and Vanderby, R., 1997. "A structurally based stress-stretch relationship for tendon and ligament". *Journal of Biomechanical Engineering-Transactions of the ASME,* ***119***(4), pp. 392–399.

[86] Puso, M., and Weiss, J., 1998. "Finite element implementation of anisotropic quasi-linear viscoelasticity using a discrete spectrum approximation". *Journal of Biomechanical Engineering-Transactions of the ASME,* ***120***(1), pp. 62–70.

[87] Quapp, K., and Weiss, J., 1998. "Material characterization of human medial collateral ligament". *Journal of Biomechanical Engineering-Transactions of the ASME,* ***120***, pp. 757–763.

[88] Linz, P., 1985. *Analytical and Numerical Methods for Volterra Equations*, Vol. 7. SIAM.

[89] Pioletti, D. P., and Rakotomanana, L. R., 2000. "On the independence of time and strain effects in the stress relaxation of ligaments and tendons". *Journal of Biomechanics,* ***33***(12), pp. 1729–1732.

[90] De Vita, R., and Slaughter, W. S., 2006. "A structural constitutive model for the strain rate-dependent behavior of anterior cruciate ligaments". *International Journal of Solids and Structures,* ***43***, pp. 1561–1570.

[91] Horgan, C. O., and Murphy, J. G., 2011. "Simple shearing of soft biological tissues". *Proceedings of the Royal Society A-Mathematical Physical and Engineering Sciences,* ***467***, pp. 760–777.

[92] Guo, D. L., Chen, B. S., and Liou, N. S., 2007. "Investigating full-field deformation

of planar soft tissue under simple-shear tests". *Journal of Biomechanics,* ***40***(5), pp. 1165–1170.

[93] Zhang, D., and Arola, D. D., 2004. "Applications of digital image correlation to biological tissues". *Journal of Biomedical Optics,* ***9***(4), pp. 691–699.

[94] Bump, R. C., and Norton, P. A., 1998. "Epidemiology and natural history of pelvic floor dysfunction". *Obstetrics and Gynecology Clinics of North America,* ***25***(4), pp. 723 – 746.

[95] Davis, K., and Kumar, D., 2003. "Pelvic floor dysfunction: A conceptual framework for collaborative patient-centred care". *Journal of Advanced Nursing,* ***43***(6), pp. 555–568.

[96] Olsen, A. L., Smith, V. J., Bergstrom, J. O., Colling, J. C., and Clark, A. L., 1997. "Epidemiology of surgically managed pelvic organ prolapse and urinary incontinence". *Obstetrics & Gynecology,* ***89***(4), pp. 501 – 506.

[97] Hendrix, S., Clark, A., Nygaard, I., Aragaki, A., Barnabei, V., and McTiernan, A., 2002. "Pelvic organ prolapse in the women's health initiative: gravity and gravidity". *American Journal of Obstetrics and Gynecology,* ***186***(6), pp. 1160–1166.

[98] MacLennan, A., Taylor, A., Wilson, D., and Wilson, D., 2000. "The prevalence of pelvic floor disorders and their relationship to gender, age, parity and mode of delivery". *British Journal of Obstetrics and Gynaecology,* ***107***(12), pp. 1460–1470.

[99] Summers, A., Winkel, L. A., Hussain, H. K., and DeLancey, J. O., 2006. "The relationship between anterior and apical compartment support". *American Journal of Obstetrics and Gynecology,* ***194***(5), pp. 1438 – 1443.

[100] Ramanah, R., Berger, M. B., Parratte, B. M., and DeLancey, J. O., 2012. "Anatomy and histology of apical support: A literature review concerning cardinal and uterosacral ligaments". *International Urogynecology Journal*, pp. 1–12.

[101] Huang, T. C., Toraya, H., Blanton, T. N., and Wu, Y., 1993. "X-ray powder diffraction analysis of silver behenate, a possible low-angle diffraction standard". *Journal of Applied Crystallography,* ***26***(2), pp. 180–184.

[102] Mosler, E., Folkhard, W., Knörzer, E., Nemetschek-Gansler, H., Nemetschek, T., and Koch, M., 1985. "Stress-induced molecular rearrangement in tendon collagen". *Journal of Molecular Biology,* ***182***(4), pp. 589 – 596.

[103] Folkhard, W., Mosler, E., Geercken, W., Knörzer, E., Nemetschek-Gansler, H., Nemetschek, T., and Koch, M., 1987. "Quantitative analysis of the molecular sliding mechanisms in native tendon collagen – time-resolved dynamic studies using synchrotron radiation". *International Journal of Biological Macromolecules,* ***9***(3), pp. 169 – 175.

[104] Purslow, P. P., Wess, T. J., and Hukins, D. W. L., 1998. "Collagen orientation and molecular spacing during creep and stress-relaxation in soft connective tissues". *Journal of Experimental Biology,* ***201***(1), pp. 135–142.

[105] Holzapfel, G., Sommer, G., Auer, M., Regitnig, P., and Ogden, R., 2007. "Layer-specific 3D residual deformations of human aortas with non-atherosclerotic intimal thickening". *Annals of biomedical engineering,* ***35***(4), pp. 530–545.

[106] Gruber, D., Warner, W., Lombardini, E., Zahn, C., and Buller, J., 2011. "Anatomical and histological examination of the porcine vagina and supportive structures: In search of an ideal model for pelvic floor disorder evaluation and management". *Female Pelvic Medicine & Reconstructive Surgery,* ***17***(3), pp. 110–114.

[107] Geary, T., and Doherty, R., 1977. "Uterine prolapse in the sow". *Veterinary Record,* ***100***(16), p. 348.

[108] Abramowitch, S. D., Feola, A., Jallah, Z., and Moalli, P. A., 2009. "Tissue mechanics, animal models, and pelvic organ prolapse: A review". *European Journal of Obstetrics & Gynecology and Reproductive Biology,* ***144***, pp. S146–S158.

[109] Schimpf, M., and Tulikangas, P., 2005. "Evolution of the female pelvis and relationships to pelvic organ prolapse". *International Urogynecology Journal,* ***16***(4), pp. 315–320.

[110] Bustamante, R., and Merodio, J., 2010. "On simple constitutive restrictions for transversely isotropic nonlinearly elastic materials and isotropic magneto-sensitive elastomers". *Journal of Engineering Mathematics,* ***68***(1), pp. 15–26.

[111] Murphy, J., 2012. "Tension in the fibres of anisotropic non-linearly hyperelastic materials. some stability results and constitutive restrictions.". *International Journal of Solids and Structures*.

[112] Merodio, J., and Ogden, R. W., 2003. "A note on strong ellipticity for transversely isotropic linearly elastic solids". *The Quarterly Journal of Mechanics and Applied Mathematics,* ***56***(4), pp. 589–591.

[113] Slaughter, W., 2002. *The Linearized Theory of Elasticity*. Birkhauser.

A

Restrictions on the Model Parameters

Restrictions were imposed on the values of the model parameters given in Chapters 3 and 4 to ensure that the material response was physically reasonable. Here the purpose is to explain how those restrictions were derived. Since the constitutive functions outlined in Ch. 3 were built upon in Ch. 4, only the more general case outlined in Ch. 4 will be addressed. The restrictions on the elastic parameters c_1, c_2, c_3, and c_4 are found first followed by the restrictions on the viscoelastic parameters a and b and the functions $\alpha(I_4)$ and $\beta(I_4)$.

A.1 Restrictions on the Elastic Model Parameters

Bustamante and Merodio [110] have extended the Baker-Ericksen inequality presented for isotropic materials [69] to transversely isotropic solids and concisely presented the restrictions that would be imposed on the strain energy function. The methods outlined in their paper will be employed to identify the restrictions on the elastic model parameters c_1 and c_2. Constitutive restrictions for the fiber reinforcement in a transversely isotropic solid have been presented by Murphy [111] and will be used to identify the restrictions on the elastic model parameters c_3 and c_4. Finally, the model is collapsed to the linear elastic case and further restrictions are imposed on the model parameters so that the strong ellipticity conditions from the linear theory of elasticity are satisfied [112].

A.1.a Preliminaries

Let W denote the so-called strain energy function. For an incompressible transversely isotropic solid the strain energy depends on four independent invariants, $W = W(I_1, I_2, I_4, I_5)$.

These invariants are:

$$I_1 = \mathrm{tr}(\mathbf{C})\,, \quad I_2 = \frac{1}{2}\left(I_1^2 - \mathrm{tr}\left(\mathbf{C}^2\right)\right)\,, \quad I_4 = \mathbf{M}\cdot\mathbf{CM}\,, \quad I_5 = \mathbf{M}\cdot\mathbf{C}^2\mathbf{M} \tag{A.1}$$

where $\mathbf{M}$ is the unit vector that defines the axis of transverse isotropy in the reference configuration and $\mathbf{C}$ is the right Cauchy-Green tensor. The strain energy function that captures the nonlinear elastic response of ligaments described in Chapter 4 is

$$W = \begin{cases} c_1 \mathrm{e}^{c_2(I_1-3)} - \frac{c_1 c_2}{2}\left(I_2 - 3\right) + c_3\left(\frac{\mathrm{e}^{c_4(I_4-1)}}{c_4} - I_4\right) & I_4 \geq 1 \\ c_1 \mathrm{e}^{c_2(I_1-3)} - \frac{c_1 c_2}{2}\left(I_2 - 3\right) & I_4 < 1 \end{cases} \tag{A.2}$$

where the strain energy function, W, can be related to the tensorial relaxation function, $\mathbf{R}\left[\mathbf{C}, 0\right]$, given by Eqs. (4.9)-(4.12) and (4.34) by substituting W into (4.5).

The Cauchy stress tensor for an incompressible transversely isotropic solid is given by [69]

$$\mathbf{T} = -p\mathbf{I} + 2\left(W_1\mathbf{B} + W_2\left(I_1\mathbf{B} - \mathbf{B}^2\right) + W_4\mathbf{m}\otimes\mathbf{m} + W_5\left(\mathbf{m}\otimes\mathbf{Bm} + \mathbf{Bm}\otimes\mathbf{m}\right)\right) \tag{A.3}$$

where p is the Lagrange multiplier arising from the incompressibility constraint, $\mathbf{F}$ is the deformation gradient, $\mathbf{B} = \mathbf{F}\mathbf{F}^{\mathrm{T}}$ is the left Cauchy-Green tensor, $\mathbf{m}$ is the unit vector that defines the axis of transverse isotropy in the deformed configuration ($\mathbf{m} = \mathbf{FM}$), and W_j denotes the partial derivative of W with respect to I_j.

A.1.b Constitutive restrictions for the isotropic matrix

Two constitutive restrictions are presented for the isotropic contribution to the strain energy function. The first restriction considers the material behavior for simple shear in the fiber direction and requires that the proposed strain energy function is a convex function of the amount of shear. Next, the conditions on the model parameters needed to satisfy the Baker-Ericksen inequality for a triaxial extension are determined. Note that the Baker-Ericksen inequality requires the greater principal stress to always occur in the same direction as the greater principal stretch.

Constitutive Restrictions for Simple Shear in the Fiber Direction

Consider the isochoric homogeneous deformation defined by

$$x_1 = X_1\,, \quad x_2 = X_2\,, \quad x_3 = \gamma X_1 + X_3 \tag{A.4}$$

where (X_1, X_2, X_3) and (x_1, x_2, x_3) represent the Cartesian coordinates of a generic point in the reference and deformed configurations, respectively, and γ is the amount of shear. The orthonormal bases $\{\mathbf{E}_1, \mathbf{E}_2, \mathbf{E}_3\}$ and $\{\mathbf{e}_1, \mathbf{e}_2, \mathbf{e}_3\}$ in the reference and deformed configurations, respectively, are aligned such that the axis of transverse isotropy is parallel to $\mathbf{E}_3$ in the reference configuration ($\mathbf{M} = \mathbf{E}_3$).

It follows that the deformation gradient tensor, $\mathbf{F}$, and the left Cauchy-Green deformation tensor, $\mathbf{B}$, are given by

$$\mathbf{F} = \mathbf{e}_1 \otimes \mathbf{E}_1 + \mathbf{e}_2 \otimes \mathbf{E}_2 + \gamma\, \mathbf{e}_3 \otimes \mathbf{E}_1 + \mathbf{e}_3 \otimes \mathbf{E}_3 \,,$$
$$\mathbf{B} = \mathbf{e}_1 \otimes \mathbf{e}_1 + \gamma\,(\mathbf{e}_1 \otimes \mathbf{e}_3 + \mathbf{e}_3 \otimes \mathbf{e}_1) + \mathbf{e}_2 \otimes \mathbf{e}_2 + \left(1 + \gamma^2\right)\, \mathbf{e}_3 \otimes \mathbf{e}_3 \,. \quad \text{(A.5)}$$

For the case of simple shear in the fiber direction the strain energy function in Eq. (A.2) can be expressed in terms of the amount of shear, $\hat{W} = W(\gamma)$, and the shear stress $T_{13} = \frac{d\hat{W}}{d\gamma}$. For the strain energy function given in Eq. (A.2), the function $\hat{W} = c_1 \mathrm{e}^{c_2\gamma^2} - \frac{c_1 c_2}{2}\gamma^2$ and the shear stress is $T_{13} = c_1 c_2 \gamma \left(2\mathrm{e}^{c_2\gamma^2} - 1\right)$.

To ensure that the response for simple shear in the fiber direction is physically reasonable we require that the shear stress is positive for a positive shear and vice versa [110]. To meet these restrictions the following inequalities must be satisfied:

$$\frac{d\hat{W}}{d\gamma} > 0 \;\text{ when } \gamma > 0\,, \qquad \frac{d\hat{W}}{d\gamma} < 0 \;\text{ when } \gamma < 0 \quad \text{(A.6)}$$

which require $c_1 c_2 > 0$.

Constitutive Restrictions for a Triaxial Extension

Consider the isochoric homogeneous axisymmetric deformation defined by

$$x_1 = \lambda_1 X_1 \,, \quad x_2 = \lambda_2 X_2 \,, \quad x_3 = \lambda_3 X_3 \quad \text{(A.7)}$$

where λ_i, $i = 1, 2, 3$ are the axial stretches. Again the axis of transverse isotropy is parallel to $\mathbf{E}_3$ in the reference configuration ($\mathbf{M} = \mathbf{E}_3$).

It follows that the deformation gradient tensor, $\mathbf{F}$, and the left Cauchy-Green deformation tensor, $\mathbf{B}$, are given by

$$\mathbf{F} = \lambda_1\, \mathbf{e}_1 \otimes \mathbf{E}_1 + \lambda_2\, \mathbf{e}_2 \otimes \mathbf{E}_2 + \lambda_3\, \mathbf{e}_3 \otimes \mathbf{E}_3 \,,$$
$$\mathbf{B} = \lambda_1^2 \mathbf{e}_1 \otimes \mathbf{e}_1 + \lambda_2^2\, \mathbf{e}_2 \otimes \mathbf{e}_2 + \lambda_3^2\, \mathbf{e}_3 \otimes \mathbf{e}_3 \,. \quad \text{(A.8)}$$

Since the material is assumed to be incompressible, we also require $\lambda_1\lambda_2\lambda_3 = 1$.

To ensure that the Baker-Ericksen inequality is satisfied for a triaxial extension Bustamante and Merodio [110] found that the following condition must be met

$$W_1 + \frac{1}{\lambda_1^2\lambda_2^2}W_2 > 0. \tag{A.9}$$

For the transversely isotropic strain energy function given in Eq. (A.2), Eq. (A.9) gives the following result:

$$c_1c_2\left(2\mathrm{e}^{c_2\left(\lambda_1^2+\lambda_2^2+\lambda_1^{-2}\lambda_2^{-2}-3\right)} - \frac{1}{\lambda_1^2\lambda_2^2}\right) > 0\,. \tag{A.10}$$

The restriction found for simple shear in the fiber direction requires that the product c_1c_2 must be greater than zero; therefore the function $f = \left(2\mathrm{e}^{c_2\left(\lambda_1^2+\lambda_2^2+\lambda_1^{-2}\lambda_2^{-2}-3\right)} - \frac{1}{\lambda_1^2\lambda_2^2}\right)$ must also be greater than zero. To determine the values of c_2 that satisfy $f > 0$, the function f was set to zero and solved for c_2.

$$c_2 = \frac{\ln\left(\frac{1}{2\lambda_1^2\lambda_2^2}\right)}{\lambda_1^2+\lambda_2^2+\lambda_1^{-2}\lambda_2^{-2}-3} \tag{A.11}$$

The values of λ_1 and λ_2 where the maximum value of c_2 occurs were found to be $\lambda_1 = \lambda_2 = 0.726$. Substituting these values of λ_1 and λ_2 into Eq. (A.11) the maximum value of c_2 was found to be approximately 0.355. As a result, the following restrictions were imposed on the model parameters: $c_2 > 0.36$ and hence $c_1 > 0$ since $c_1c_2 > 0$.

A.1.c Restrictions on the response of the fiber reinforcement

To derive the restrictions on the model parameters c_3 and c_4 the following three requirements proposed by Murphy [111] on the fiber contribution to the strain energy function were enforced.

1. The tension in unstretched fibers must be zero.
2. The slope of the stress-stretch curve in the reference configuration must be greater than zero.
3. The tension in the fibers must be a monotonically increasing function of stretch.

To meet the first requirement, W_4 must equal zero when evaluated in the reference configuration. For the transversely isotropic strain energy given in Eq. (A.2) this requirement is

clearly met with no constraint on the model parameters c_3 and c_4.

$$W_4 = c_3 \left(\mathrm{e}^{c_4(I_4-1)} - 1 \right) , \qquad W_4|_{I_4=1} = 0 \tag{A.12}$$

The second requirement ensures that for small extensions the modulus of the fibers is greater than zero and can be expressed mathematically as $\frac{dW_4}{d\lambda_f}|_{I_4=1} > 0$ where $\lambda_f = \sqrt{I_4}$ and is the stretch in the fiber direction.

$$\frac{dW_4}{d\lambda_f} = 2c_3c_4\lambda_f \mathrm{e}^{c_4\left(\lambda_f^2-1\right)} , \qquad \left.\frac{dW_4}{d\lambda_f}\right|_{\lambda_f=1} = 2c_3c_4 \tag{A.13}$$

Evaluating Eq. (A.13) at $\lambda_f = 1$, one finds that c_3c_4 must be greater than zero.

The final condition requires that $\frac{d^2W_4}{d\lambda_f{}^2} > 0$ for $\lambda_f > 0$.

$$\frac{d^2W_4}{d\lambda_f{}^2} = 2\, c_3c_4\, \mathrm{e}^{c_4\left(\lambda_f^2-1\right)} + 4\, c_3c_4^2\, \lambda_f^2\, \mathrm{e}^{c_4\left(\lambda_f^2-1\right)} \tag{A.14}$$

Imposing the constraint that $c_3 > 0$ is sufficient to ensure that $\frac{d^2W_4}{d\lambda_f{}^2} > 0$ and thus requires that $c_4 > 0$ since $c_3c_4 > 0$.

A.1.d Connection with linear elasticity

A transversely isotropic linear elastic solid can be described with five elastic constants, s_{11}, s_{12}, s_{33}, s_{13}, and s_{44}. The constitutive relationship for a linear elastic transversely isotropic material is the following [113]:

$$\begin{bmatrix} \sigma_{11} \\ \sigma_{22} \\ \sigma_{33} \\ \sigma_{23} \\ \sigma_{31} \\ \sigma_{12} \end{bmatrix} = \begin{bmatrix} s_{11} & s_{12} & s_{13} & 0 & 0 & 0 \\ s_{12} & s_{11} & s_{13} & 0 & 0 & 0 \\ s_{13} & s_{13} & s_{33} & 0 & 0 & 0 \\ 0 & 0 & 0 & s_{44} & 0 & 0 \\ 0 & 0 & 0 & 0 & s_{44} & 0 \\ 0 & 0 & 0 & 0 & 0 & \frac{1}{2}\left(s_{11} - s_{12}\right) \end{bmatrix} \begin{bmatrix} \varepsilon_{11} \\ \varepsilon_{22} \\ \varepsilon_{33} \\ \varepsilon_{23} \\ \varepsilon_{31} \\ \varepsilon_{12} \end{bmatrix} \tag{A.15}$$

where σ_{ij} is the stress, ε_{ij} is the infinitesimal strain, and the axis of transverse isotropy is parallel to $\mathbf{E}_3$. Note that when the material is also incompressible the number of independent material constants reduces to three. Merodio and Ogden [70] have shown that for a hyperelastic incompressible transversely isotropic material s_{11}, s_{12}, s_{33}, s_{13}, and s_{44} can be

found from the strain energy function, W, using the following expressions:

$$W_1 + W_2 = (s_{11} - s_{12})/4 \tag{A.16}$$
$$W_1 + W_2 + W_5 = s_{44}/2 \tag{A.17}$$
$$W_{44} + 4W_{45} + 4W_{55} = (s_{11} + s_{33} - 2s_{13} - 4s_{44})/4 \tag{A.18}$$

where Eqs. (A.16)-(A.18) are evaluated in the reference configuration. Further, the strong ellipticity conditions for linear elasticity require [112]

$$s_{11} > s_{12}\,, \quad s_{44} > 0\,, \quad s_{11} + s_{33} - 2s_{13} > 0\,. \tag{A.19}$$

For the strain energy function given in Eq. (A.2), $W_1 = c_1 c_2 \mathrm{e}^{c_2(I_1-3)}$, $W_2 = -c_1 c_2/2$, and $W_{44} = c_3 c_4 \mathrm{e}^{c_4(I_4-1)}$ and hence from Eqs. (A.16)-(A.18) we find

$$(s_{11} - s_{12}) = 2c_1 c_2 \tag{A.20}$$
$$s_{44} = c_1 c_2 \tag{A.21}$$
$$(s_{11} + s_{33} - 2s_{13} - 4s_{44}) = 4c_3 c_4\,. \tag{A.22}$$

The strong ellipticity conditions from linear elasticity given in Eq. (A.19) can be satisfied by requiring $c_1 c_2 > 0$ and $c_3 c_4 > 0$.

The classical shear moduli, G_{ij}, and elastic moduli, E_i, can be calculated from the elastic constants s_{11}, s_{12}, s_{33}, s_{13}, and s_{44}.

$$G_{12} = G_{21} = (s_{11} - s_{12})/2 \tag{A.23}$$
$$G_{32} = G_{23} = G_{13} = G_{31} = s_{44} \tag{A.24}$$
$$E_1 = E_2 = (s_{11} - s_{12})\left(1 + \left(1 - \frac{s_{11} - s_{12}}{s_{11} + s_{33} - 2s_{13}}\right)\right) \tag{A.25}$$
$$E_3 = (s_{11} - s_{12})\left(\frac{s_{11} + s_{33} - 2s_{13}}{s_{11} - s_{12}} - \frac{1}{2}\right) \tag{A.26}$$

For the values determined in Eqs. (A.20)-(A.22) the classical shear moduli, G_{ij}, and elastic moduli, E_i, are

$$G_{12} = G_{21} = G_{32} = G_{23} = G_{13} = G_{31} = G = c_1 c_2 \tag{A.27}$$
$$E_1 = E_2 = 2c_1 c_2\left(1 + \frac{c_3 c_4}{c_1 c_2 + c_3 c_4}\right) \tag{A.28}$$
$$E_3 = 4\,c_3 c_4 + 3\,c_1 c_2\,. \tag{A.29}$$

For the values of the parameters determined in Ch. 4, $c_1 = 0.86$ MPa, $c_2 = 8.16$, $c_3 = 21.77$ MPa, $c_4 = 3.30$, the values of the shear modulus, G, and the elastic moduli E_1 and E_3 are 7 MPa, 13 MPa, and 308 MPa, respectively. For comparison purposes, the slopes of the axial stress-strain curves for ligament samples cut in the transverse and longitudinal directions at zero strain were calculated from the experimental data collected by Quapp and Weiss [87] and found to be 7 MPa and 107 MPa, respectively. The tangent moduli (slope of the linear region of the axial stress-strain curve) reported by Quapp and Weiss [87] for samples cut in the transverse and longitudinal direction were 11.02 ± 3.57 MPa and 332.15 ± 58.27 MPa, respectively.

A.2 Restrictions on the Viscoelastic Model Parameters

In order to meet fading memory requirements, the tensorial relaxation function must be a monotonically decreasing function of time: the partial derivative of $\mathbf{R}[\mathbf{C}, t-\tau]$ with respect to $t-\tau$ must be always negative [69]. To meet this requirement the products $(1-a)\,b$ and $(1-\alpha(I_4))\,\beta(I_4)$ must be greater than zero. For the normalized stress relaxation response to be bounded between 0 and 1, the values of a and $\alpha(I_4)$ must also lie between 0 and 1. Knowing that $0 < a < 1$ and $0 < \alpha(I_4) < 1$ requires the values of b and $\beta(I_4)$ to be greater than zero so that $(1-a)\,b$ and $(1-\alpha(I_4))\,\beta(I_4)$ are greater than zero.

B

Tensile Properties of the Swine Cardinal Ligament

B.1 Experimental Methods

B.1.a SEM examination

Prior to SEM examination, one ligament was allowed to thaw for one hour and three samples were cut down to a length of approximately 30 mm. The specimens were placed in 2% glutaraldehyde-0.01 M sodium cacodylate buffer, fixed in osmium tetraoxide and then critical point dried. To visualize the cross-section, each sample was frozen in liquid nitrogen and cut with a sharp razor blade; then a gold coating was applied by vacuum evaporation. Images of the samples were collected using an environmental scanning electron microscope (Quanta 600 FEG, FEI).

B.1.b Uniaxial testing

Ten samples were removed from the freezer and allowed to come to room temperature for one hour. They were kept continuously hydrated by spraying them with PBS throughout the sample preparation. Images of each sample were collected using a microscope (Stemi 2000C, Zeiss) to determine the width of each specimen at five locations. A caliper instrumented with a force gauge was used to measure the thickness of each specimen at five locations under a 50 g compressive load (Mitutoyo 573-291-20). Assuming a rectangular cross-section, the area for each specimen was calculated using the average width and thickness. Black ink was sprayed on the surface of the ligament to produce marks with suitable contrast for strain calculation.

The specimens were tested using a tensile testing machine (ElectroPuls E1000, Instron). Each sample was pre-loaded to 0.1 N. It was then stretched at 0.75 mm/sec until failure

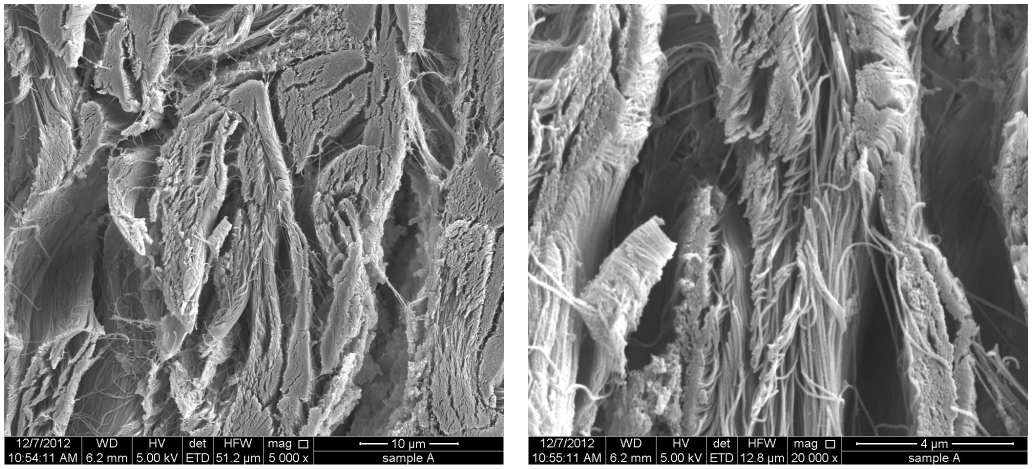

(a) (b)

Figure B.1: Scanning electron micrographs of the cardinal ligament illustrating (a) the bundled groups of collagen fibers and (b) an individual bundle within the ligament.

occurred. The motion of the ink marks was tracked using a digital image correlation method (MATLAB v. 7.10, MathWorks) and the axial strain was computed. The nominal axial stress was calculated by dividing the load by the measured cross-sectional area.

B.2 Results

Scanning electron micrographs of the ligament cross-section revealed multiple bundles of collagen fibers [Figure B.1(a)]. When examining the collagen network within one bundle one finds collagen fibrils approximately 60 nm in diameter that are organized into fibers primarily pointing into the page [Figure B.1(b)]. However, the fibers at the bottom center of the image are clearly aligned in the vertical direction [Figure B.1(b)]. This arrangement of the collagen network suggests that the cardinal ligament may need to resist loads in multiple directions.

A representative stress-strain curve for the cardinal ligament is shown in Figure B.2. The ligaments exhibited the strain-stiffening behavior generally observed in soft collagenous tissues. In the failure region of the stress-strain curve, multiple peaks can be observed when a tear initiates in one location and is then halted. While the tear is halted the load increases, until the tear begins to propagate again. Eventually the tear propagates through the width of the tissue and the stress drops to zero.

To quantify the mechanical properties of the cardinal ligament, the average values of the elastic modulus of the linear region and the ultimate stress were determined. A line was

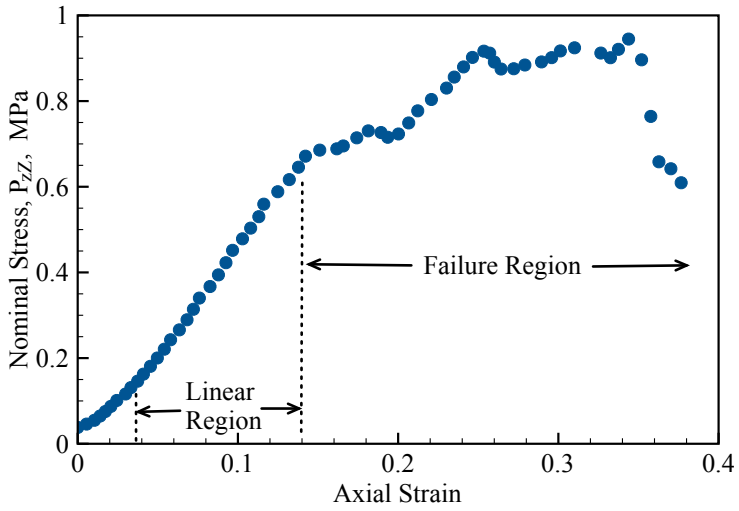

Figure B.2: Typical tensile axial stress-strain curve for swine cardinal ligament. For this sample the modulus in the linear region is 0.45 MPa.

fit to the points in the linear region using the linear least squares fitting routine *polyfit* in MATLAB. The slope found from the linear regression is taken as the modulus of the linear region. Across all 10 samples the average elastic modulus of the linear region was found to be 0.40 $\pm$ 0.19 MPa, while the average ultimate stress was 1.49 $\pm$ 0.66 MPa.

C

Copyright Permissions for Figures

Secure permission for figure

2 messages

Frances Davis <fmdavis@vt.edu> Wed, Mar 27, 2013 at 7:44 PM
To: permissions@sagepub.com

I attempted to request use of the following figure using RightsLink and was directed to email Sage for permission directly. Find the information for the requested figure and the requested use below:

Journal name: American Journal of Sports Medicine, The

Article title: Augmentation of Achilles Tendon Repair With Extracellular Matrix Xenograft:A Biomechanical Analysis

Authors: Robert A. Magnussen, Richard R. Glisson, Claude T. Moorman III

Volume Number: 39

Issue Number: 7

Pages: 1522 -- 1527

Use: For thesis or dissertation

Portion: Figure 2

Requester: Frances Davis

Title of Disseration: Nonlinear viscoelastic behavior of ligaments and tendons: models and experiments

Expected completion date: May 2013

~~~~~~~~~~~~~~~~
Frances M. Davis
PhD Candidate
Engineering Science and Mechanics
Virginia Tech

Binur, Michelle <Michelle.Binur@sagepub.com> Thu, Mar 28, 2013 at 12:48 PM
To: Frances Davis <fmdavis@vt.edu>

Dear Frances,

Thank you for your request. Please consider this e-mail as permission to reprint the material as detailed below in your upcoming thesis. Please note that this permission does not cover any 3rd party material that may be found within the work. We do ask that you credit the original source, SAGE Publications. Please contact us for any further usage.
~~~~~~~~~~~~~~~~

Good luck with your thesis,

Michelle Binur

From: Frances Davis [mailto:fmdavis@vt.edu]
Sent: Wednesday, March 27, 2013 4:45 PM
To: permissions (US)
Subject: Secure permission for figure

[Quoted text hidden]

SPRINGER LICENSE
TERMS AND CONDITIONS

Mar 27, 2013

This is a License Agreement between Frances M Davis ("You") and Springer ("Springer") provided by Copyright Clearance Center ("CCC"). The license consists of your order details, the terms and conditions provided by Springer, and the payment terms and conditions.

All payments must be made in full to CCC. For payment instructions, please see information listed at the bottom of this form.

License Number	3117311399640
License date	Mar 27, 2013
Licensed content publisher	Springer
Licensed content publication	World Journal of Urology
Licensed content title	Surgical management of pelvic organ prolapse: abdominal and vaginal approaches
Licensed content author	Kristina Cvach
Licensed content date	Jan 1, 2011
Volume number	30
Issue number	4
Type of Use	Thesis/Dissertation
Portion	Figures
Author of this Springer article	No
Order reference number	
Title of your thesis / dissertation	Nonlinear viscoelastic behavior of ligaments and tendons: models and experiments
Expected completion date	May 2013
Estimated size(pages)	100
Total	0.00 USD
Terms and Conditions	

Introduction
The publisher for this copyrighted material is Springer Science + Business Media. By clicking "accept" in connection with completing this licensing transaction, you agree that the following terms and conditions apply to this transaction (along with the Billing and Payment terms and conditions established by Copyright Clearance Center, Inc. ("CCC"), at the time that you opened your Rightslink account and that are available at any time at http://myaccount.copyright.com).

Limited License
With reference to your request to reprint in your thesis material on which Springer Science and Business Media control the copyright, permission is granted, free of charge, for the use

Indemnity
You hereby indemnify and agree to hold harmless Springer Science + Business Media and CCC, and their respective officers, directors, employees and agents, from and against any and all claims arising out of your use of the licensed material other than as specifically authorized pursuant to this license.

No Transfer of License
This license is personal to you and may not be sublicensed, assigned, or transferred by you to any other person without Springer Science + Business Media's written permission.

No Amendment Except in Writing
This license may not be amended except in a writing signed by both parties (or, in the case of Springer Science + Business Media, by CCC on Springer Science + Business Media's behalf).

Objection to Contrary Terms
Springer Science + Business Media hereby objects to any terms contained in any purchase order, acknowledgment, check endorsement or other writing prepared by you, which terms are inconsistent with these terms and conditions or CCC's Billing and Payment terms and conditions. These terms and conditions, together with CCC's Billing and Payment terms and conditions (which are incorporated herein), comprise the entire agreement between you and Springer Science + Business Media (and CCC) concerning this licensing transaction. In the event of any conflict between your obligations established by these terms and conditions and those established by CCC's Billing and Payment terms and conditions, these terms and conditions shall control.

Jurisdiction
All disputes that may arise in connection with this present License, or the breach thereof, shall be settled exclusively by arbitration, to be held in The Netherlands, in accordance with Dutch law, and to be conducted under the Rules of the 'Netherlands Arbitrage Instituut' (Netherlands Institute of Arbitration).***OR:***

All disputes that may arise in connection with this present License, or the breach thereof, shall be settled exclusively by arbitration, to be held in the Federal Republic of Germany, in accordance with German law.

Other terms and conditions:

v1.3

If you would like to pay for this license now, please remit this license along with your payment made payable to "COPYRIGHT CLEARANCE CENTER" otherwise you will be invoiced within 48 hours of the license date. Payment should be in the form of a check or money order referencing your account number and this invoice number RLNK500987351.
Once you receive your invoice for this order, you may pay your invoice by credit card. Please follow instructions provided at that time.

Make Payment To:
Copyright Clearance Center
Dept 001
P.O. Box 843006
Boston, MA 02284-3006